

SUBMICROSCOPIC DEFORMATION IN CEMENT PASTE AND MORTAR AT HIGH LOAD RATES

By AFOSR-TR- 88 - 0955

David Darwin
Emmanuel K. Attiogbe
Shraadhakar Harsin
Shen Zhenjia
George R. Dewey

DTIC
SELECTED
OCT 06 1988
S D

AD-A205 016

A Report on Research Sponsored by
THE AIR FORCE OFFICE OF SCIENTIFIC RESEARCH
Research Grant AFOSR-85-0194

DISTRIBUTION STATEMENT A
Approved for public release;
Distribution Unlimited

Structural Engineering and Engineering Materials
SL Report 88-1
August 1988



THE UNIVERSITY OF KANSAS CENTER FOR RESEARCH, INC.
2291 Irving Hill Drive—Campus West, Lawrence, Kansas 66045

Reproduced From
Best Available Copy

88 10 5 161

REPORT DOCUMENTATION PAGE

1a. REPORT SECURITY CLASSIFICATION Unclassified			1b. RESTRICTIVE MARKINGS			
2a. SECURITY CLASSIFICATION AUTHORITY			3. DISTRIBUTION/AVAILABILITY OF REPORT Approved for Public Release; distribution is unlimited			
2b. DECLASSIFICATION/DOWNGRADING SCHEDULE						
4. PERFORMING OR ORGANIZATION REPORT NUMBER(S)			5. MONITORING ORGANIZATION REPORT NUMBER(S) AFOSR-TX-88-0955			
6a. NAME OF PERFORMING ORGANIZATION University of Kansas Center for Research, Inc.		6b. OFFICE SYMBOL (if applicable)	7. NAME OF MONITORING ORGANIZATION Air Force Office of Scientific Research			
6c. ADDRESS (City, State, and ZIP Code) Lawrence, KS 66045			7b. ADDRESS (City, State, and ZIP Code) AFOSR/NA BK410 Bolling Air Force Base Washington, DC 20332			
8a. NAME OF FUNDING/SPONSORING ORGANIZATION AFOSR/NA Bolling AFB, DC 20332		8b. OFFICE SYMBOL (if applicable) NA	9. PROCUREMENT INSTRUMENT IDENTIFICATION NUMBER AFOSR-85-0194			
8c. ADDRESS (City, State, and ZIP Code) AFOSR/NA BK410 Bolling AFB, DC 20332			10. SOURCE OF FUNDING NUMBERS			
			PROGRAM ELEMENT NO. 61102F	PROJECT NO. 2302	TASK NO. C2	WORK UNIT ACCESSION NO.
11. TITLE (Include Security Classification) Submicroscopic Deformation in Cement Paste and Mortar at High Load Rates						
12. PERSONAL AUTHOR(S) Darwin, David						
13a. TYPE OF REPORT Final		13b. TIME COVERED FROM 850401 TO 880731		14. DATE OF REPORT (Year, Month, Day) 880815	15. PAGE COUNT 105	
16. SUPPLEMENTARY NOTATION						
17. COSATI CODES			18. SUBJECT TERMS (Continue on reverse if necessary and identify by block number) cement pastes; compression; concretes; cracking (fracturing), electron microscopes; image analysis; isotropy; measurement; microcracking; microscopic; microstructures; mortars (material); strains; strain rate; stress; stress-strain diagram; submicro-			
FIELD	GROUP	SUB-GROUP				
			19. ABSTRACT (Continue on reverse if necessary and identify by block number) Submicroscopic cracking and strain-rate response of cement paste and mortar under uniaxial compression were measured and correlated with applied strain. Cement paste specimens with water-cement ratios of 0.3, 0.4, 0.5, and 0.7 and mortar specimens with water-cement ratios of 0.3, 0.4, and 0.5 were subjected to monotonic load at strain rates ranging from 0.3 to 300,000 microstrain per second. Specimens were tested at ages ranging from 27 to 29 days. After loading, slices of material were removed from selected specimens for study at magnifications of 1250x and 2500x in a scanning electron microscope. Image analysis instrumentation was used in later stages of the study. Cracks on transverse and longitudinal surfaces were measured, and three-dimensional crack distributions were obtained from the crack data. The portion of the nonlinear material response caused by the cracks was estimated using a self-consistent material model. The strength and stiffness of cement paste and mortar increase with increasing strain rate. The relative effects of strain rate are largely independent of water-cement ratio and sand content. Submicrocracking accounts for a significant portion of the nonlinear response at all			
20. DISTRIBUTION/AVAILABILITY OF ABSTRACT <input checked="" type="checkbox"/> UNCLASSIFIED/UNLIMITED <input type="checkbox"/> SAME AS RPT <input type="checkbox"/> DTIC USERS			21. ABSTRACT SECURITY CLASSIFICATION Unclassified			
22a. NAME OF RESPONSIBLE INDIVIDUAL Dr. Spencer T. Wu			22b. TELEPHONE (Include Area Code) (202) 767-6962	22c. OFFICE SYMBOL AFOSR/NA		

TABLE OF CONTENTS

	PAGE
REPORT DOCUMENTATION PAGE.	ii
LIST OF TABLES	vi
LIST OF FIGURES.	vii
CHAPTER 1 INTRODUCTION	1
CHAPTER 2 EXPERIMENTAL PROGRAM	3
2.1 Materials	3
2.2 Test Specimens.	4
2.3 Loading Procedure	5
2.4 Submicrocracking Studies.	6
CHAPTER 3 EXPERIMENTAL RESULTS AND DISCUSSION - PHASE 1.	9
3.1 Submicrocracks.	9
3.2 Conversion of Surface to Three-Dimensional Crack Distributions	11
3.3 Three Dimensional Crack Parameters.	14
3.4 Strain Due to Submicrocracking.	18
CHAPTER 4 EXPERIMENTAL RESULTS AND DISCUSSION - PHASE 2.	29
4.1 Stress-Strain Curves.	29
4.2 Strength.	30
4.3 Strain at Peak Stress	31
4.4 Initial Modulus of Elasticity	31
4.5 Effect of Sand Content.	32
4.6 Submicrocracks.	34
4.7 Strain Due to Submicrocracking.	36

TABLE OF CONTENTS, Continued

CHAPTER 5	SUMMARY AND CONCLUSIONS.	37
5.1	Summary	37
5.2	Conclusions	37
5.3	Future Studies.	40
REFERENCES.	42
APPENDIX A	NOTATION	61
APPENDIX B	REPORTS AND PUBLICATIONS SUPPORTED BY THE AIR FORCE OFFICE OF SCIENTIFIC RESEARCH UNDER GRANT AFOSR-85-0194.	63

LIST OF TABLES

<u>Table No.</u>		<u>Page</u>
3.1	Three-Dimensional Crack Parameters	46
3.2	Effective Moduli and Axial Strain Due to Submicrocracking - Linear Matrix Material, Pre-Existing Cracks.	48
3.3	Moduli of Matrix and Axial Strain Due to Submicrocracking - Nonlinear Matrix Material, Pre-Existing Cracks	49
3.4	Moduli of Matrix and Axial Strain Due to Submicrocracking - Nonlinear Matrix Material, No Pre-Existing Cracks	50
4.1	Summary of Strain Rate Tests.	51
4.2	Comparison of Three-Dimensional Crack Parameters for Cement Paste, W/C = 0.3	59
4.3	Estimated Effective Moduli and Axial Strain Due to Submicrocracking Linear Material - Phase 2.	60

LIST OF FIGURES

<u>Figure No.</u>		<u>Page</u>
3.1	Stress-strain curves for cement paste and mortar, W/C = 0.5 (1 psi = 6.89 kPa).	61
3.2	Crack through calcium silicate hydrate in cement paste, μ marker = 3.6×10^{-4} in. (9.1 μ m).	62
3.3	Crack through calcium silicate hydrate and calcium hydroxide in cement paste, μ marker = 3.6×10^{-4} in. (9.1 μ m)	62
3.4	Sand grain adjacent to calcium silicate hydrate in mortar. Cracks at interface and within calcium silicate hydrate, μ marker = 3.6×10^{-3} in. (90.9 μ m)	63
3.5	Surface crack density versus compressive strain for cement paste, W/C = 0.5 (1 in./in. ² = 0.039 mm/mm ²).	64
3.6	Surface crack density versus compressive strain for mortar, W/C = 0.5 (1 in./in. ² = 0.039 mm/mm ²).	65
3.7	Mean crack width versus compressive strain for cement paste and mortar, W/C = 0.5 (1 in. = 25.4 mm).	66
3.8	Surface crack density versus compressive strain for cement paste W/C = 0.3 (1 in./in. ² = 0.039 mm/mm ²).	67
3.9	Cracks as seen with limited field of view.	68
3.10	Elliptic crack	68
3.11	Mean characteristic crack size, $\langle a \rangle$, versus compressive strain for cement paste, W/C = 0.5 (1 in. = 25.4 mm)	69
3.12	Coefficient of variation of crack size versus compressive strain for cement paste, W/C = 0.5 (1 in. = 25.4 mm)	70
3.13	Number of cracks per unit volume versus compressive strain for cement paste, W/C = 0.7, 0.5, and 0.3, and mortar, W/C = 0.5 (10^6 in. ⁻³ = 61 mm ⁻³).	71
3.14	Measure of volumetric crack density, $N_V \langle a^3 \rangle$, versus compressive strain for cement paste, W/C = 0.7, 0.5, 0.3, and mortar, W/C = 0.5	72
3.15	Secant modulus, E_s , and strain associated with submicrocracking and other inelastic deformation	73
3.16	Normalized calculated secant stiffness moduli versus compressive strain for cement paste, W/C = 0.7, 0.5, and 0.3, and mortar, W/C = 0.5	74

LIST OF FIGURES, Continued

<u>Figure No.</u>		<u>Page</u>
3.17	Stress-strain curves for cement paste, W/C = 0.5. Linear matrix (1 psi = 6.89 kPa).	75
3.18	Stress-Strain curves for mortar, W/C = 0.5. Linear matrix (1 psi = 6.89 kPa)	76
3.19	Comparison of calculated secant stiffness moduli of cement paste, W/C = 0.5, with and without pre-existing cracks. Linear matrix (1 psi = 6.89 kPa)	77
3.20	Stress-strain curves for cement paste, W/C = 0.5. Nonlinear matrix (1 psi = 6.89 kPa).	78
3.21	Stress-strain curves for mortar, W/C = 0.5. Nonlinear matrix (1 psi = 6.89 kPa).	79
3.22	Stress-strain curves for cement paste, W/C = 0.3. Calculated curves both with and without pre-existing cracks. Nonlinear matrix (1 psi = 6.89 kPa)	80
4.1	Stress-strain curves for cement paste, W/C = 0.3, strain rates = 0.3, 3.0, 30, 300, 3000, 30,000 and 300,000 microstrain per second	81
4.2	Stress-strain curves for mortar, W/C = 0.3, strain rates = 0.3, 3.0, 30, 300, 3000, 30,000 and 300,000 microstrain per second.	82
4.3	Compressive strength versus strain rate ($\dot{\epsilon}_{50-99}$) for cement paste, W/C = 0.3, 0.4, and 0.5.	83
4.4	Compressive strength versus strain rate ($\dot{\epsilon}_{50-99}$) for mortar, W/C = 0.3, 0.4, and 0.5.	84
4.5	Maximum stress ratios for cement paste and mortar versus strain rate ($\dot{\epsilon}_{50-99}$).	85
4.6	Strain at the peak of the stress-strain curve versus strain rate ($\dot{\epsilon}_{50-99}$) for cement paste, W/C = 0.3, 0.4, and 0.5.	86
4.7	Post-peak strain at a stress equal to 90 percent of the peak stress versus strain rate ($\dot{\epsilon}_{50-99}$) for cement paste, W/C = 0.3, 0.4, and 0.5	87
4.8	Post-peak strain at a stress equal to 90 percent of the peak stress versus water-cement ratio for cement paste and mortar at different strain rates ($\dot{\epsilon}_{50-99}$)	88
4.9	Ratio of initial modulus of elasticity to modulus at $\dot{\epsilon} = 3.0$ microstrain per second versus strain rate ($\dot{\epsilon}_{5-20}$).	89

LIST OF FIGURES, Continued

<u>Figure No.</u>		<u>Page</u>
4.10	Crack density measured with image analysis system versus compressive strain for cement paste, W/C = 0.3, for $\dot{\epsilon} = 3.0$ and 300,000 microstrain per second (1 in./in. ² = 0.039 mm/mm ²).	90
4.11	Stress-strain curves for cement paste, W/C = 0.3. Linear matrix, $\dot{\epsilon} = 3.0$ microstrain per second.	91
4.12	Stress-strain curve for cement paste, W/C = 0.3. Linear matrix, $\dot{\epsilon} = 300,000$ microstrain per second.	92

CHAPTER 1

INTRODUCTION

Concrete behaves as a nonlinear material when subjected to uniaxial compression. Work in the early 1960's showed that the stress-strain curve of concrete is associated closely with the formation of microcracks: cracks that form at coarse aggregate boundaries (bond microcracks) and propagate through the surrounding mortar (mortar microcracks)(12, 14, 21, 29, 33, 35). Microcracks have a surface density of 1 to 3.5 in./in.² (0.04 to 0.14 mm/mm²) and can be seen at magnifications below 50x (9, 21).

During the early microcracking studies, concrete was considered to be made up of two linear elastic brittle materials - cement paste and aggregate - and microcracks were considered to be the major cause of nonlinearity (21, 32).

This picture began to change in the 1970's. As shown in Fig. 3.1, cement paste is, in fact, a nonlinear softening material, as is the mortar constituent of concrete. The nonlinearity of concrete appears to be highly dependent on the response of these two materials (11, 26, 32, 38-40) and less dependent upon bond and mortar microcracks than originally thought.

The effects of load rate on the response of concrete have been under study for over 70 years (1). An increased rate of loading will increase both stiffness (27, 28) and strength. However, the sensitivity of strength to strain rate seems to vary with different studies. Some researchers have obtained little or no increase in strength for increases in loading rate of several orders of magnitude (15-17, 30). Others have obtained large increases in strength (1, 5, 6, 22-24, 27, 28, 31, 36-38, 41-43, 45), in some

cases over 80 percent. The differences appear to be due to differences in test specimens, such as curing conditions (23, 37, 43), concrete strength (1, 5, 23, 27, 38), age of concrete (23), type of aggregate (34), and moisture content (24). The largest variations appear to be due to differences in moisture content (24). Specimens that are dry show very little sensitivity to strain rate, while specimens that are fully saturated show the greatest increase in strength with rate of loading.

The studies presented in this report are aimed at improving the understanding of concrete by determining why its cement paste and mortar constituents are nonlinear, how these materials respond at different strain rates, and what structural changes occur as a function of water-cement ratio, sand content, and strain rate. Special emphasis is paid to very small microcracks that form in cement paste and mortar under load. The term "submicrocracks" is used to distinguish these cracks from the much larger bond and mortar microcracks observed in earlier studies.

The following chapters describe the experimental program and the experimental and analytical techniques developed to support that program, discuss the implications of the observations, and present the key conclusions.

This research has involved a wide number of technical and scientific areas. The details of the work are presented in a number of other documents. This report summarizes the most significant findings of the study. Appendix B includes a complete listing of the publications produced through this research effort.

CHAPTER 2

EXPERIMENTAL PROGRAM

The experimental program consisted of two major phases, 1) a study of cement paste and mortar subjected to monotonic uniaxial compressive loading at low strain rates and 2) a study of cement paste and mortar subjected to monotonic uniaxial compressive loading at strain rates ranging from 0.3 to 300,000 microstrain per second.

2.1 Materials

Cement: Type I portland cement was used. For phase 1, the cement consisted of 51.1 percent tricalcium silicate, 22.3 percent dicalcium silicate, 9.5 percent tetracalcium aluminoferrite, and 8.6 percent tricalcium aluminate. For phase 2, the cement consisted of 54.4 percent tricalcium silicate, 22 percent dicalcium silicate, 8 percent tetracalcium aluminoferrite, and 7 percent tricalcium aluminate.

Fine Aggregate: The fine aggregate was river sand consisting mainly of quartz, with 10-15 percent chert. Larger particles contain some limestone and dolomite. Fineness modulus = 2.9, bulk specific gravity (saturated surface dry) = 2.61, absorption = 0.79 percent. Source: Kansas River, Lawrence, Kansas. The sand was passed through a No. 4 sieve before use.

Mix Proportions: For phase 1, concrete mixes were designed in order to obtain proportions of the corresponding mortar constituent. Three water-cement ratios (W/C), 0.3, 0.5, and 0.7, were used for cement paste. A single mortar mix, with W/C = 0.5, was used and had a sand-cement ratio (S/C) of 2.27.

For phase 2, W/C's 0.3, 0.4, and 0.5 were used for cement paste and mortar. Concrete mixes were designed in order to obtain the sand-cement for one mortar for each water-cement ratio (mortar A). Sand-cement ratios of 0.97, 1.59, and 1.97 were used for W/C's of 0.3, 0.4, and 0.5, respectively. For W/C's 0.4 and 0.5, a second mortar (mortar B) was used to evaluate the effect of a modification in sand-cement ratio upon response (S/C = 1.97 and 1.29 for W/C = 0.4 and 0.5, respectively).

2.2 Test Specimens

Prismatic test specimens, 2 in. (51 mm) square by 8 in. (203 mm) long for phase 1 and 1 in. (25 mm) square by 5 in. (127 mm) long for phase 2, were prepared using steel molds. The specimens were cast in a vertical position. For phase 1 and phase 2, the molds were filled in three layers, each layer rodded 25 times. $\frac{3}{8}$ in. (9.5 mm) and $\frac{1}{4}$ in. (6.4 mm) diameter rods were used for the large and small specimens, respectively. For phase 2, specimens with W/C = 0.3 and 0.4 were placed in three layers and consolidated on a vibratory table. The molds were then sealed at the top.

During the first 24 hours, the molds were stored in the laboratory in a horizontal position to reduce the effects of bleeding. The specimens were then removed from the molds and stored in lime saturated water until the time of testing.

Prior to loading, the specimens were shortened by removing 1 in. portions from each end, using a high speed masonry saw. Specimens were tested 27 to 29 days after casting. Specimens were wrapped in plastic to ensure that they would remain saturated during the test.

2.3 Loading Procedure

For phase 1, specimens were loaded to pre-selected values of compressive strain and immediately unloaded using a closed-loop servo-hydraulic testing machine. The monotonically loaded specimens were loaded and unloaded at a strain rate of 6.7 microstrain per second. Cement paste specimens were loaded to strains of 0.0005, 0.001, 0.002, 0.004, and 0.006, while mortar specimens were loaded to strains of 0.0005, 0.001, 0.002, 0.003, and 0.004. Specimens were instrumented with a 5 in. gage length compressometer to measure axial strain and a 2 in. gage length extensometer to measure lateral strain.

For phase 2, specimens were loaded in compression at seven strain rates ranging from 0.3 microstrain per second to over 300,000 microstrain per second. Successive strain rates were separated by a factor of 10 (one order of magnitude). The slowest tests took 12 hours, while the fastest tests took about 0.03 sec. A typical compression test for concrete is made at a strain rate of about 15 microstrain per second and takes about 2 minutes. Longitudinal strain was monitored and controlled using two parallel linear variable differential transformers (LVDT's). Virtually constant strain rates were obtained, except at the highest strain rate. At a nominal strain rate of 300,000 microstrain per second, the initial response of the actuator was below the desired strain rate. The strain rate stabilized only at a stress corresponding to approximately 30 percent of the compressive strength of the material. Over the final range of strain a nearly constant strain rate, in excess of 300,000 microstrain per second, was obtained. In the data that follows, three strain rates are shown: The average strain rate

from zero stress to the peak stress, $\dot{\epsilon}_{0-100}$, the strain rate obtained between strains corresponding to 5 and 20 percent of the peak stress, $\dot{\epsilon}_{5-20}$, and the strain rate obtained from a strain corresponding to 50 percent of the compressive strength to a strain past the peak of the stress-strain curve, corresponding to a stress of 99 percent of the compressive strength $\dot{\epsilon}_{50-99}$.

2.4 Submicrocracking Studies

Specimen preparation: After the test specimens were loaded, they were submerged in lime saturated water for no longer than 24 hours. To prepare the specimens for viewing in the scanning electron microscope (SEM), 1/8 in. (3.2 mm) thick slices were removed along the longitudinal (or loading) direction with a high speed masonry saw, using a saturated solution of calcium hydroxide as the lubricant. The edges of the slice were removed, leaving the middle portion of each slice. The slice was rinsed with lime saturated water and placed in an oven at a temperature of 217°F (103° C). A constant weight was attained in 24 hours.

After drying, the specimens were stored in a vacuum desiccator. Prior to viewing in the SEM, the slices were fractured to produce two SEM specimens. The SEM specimens had edges which were either perpendicular or parallel to the direction of loading (i.e., transverse or longitudinal edges). The two specimens had dimensions of about 1/8 in. (3.2 mm) thick by 1/2 in. (12.7 mm) long by 1/4 in. (6.4 mm) high. Just prior to viewing in the SEM, the fractured specimens were coated with 200 angstroms of gold-palladium, a conducting material used to allow high quality images to be obtained for nonmetallic materials with an SEM.

Crack measurements: Within the SEM, each specimen was scanned in 10 (phase 1) or 5 (phase 2) pre-selected bands across the 1/8 in. (3.2 mm) specimen thickness. A Philips 501 Scanning Electron Microscope was used for phase 1, while a Philips 515 SEM, in conjunction with a LeMont Scientific OASYS Image Analysis System, was used for phase 2. Crack trace lengths, widths, angles, and microstructural features through which the cracks passed were recorded.

For phase 1, measurements were made at a magnification of 1250x, except crack widths below 10^{-4} in. (2.5 μm) were measured at 2500x. Only portions of cracks within the field of view were measured in order to obtain an accurate estimate of the density of cracks within the scanned areas. Crack lengths and widths were measured with a ruler on the SEM viewing monitor operating in the "TV" mode. Markers having units of micrometers were displayed on the viewing monitor and were used to convert the ruler measurements to true dimensions. Crack trace angles were measured by means of the rotation control on the SEM. For easy recording, crack trace lengths were recorded at intervals of 2×10^{-4} in. (5.1 μm) [= 0.25 in. (6.4 mm) with the ruler], and crack trace angles were recorded at intervals of 5° from 0-180° (i.e., $5^\circ = 2.5^\circ$ to 7.5° , etc.).

The process of obtaining the crack data was quite tedious and required about 2 hours per specimen. To maintain objectivity, crack surveys were made at the same time each day and limited to a single specimen. To further insure objectivity, specimens were selected and surveyed using a double blind coding system. A total of 150 individual SEM specimens were studied.

In phase 2, procedures were developed to carry out crack surveys using a new SEM in conjunction with an image analysis system. The new system has

greatly improved resolution (crack width = 0.05 μm versus 0.15 to 0.5 μm for phase 1) and allows greater accuracy in crack data acquisition. Measurements were made at a magnification of 3750x. Crack lengths and orientations were obtained directly from the system in an interactive mode, using a digitizing pad and stylus. The improved resolution and accuracy provide data with much less scatter than observed in phase 1. This allows crack surveys to be obtained with fewer scans across a specimen.

These developments occurred late in the project, but enough data was obtained with the new techniques to demonstrate their power and to support the accuracy of the extensive studies performed in phase 1. A more detailed discussion of image analysis of cracks is presented in Reference 13.

CHAPTER 3

EXPERIMENTAL RESULTS AND DISCUSSION - PHASE 1

Fig. 3.1 illustrates typical stress-strain curves for cement paste and mortar in compression. The nonlinearity of concrete is closely tied to the nonlinear response of these two materials. The principal goal of phase 1 was to determine the role of submicrocracks in this behavior.

3.1 Submicrocracks

Typical cracks are illustrated in Fig. 3.2-3.4. Fig. 3.2 shows a crack in cement paste through calcium silicate hydrate (CSH), one of the prime hydration products of portland cement. Fig. 3.3 illustrates a crack through both CSH and calcium hydroxide (the second major product of hydration). Fig. 3.4 shows cracking in mortar. In this figure, a crack runs adjacent to the sand grain-CSH interface. Additional cracks are apparent within the CSH.

Cracks range in length from about 4×10^{-4} in. ($10 \mu\text{m}$) to about 8×10^{-3} in. ($200 \mu\text{m}$). Interfacial cracks within mortar can attain even greater lengths, as illustrated in Fig. 3.4. Cracks appeared to range in width from 0.8×10^{-5} in. ($0.20 \mu\text{m}$) to 2.8×10^{-4} in. ($7.0 \mu\text{m}$) in cement paste and from 0.6×10^{-5} in. ($0.15 \mu\text{m}$) to over 12×10^{-4} in. ($30 \mu\text{m}$) in mortar. However, very few of the narrow cracks were observed.

The raw data can be summarized in terms of the crack density and the mean crack width on the transverse and longitudinal surfaces. The variations in surface crack density (expressed in in./in.^2) with applied strain are illustrated for cement paste and mortar with $W/C = 0.5$ in Fig. 3.5 and 3.6. Variations in mean crack width are presented in Fig. 3.7.

The crack densities in cement paste and mortar range from about 15 in./in. (0.59 mm/mm²) to about 50 in./in.² (1.97 mm/mm²), which is an order of magnitude greater than that obtained for bond and mortar microcracking in concrete (9, 21). Fig. 3.5 and 3.6 illustrate that crack density increases with strain. The best fit lines are shown for the data. Equations of the lines are given in the figures. The correlation coefficients, R, indicate that the relationships between crack density and applied strain are strongly linear. This linear trend was also obtained for cement paste with W/C = 0.7 (2). Contrary to the linear trend exhibited by the other materials, cement paste with W/C = 0.3 exhibits a crack density-strain relationship that is parabolic (Fig. 3.8).

In all cases, crack density begins to increase at very small applied strains, suggesting that even low strains result in some damage to cement paste and mortar. The specimens also exhibit greater crack densities on the transverse surface than the longitudinal surface. This is a function of the preferential orientation of the submicrocracks toward the longitudinal direction, as will be demonstrated later.

Fig. 3.7 illustrates that the mean crack width [typically 3.0 to 5.0 x 10⁻⁵ in. (0.76 to 1.27 μm)] increases with increasing compressive strain for cement paste and mortar. The magnitude of the increase appears to be nearly the same in the two materials. Except for nonloaded specimens, the average crack widths in mortar exceed those in cement paste.

Like the data produced in the earlier microcracking studies of concrete, the relationships illustrated in Figs. 3.5, 3.6, and 3.8 are largely of qualitative, not quantitative, interest. The data, in fact, represent only the traces of three-dimensional cracks on selected planes. Thus, this

data does not directly provide information about cracking as it occurs throughout the volume of a specimen. The dimensions and orientations of three-dimensional cracks are needed if a full understanding of material response to cracking is to be obtained. Therefore, the surface crack data must be further analyzed to obtain estimates of the three-dimensional crack distributions. The three-dimensional distributions are used to estimate the effects of cracks on the stress-strain behavior of the materials (Sections 3.4 and 4.7).

3.2 Conversion of Surface to Three-Dimensional Crack Distributions

Surface Distributions: The accurate estimation of three-dimensional crack distributions requires a number of steps. First, the experimental surface crack distributions must be modified to obtain "true" surface distributions. This is necessary because only crack traces that lie within the field of view are measured (Fig. 3.9). Segments of some cracks project outside the viewing area, and their measured lengths are shorter than their true lengths. This causes the length distribution to be skewed towards low values. A crack whose center is located outside the viewing area may have a portion within the field of view (Fig. 3.9). A crack centered at the same point, but at a lower angle, θ , may lie completely outside the viewing area. The observed number of cracks at low angles will, therefore, be relatively less than the number at high angles, resulting in the angle distribution being skewed towards $\theta = 90^\circ$. Thus, the observed distributions may not be good estimates of the true surface distributions. True trace length and angle distributions are obtained from the observed surface distributions using statistical procedures described in References 2 and 3.

Three-dimensional crack distributions: True surface crack distributions are converted to three-dimensional distributions using stereological procedures described in Reference 2. These procedures include steps that filter out cracks induced by specimen preparation (2). The filtering removes the non-isotropic components of crack distributions caused by specimen preparation, but retains isotropic components which cannot be separated from isotropic components that may occur during hydration. For the purposes of this analysis, if a crack trace is nonlinear, it is treated as an equivalent linear trace which spans end to end of the nonlinear crack trace.

To derive the relationships between the surface and three-dimensional crack distributions, each crack is assumed to be elliptic with a semi-major axis length, a , aspect ratio, r ($= b/a$, b = semi-minor axis length), and angular coordinates ψ , ϕ , and η (Fig. 3.10). Comparisons of experimental crack trace distributions with distributions generated using elliptic cracks (2) show little loss in accuracy due to this simplifying assumption. The length of the semi-major axis, a , is the "characteristic crack size".

The parameters which describe the three-dimensional crack distributions are the orientation distribution, $f(\psi)$, the size distribution, $f(a|\psi)$, at each orientation, ψ , the mean and variance of $f(a|\psi)$, $\langle a_\psi \rangle$ and $\text{var}(a_\psi)$, the crack aspect ratio, r , the rotation of the crack about its normal, defined by the angle η , and the number of cracks per unit volume, N_V .

For the crack distributions obtained in this study, the crack orientation distribution, $f(\psi)$, can be represented satisfactorily by a Marriott distribution (44). This distribution describes the orientation of a

transversely isotropic system of cracks with a mild degree of anisotropy.

The Marriott distribution is expressed as:

$$f(\psi) = \frac{1}{1 - K/3} (1 + K \cos 2\psi) \sin \psi \quad (3.1)$$

$$-1 \leq K \leq 1$$

The longitudinal direction (direction of applied stress) corresponds to $\psi = 90^\circ$. K is a measure of the degree of anisotropy. A negative value of K indicates a system in which more cracks are oriented in the longitudinal direction than in the transverse direction, while a positive value of K indicates a system in which more cracks are oriented in the transverse direction than in the longitudinal direction. $K = 0$ represents an isotropic crack distribution. K can range from $+\infty$ (all cracks with $\psi = 0$) to $-\infty$ (all cracks with $\psi = 90^\circ$), although the range is much narrower for cement paste and mortar. Even small values of K , such as obtained in this study, have a major effect on material properties (2, 4). K is obtained from the surface crack densities on the transverse and longitudinal surfaces (44).

The crack size distributions, $f(a|\psi)$, are conveniently represented by a gamma distribution (2).

$$f(a|\psi) = \frac{1}{\beta^\alpha \Gamma(\alpha)} a^{\alpha-1} e^{-a/\beta} \quad (3.2)$$

in which α and β are functions of the mean and variance of $f(a|\psi)$, $\langle a_\psi \rangle$ and $\text{var}(a_\psi)$.

$$\alpha = \frac{\langle a_\psi \rangle^2}{\text{var}(a_\psi)}; \quad \beta = \frac{\text{var}(a_\psi)}{\langle a_\psi \rangle} \quad (3.3)$$

$\Gamma(\alpha)$ is the gamma function and is defined as

$$\Gamma(\alpha) = \int_0^{\infty} y^{\alpha-1} e^{-y} dy \quad (3.4)$$

Gaussian quadrature with four integration points over the range of y from 0 to 50 is sufficient for the integration in Eq. (3.4).

Of the parameters which describe the three-dimensional crack distributions, the analyses (2) show that the crack aspect ratio, r , is affected only slightly by the load regime and applied strain. r varies within a narrow range from 1.0 to 0.85. For many values of strain, $r = 1$. The analyses also show that the optimum solutions for three-dimensional crack distributions are obtained when the rotation of the crack about its normal, η , is equal to 0. As a result, the three-dimensional distributions are best described by the skewness or degree of anisotropy of the crack orientation, represented by K of the Marriott distribution, the variation of the mean characteristic crack size, $\langle a_{\psi} \rangle$, with orientation ψ , and the number of cracks per unit volume, N_V . An additional crack parameter, $N_V \langle a^3 \rangle$, the product of the number of cracks per unit volume, N_V , and the mean of the cubed crack size $\langle a^3 \rangle$, is a measure of the volume density of the cracks. $N_V \langle a^3 \rangle$ is useful since it plays an important role in controlling material behavior (2, 4, 8). Average values of these parameters are summarized in Table 3.1 for the cement paste and mortar specimens tested in this study.

3.3 Three-Dimensional Crack Parameters

The results presented in this section are obtained from the average surface crack data for all specimens loaded to a given strain--typically three specimens for cement paste with $W/C = 0.3$ and 0.5 , and two specimens for cement paste with $W/C = 0.7$, and mortar with $W/C = 0.5$. The crack

parameters obtained for the individual specimens varied less than 2 percent from those obtained from the mean values (2).

Mean Characteristic Crack Size: Typical relationships between the mean characteristic crack size, $\langle a_\psi \rangle$, and strain, and between the coefficient of variation of crack size, $[\text{var}(a_\psi)]^{1/2}/\langle a_\psi \rangle$, and strain are illustrated in Fig. 3.11 and 3.12 for cement paste with a W/C = 0.5. Crack orientations of 0°, 45°, and 90° are used in these figures. The lines shown are best fit lines through the data. Fig. 3.11 and Table 3.1 show that crack size, $\langle a_\psi \rangle$, increases with increasing strain and with increasing orientation angle, ψ . The increase in $\langle a_\psi \rangle$ with increasing angle indicates that cracks are larger the closer their orientation is to the direction of the applied compressive stress. The coefficients of variation are approximately constant (Fig. 3.12), indicating that crack sizes have about the same spread relative to their means for all applied strains and crack orientations.

Degree of Anisotropy: For nonloaded cement paste and mortar with W/C = 0.5, the degree of anisotropy, K , is 0.00, while for nonloaded cement pastes with W/C = 0.7 and 0.3, K is -0.02 (Table 3.1). As pointed out earlier, $K = 0$ indicates an isotropic orientation distribution. $K = -0.02$ gives an orientation distribution, $f(\psi)$, that differs from an isotropic distribution by less than 1 percent. Thus, the orientation distributions are virtually isotropic in all of the nonloaded materials.

For the loaded specimens, K becomes increasingly negative with increasing compressive strain (Table 3.1), indicating that the crack distributions become skewed towards the direction of applied stress as the strain increases. For cement paste with W/C = 0.5, values of K range from 0.00 for nonloaded specimens to -0.30 for specimens at a strain of 0.006, while for paste with W/C = 0.7 and 0.3, they range from -0.02 for nonloaded specimens

to -0.29 and -0.31, respectively, for specimens at a strain of 0.006. For mortar with W/C = 0.5, values of K range from 0.00 for nonloaded specimens to -0.24 for specimens at a strain of 0.004.

Aspect Ratio: At low strains, the crack aspect ratio, r , is 1.0; i.e., the cracks may be approximated as circular (Table 3.1). At high compressive strains, the cracks become slightly elongated (i.e., $r < 1.0$). At a strain of 0.006, the values of r are 0.90, 0.87, and 0.85 for cement pastes with W/C = 0.7, 0.5, and 0.3, respectively. At an applied strain of 0.004 in mortar with W/C = 0.5, the value of r is 0.90. These results imply that each crack has a slightly preferred direction of propagation (or characteristic direction) in its plane. Since $\eta = 0^\circ$ for all load cases (2), that direction is such that the crack normal and the major axis of the crack lie in a plane that is parallel to the direction of loading.

Number of Cracks per Unit Volume: The number of cracks per unit volume, N_V , decreases with increasing applied strain (Table 3.1, Fig. 3.13). For example, for cement paste with W/C = 0.5, N_V decreases from 2.3×10^6 in.⁻³ (140 mm^{-3}) in nonloaded specimens to 0.7×10^6 in.⁻³ (43 mm^{-3}) in specimens loaded to a strain of 0.006. Similar variations occur for paste with W/C = 0.3 and 0.7. At any given strain, the lower water-cement ratio pastes exhibit a greater number of cracks per unit volume. For mortar with W/C = 0.5, N_V decreases from 1.5×10^6 in.⁻³ (92 mm^{-3}) in nonloaded specimens to 0.6×10^6 in.⁻³ (37 mm^{-3}) in specimens loaded to a strain of 0.004. While the number of cracks per unit volume decreases with increasing strain (Fig. 3.13), the mean crack size increases (Fig. 3.11). The two results suggest that as compressive strain increases, small cracks join to form larger cracks.

Volumetric Crack Density: The variation of the "volume density" of cracks, $N_V \langle a^3 \rangle$, with applied strain is shown in Fig. 3.14 for cement pastes with W/C = 0.7, 0.5, and 0.3. $N_V \langle a^3 \rangle$ increases with increasing strain, suggesting that cement paste is damaged progressively during loading. The best fit lines in Fig. 3.14 show that the average increase in $N_V \langle a^3 \rangle$ with strain is virtually the same for all three cement pastes. This observation suggests that the volume density of submicrocracks is more a function of compressive strain, than of water-cement ratio. The close agreement in volumetric crack densities also suggests that the degree of softening caused by submicrocracking should be approximately the same for the three cement pastes. The validity of this conclusion, however, depends on other non-linear behavior that may occur (Section 3.4).

A study of the individual data points in Fig. 3.14 shows that below a strain of 0.004, $N_V \langle a^3 \rangle$ increases more rapidly the higher the water-cement ratio. Above 0.004, the trend is reversed, and $N_V \langle a^3 \rangle$ increases most rapidly for cement paste with W/C = 0.3.

Fig. 3.14 also compares $N_V \langle a^3 \rangle$ to compressive strain for mortar with W/C = 0.5. The value of $N_V \langle a^3 \rangle$ for nonloaded mortar is lower than that for nonloaded cement paste. This reflects the lower percentage of paste in mortar and the restraint of shrinkage exerted by the sand grains. With increasing strain, $N_V \langle a^3 \rangle$ increases more rapidly in mortar than in cement paste. Thus under load, sand particles appear to act as stress raisers, resulting in a larger volumetric crack density at strains above 0.001, a greater degree of softening, and a lower strain capacity compared to cement paste.

3.4 Strain Due to Submicrocracking

The portion of material nonlinearity due to the submicrocracking is estimated through the use of a self-consistent material model (4). The model was designed specifically to account for anisotropic crack distributions of the type obtained in cement paste and mortar under uniaxial compression.

Self-Consistent Material Model: In the self-consistent method, the strain energy of a cracked solid, ϕ_c , is represented as the sum of the strain energy of the uncracked solid, ϕ , and the change in strain energy due to the presence of cracks, $\Delta\phi$.

$$\phi_c = \phi + \Delta\phi \quad (3.5)$$

The "self-consistent" approximation is obtained by assuming that each crack contributes to $\Delta\phi$ as if it were an isolated crack in an infinite matrix having the elastic moduli of the fully cracked solid (7, 8, 18-20).

The self-consistent model used here represents a transversely isotropic cracked solid (4). Transverse isotropy (isotropic behavior within transverse planes but orthotropic behavior in longitudinal planes) is the type of anisotropy expected in an initially isotropic, uniaxially loaded material. In the model, crack closure effects are neglected. Cracks are assumed to be elliptic (Fig. 3.10) with known size and orientation distributions (obtained from the crack analysis), and crack centroids are assumed to be randomly distributed throughout the material. The material between cracks (matrix material) is assumed to be locally isotropic and homogeneous, making the model somewhat less applicable to mortar than to cement paste.

Although isotropic and homogeneous, the matrix material may be either linear or nonlinear.

Using the global coordinate system in Fig. 3.10 as a reference, a transversely isotropic material has six material moduli, five of which are independent. The five independent moduli are the stiffness modulus in the plane of perpendicular to the direction of loading (plane of isotropy), E_1 , the stiffness modulus in the direction of loading (longitudinal direction), E_3 , Poisson's ratio in the plane of isotropy, ν_{12} , Poisson's ratio in any longitudinal plane, ν_{31} , and the shear modulus in a longitudinal plane, G_{31} . The sixth modulus, G_{12} , is the shear modulus in the plane of isotropy. G_{12} is dependent upon E_1 and ν_{12} through the relation

$$G_{12} = \frac{E_1}{2(1 + \nu_{12})} \quad (3.6)$$

The five independent elastic constants for a given crack distribution require the solution of five simultaneous nonlinear equations (4). These equations are solved iteratively to obtain the elastic moduli, which depend only on the crack distribution and the elastic moduli of the matrix material, E_m , Young's modulus, and ν_m , Poisson's ratio.

As the crack distributions change with increasing strain, the elastic moduli decrease. Since the representation is elastic, nonlinear material behavior is represented by decreasing secant moduli, as illustrated in Fig. 3.15.

Application of the Model: To determine the effects of submicrocracking on material behavior, the effective moduli of interest are E_3 and ν_{31} , the modulus of elasticity and Poisson's ratio, respectively, that are normally measured in a uniaxial compression test. The specific procedures used to

calculate E_3 and $\nu_{3,1}$ depend upon whether or not cracks exist prior to loading.

Pre-existing cracks: In this case, the crack distribution obtained for a nonloaded specimen is assumed to exist prior to loading. The moduli of the matrix material, E_m and ν_m , are obtained by selecting values which, when combined with this distribution, produce the measured values of the initial moduli, E_1 and ν_1 . The effective moduli, E_3 and $\nu_{3,1}$, are then calculated using E_m and ν_m and the full three-dimensional crack distribution at each stage of loading.

For application in the self-consistent model, the average experimental values are used for the initial moduli, E_1 and ν_1 (2): $E_1 = 1.78 \times 10^6$ psi (1.23×10^4 MPa), 2.54×10^6 psi (1.75×10^4 MPa), and 3.31×10^6 psi (2.28×10^4 MPa) for cement pastes with W/C = 0.7, 0.5, and 0.3, respectively, and 4.79×10^6 psi (3.30×10^4 MPa) for mortar with a W/C = 0.5. $\nu_1 = 0.24$ for the three cement pastes, and 0.20 for mortar.

No pre-existing cracks: If no cracks exist prior to loading, the cracks in nonloaded specimens represent cracks caused by specimen preparation, and the cracks in loaded specimens consist of both load-induced and preparation cracks. Since the calculation of the effective moduli of loaded material should only account for the load-induced cracks, distributions representing load-induced cracks are obtained by subtracting the three-dimensional crack distribution (size, orientation, and density) obtained for the nonloaded specimen from the distribution obtained for the loaded specimen. The altered distribution is used to calculate E_3 and $\nu_{3,1}$. In this case, E_m and ν_m equal the initial experimental moduli.

Linear Elastic Material Matrix: For a given crack distribution, the strain associated with the cracked elastic material, ϵ_{ec} , depends on the effective stiffness modulus, E_s , and the applied stress, σ (Fig. 3.15).

$$\epsilon_{ec} = \frac{\sigma}{E_s} \quad (3.7)$$

ϵ_{ec} includes a component due to elastic deformation, ϵ_e , and a component due to submicrocracking, ϵ_c . The strain due to submicrocracking is

$$\epsilon_c = \epsilon_{ec} - \epsilon_e = \frac{\sigma}{E_s} - \frac{\sigma}{E_1} = \sigma \left(\frac{E_1 - E_s}{E_1 E_s} \right) \quad (3.8)$$

The total inelastic strain, $\epsilon - \epsilon_e$, is the difference between the applied strain, ϵ , and the elastic strain, ϵ_e .

Pre-existing cracks: The values of the moduli, E_s and ν_{s1} , and the axial strains, ϵ , ϵ_{ec} , and ϵ_c are presented in Table 3.2 for cement pastes with W/C = 0.7, 0.5, and 0.3 and mortar with W/C = 0.5. As the applied strain increases, the calculated stiffness modulus, E_s , decreases. For example, for cement paste with W/C = 0.5, E_s decreases from 2.54×10^6 psi at $\epsilon = 0$ to 2.156×10^6 psi at $\epsilon = 0.006$. For mortar with W/C = 0.5, E_s decreases from 4.79×10^6 psi at $\epsilon = 0$ to 4.06×10^6 psi at $\epsilon = 0.004$.

The effect of the cracks on E_s for the different materials is shown in Fig. 3.16 which compares the normalized stiffness modulus, E_s/E_1 , with the applied strain, ϵ . For the three cement pastes, the variation of E_s/E_1 with ϵ is virtually independent of water-cement ratio. This result is expected because the crack distributions obtained in the three cement pastes are

nearly identical (Table 3.1). At the maximum strain of 0.006, the calculated reduction in stiffness due to submicrocracking for the three cement pastes is about 15 percent.

Fig. 3.16 also shows that the reduction in E_s/E_1 is greater for mortar than for cement paste. At the maximum strain of 0.004 in mortar, the calculated reduction in stiffness is 15 percent, versus 11 percent for cement paste at the same strain. This difference is consistent with the higher rate of increase in crack density in mortar described earlier.

The stress-strain curves due to submicrocracking ($\sigma-\epsilon_{ec}$) are compared with the experimental stress-strain curves ($\sigma-\epsilon$) and linear elastic stress-strain relationships ($\sigma-\epsilon_e$) in Fig. 3.17 and 3.18 for cement paste and mortar with W/C = 0.5. The curves illustrate that the submicrocracks account for a portion, but not all, of the nonlinear response of the materials.

The total strain, ϵ , consists of elastic and inelastic components. The inelastic component, $\epsilon - \epsilon_e$, consists of a portion due to submicrocracking, ϵ_c , and a portion due to other causes, $\epsilon - \epsilon_e - \epsilon_c$.

For cement paste with W/C = 0.5, the strain due to submicrocracking, ϵ_c , increases from 0.000005 at $\epsilon = 0.0005$ to 0.000469 at $\epsilon = 0.006$ (Table 3.2). ϵ_c accounts for 18 percent of the inelastic strain at a total strain $\epsilon = 0.0005$, and 14 percent at $\epsilon = 0.006$. Similar values are obtained for paste with W/C = 0.7. For cement paste with W/C = 0.3, ϵ_c accounts for as high as 37 percent of the inelastic strain at $\epsilon = 0.0004$. This value drops to 24 percent at $\epsilon = 0.006$.

For mortar, ϵ_c represents nearly 18 percent of the inelastic strain at $\epsilon = 0.0005$. This drops to 9 percent at $\epsilon = 0.003$ and 5 percent at $\epsilon = 0.004$. After the peak stress, the applied strain increases but ϵ_{ec} and ϵ_c decrease (Fig. 3.18), indicating that the material is unloading. This

response is due in large part to the use of a linear representation for the matrix material.

The fact that ϵ_c accounts for only a portion of the inelastic strain in cement paste and mortar suggests that the matrix material is not linear and elastic at all values of strain. Rather, the matrix appears to become inelastic with increasing applied strain.

$\nu_{,1}$ is compared with the experimental Poisson's ratio, ν , in Table 3.1. ν increases from 0.24 at $\epsilon = 0$ to 0.27 at $\epsilon = 0.006$ for the three cement pastes, while $\nu_{,1}$ increases to only about 0.25 at the same strain. For mortar with W/C = 0.50, ν increases from 0.20 at $\epsilon = 0$ to 0.48 at $\epsilon = 0.004$. This compares to $\nu_{,1} = 0.218$ at $\epsilon = 0.004$. Thus, submicrocracking appears to account for only a portion of the lateral strain in cement paste and a very small portion in mortar.

No pre-existing cracks: As illustrated in Fig. 3.19, when using a linear elastic matrix material to model the effects of cracks, the question of pre-existing cracks is unimportant. The values of material moduli, E , and $\nu_{,1}$, are virtually identical whether or not the crack distributions obtained for nonloaded specimens are assumed to exist prior to loading. The reason for this similarity is due to the fact that an analysis based on no pre-existing cracks starts with a lower calculated stiffness for the matrix material, E_m , than used if cracks are assumed to pre-exist. The close match in moduli indicates that in the analysis with no pre-existing cracks, the smaller number of cracks used at each strain level and the lower value of E_m compensate for each other.

Other Inelastic Deformation: The inelastic deformations in cement paste and mortar include sizeable strains that cannot be accounted for by the recorded submicrocracking (Fig. 3.17 and 3.18). This leads to the

conclusion that the assumption of a linear matrix may be incorrect. In addition to the recorded submicrocracking, there are a number of sources of inelastic deformation.

Not all of the surface submicrocracks were seen. Since the microstructure of cement paste consists of different features (e.g., calcium silicate hydrate and calcium hydroxide), some cracks may be obscured by the boundaries between these features. This may be even more so in mortar, which contains sand. Even more important is the limitation on resolution of the SEM, since cracks were measured using the SEM monitor operating in the "TV" mode. The results obtained in Phase 2 support this point (see Section 4.6). Additions to the recorded cracks will result in a larger portion of the inelastic strain being attributed to submicrocracking.

Large microcracks and macrocracks, which are visible on the surface of some specimens at high stresses, are not included. These cracks will make an important contribution at high strains.

A portion of the inelastic strain in cement paste subjected to monotonic loading is due to flow or creep of the material (38). Thus, the mechanisms of creep account for a portion of the inelastic deformation that is not due to submicrocracking.

These observations should not come as a surprise. In fact, the properties of the matrix material should be expected to change under load. The resulting inelasticity of the matrix and the effects of larger cracks and those missed in the crack surveys need to be accounted for in order to fully assess the role of submicrocracks in the nonlinear behavior of cement paste and mortar.

Nonlinear Matrix Material: To obtain an improved estimate of the role of submicrocracks in the stress-strain response of cement paste and mortar, the analysis procedures can be altered to allow the moduli of the matrix material, E_m and ν_m , to change. For simplicity, all of the nonlinear response that is not accounted for by submicrocracking is assigned to the matrix and is reflected in changes in E_m and ν_m . This simplifying assumption lumps large microcracks and macrocracks in with flow or creep. The implications of this assumption are discussed below. The matrix material is assumed to remain isotropic.

To calculate E_m and ν_m for a given distribution of submicrocracks, the effective stiffness modulus of the cracked material, E_s , is set equal to the measured secant modulus = σ/ϵ . The effective Poisson's ratio, ν_{s1} , is set equal to the measured Poisson's ratio, ν . Values of E_m and ν_m are selected which, when combined with the three-dimensional crack distribution, produce the measured values of E_s and ν_{s1} .

If the full crack distribution is used, this computation process is similar to that used with the "pre-existing crack" assumption. If the difference between crack distributions in the loaded and nonloaded specimens is used, a procedure similar to that used with the "no pre-existing crack" assumption is obtained.

At any value of total strain, ϵ , the strain associated with the matrix material, $\epsilon_m = \sigma/E_m$, includes elastic and inelastic components. The component of the strain due to submicrocracking, ϵ_c , is the difference between the applied strain, ϵ , and ϵ_m .

$$\epsilon_c = \epsilon - \epsilon_m \quad (3.9)$$

As before, the total inelastic strain, $\epsilon - \epsilon_e$, is the difference between ϵ and the elastic strain, $\epsilon_e = \sigma/E_1$. To obtain the equivalent of ϵ_{ec} used previously (Eq. 3.7), ϵ_c must be combined with ϵ_e .

$$\epsilon_{ec} = \epsilon_e + \epsilon_c \quad (3.10)$$

Pre-existing cracks: The calculated matrix material moduli and the strain due to submicrocracking are presented in Table 3.3. $\sigma - \epsilon_{ec}$ curves are compared with experimental $\sigma - \epsilon$ curves and linear $\sigma - \epsilon_e$ relationships for cement paste and mortar with W/C = 0.5 in Fig. 3.20 and 3.21.

Softening within the matrix accounts for a significant portion of the nonlinearity at all values of applied strain. Changes in E_m are substantial, as illustrated by cement paste with W/C = 0.5 for which E_m decreases from 2.54×10^6 psi at $\epsilon = 0$ to 1.375×10^6 psi at $\epsilon = 0.006$.

Allowing the matrix to soften increases the degree of nonlinearity attributed to submicrocracking in all cases (Table 3.3). As with the elastic matrix, ϵ_c plays a larger role the lower the water-cement ratio and accounts for the greatest percentage of the inelastic strain at low applied strains. ϵ_c accounts for as much as 85 percent of the inelastic strain for 0.3 W/C paste at a strain of 0.0005 (56 percent and 65 percent for W/C = 0.7 and 0.5, respectively). The strain due to submicrocracking, as a portion of inelastic strain, $\epsilon_c/(\epsilon - \epsilon_e)$, decreases with increasing applied strain, dropping to values of 30 percent, 34 percent, and 45 percent at a strain of 0.006 for pastes with W/C = 0.7, 0.5, and 0.3, respectively. This indicates that while the contribution of submicrocracking to the nonlinear response of cement paste is significant at all levels of applied strain, the relative importance of other mechanisms, large microcracks, macrocracks, and creep,

increases with increasing strain. The relative importance of submicrocracking increases with a decrease in water-cement ratio; the majority of the nonlinear strain in 0.3 W/C paste is due to submicrocracking at all strains except 0.006, at which point macrocracks presumably play a major role.

For mortar, $\epsilon_c/(\epsilon - \epsilon_e)$ decreases with increasing applied strain from 45 percent at a strain of 0.0005 to 17 percent at a strain of 0.003, the strain at the peak stress (Table 3.3, Fig. 3.21). At a strain of 0.004, which corresponds to the descending branch of the stress-strain curve, $\epsilon_c/(\epsilon - \epsilon_e)$ increases to 22 percent, implying that the portion of the inelastic strain due to submicrocracking is larger on the descending branch of the stress-strain curve than at the peak of the stress-strain curve. If the post-peak softening of the material is due primarily to macrocracks, however, categorizing all nonlinear response other than submicrocracking as softening of the matrix material will overestimate the strain due to submicrocracking. The smaller values of $\epsilon_c/(\epsilon - \epsilon_e)$ for mortar as compared to those for cement paste may indicate that large microcracks and macrocracks play a more dominant role in mortar.

As with the elastic matrix, in this case submicrocracking explains very little of the change in Poisson's ratio. Most of the change in ν must be accounted for by changes in ν_m (Table 3.3). Thus, aspects other than submicrocracking appear to control the Poisson effect in these materials.

No pre-existing cracks: The moduli of the matrix material and strains due to submicrocracking based on the assumption that no cracks exist prior to loading are presented in Table 3.4. For this approach, $\epsilon_c/(\epsilon - \epsilon_e)$ is lower than obtained using the full crack distributions, 10 percent to 80 percent compared with 20 percent to 90 percent. This difference in results

contrasts with the virtually identical results obtained with the linear matrix (Fig. 3.19).

The effect of the pre-existing crack assumption here is due to the fact that with an inelastic matrix, the crack density is used to back-calculate the matrix moduli at each strain. As a result, the matrix stiffness and the strain due to submicrocracking, ϵ_0 , (Eq. 3.9) depend on whether or not cracks are assumed to exist prior to loading.

The differences in ϵ_0 obtained with these two approaches increase as the applied strain increases. For example, for cement paste with W/C = 0.3 (Fig. 3.22), at a strain of 0.0005, ϵ_0 with pre-existing cracks is 1.06 times the value without pre-existing cracks, while at a strain of 0.006, the ratio is 1.27. Considering the extreme assumptions used for the two approaches, these differences are not large, as seen in Fig. 3.22.

A completely accurate solution depends on the actual amount of cracking that exists prior to loading, a question not answered in the current study. It is likely that some cracks do exist prior to loading. However, it is also likely that a large number of preparation cracks remain in the crack distributions (2). Therefore, the true effect of load-induced submicrocracking should lie somewhere between the results obtained with the two approaches.

CHAPTER 4

EXPERIMENTAL RESULTS AND DISCUSSION - PHASE 2

In phase 2, a total of 207 specimens were tested. Major emphasis was placed on strain rates of 3, 3000 and 300,000 microstrain per second. With one exception, at least two specimens of each material and strain rate were tested. Table 4.1 summarizes the test program and the key results, including material, number of specimens, and average strain rates, strength, strain at peak stress, post-peak strains at 90 percent of the maximum stress, and initial moduli of elasticity.

4.1 Stress-Strain Curves

Fig. 4.1 and 4.2 illustrate the stress-strain response of specimens from single batches of cement paste and mortar with W/C = 0.3 at each of the 7 strain rates. These curves are typical of the stress strain response of cement paste and mortar at all three W/C's. The curves show that both materials increase in strength with increasing strain rate. They also show that the strain at the peak stress and the overall ductility of the materials also depend on strain rate; however, these relations are not monotonic. The strain at the peak stress is generally greatest for the slowest rate of loading (0.3 microstrain per second). As the strain rate increases, the strain at the peak stress decreases at first and then increases with increasing strain rate. The curves also show an increase in the initial modulus of elasticity with increasing strain rate. The effect of strain rate on specific aspects of the stress-strain response are discussed in the sections that follow.

4.2 Strength

The effect of strain rate on compressive strength is illustrated Fig. 4.3 and 4.4 for cement paste and mortar, respectively. For these comparisons, $\dot{\epsilon}_{50-99}$ is used to represent strain rate since the strain rate at high stresses has more of an impact on strength than the strain rate at low stresses. $\dot{\epsilon}_{50-99}$, $\dot{\epsilon}_{0-100}$, and $\dot{\epsilon}_{5-20}$ differ appreciably only for the two highest and, in some cases, three highest strain rates (Table 4.1).

Fig. 4.3 and 4.4 show that strength depends upon both water-cement ratio and strain rate. The diverging lines with increasing strain rate indicate that strength of the high strength materials is enhanced more by increasing strain rate than is the strength of lower strength materials. For the mortars, sand content does not appear to play a significant role in the response of strength to strain rate. Additional information can be obtained by normalizing the results illustrated in Fig. 4.3 and 4.4 with respect to the strength at a single strain rate. This is done in Fig. 4.5, in which the compressive strengths of the cement pastes and the "A" mortars are normalized to the strength measured at a strain rate of 3 microstrain per second to obtain "maximum stress ratios". The individual data points shown in Fig. 4.5 represent the average of all test specimens of a particular material at each strain rate. The figure indicates that the compressive strength of fully saturated cement paste and mortar increases approximately 15 percent for each order of magnitude increase in strain rate. The percentage increase in strain does not appear to be a function of the material (paste or mortar) or the water-cement ratio.

The fact that the effects of strain rate on strength are virtually the same for the materials tested indicates that the mechanisms that control the behavior of the materials are similar.

4.3 Strain at Peak Stress

Fig. 4.6 illustrates the average value of strain at peak stress, ϵ_p , versus strain rate ($\dot{\epsilon}_{50-99}$) for cement pastes with W/C = 0.3, 0.4, and 0.5. Fig. 4.7 illustrates the post-peak strain at a stress equal to 90 percent of the peak stress, ϵ_{pp90} , versus strain rate for the three cement pastes. ϵ_{pp90} provides a measure of material ductility. The nonmonotonic nature of the change in ϵ_p and ϵ_{pp90} with respect to strain rate is clearly shown. The strain at the peak stress first decreases and then increases with increasing strain rate. Tests at the lowest strain rate took 15 hours. Thus, the high strain corresponding to the peak stress for these tests is largely dependent on the effects of creep. As the strain rate increases, the effects of creep decrease, and thus, the strain at the peak stress decreases. At high strain rates, the increasing values of ϵ_p and ϵ_{pp90} are likely the result of limitations in crack velocity.

The effect of water-cement ratio on the ductility of cement paste and mortar is illustrated in Fig. 4.8, which compares average values of ϵ_{pp90} with W/C for each strain rate. With the exception of cement paste loaded at 0.3 and 3.0 microstrain per second, a decrease in water-cement ratio produced a higher strain capacity for both materials. Fig. 4.6 and 4.7 also illustrate this trend.

4.4 Initial Modulus of Elasticity

For the purposes of analysis, the initial modulus of elasticity is obtained using a least squares fit of the stress-strain data for stresses between 5 and 20 percent of the peak stress. This range was selected to remove the effects of seating errors as the specimens were initially loaded, use a strain range that was wide enough to limit the effects of scatter in the data, and limit the maximum value of stress to a value at which the

response remains essentially linear. For each material and strain rate, average values of initial moduli, E_1 , are tabulated in Table 4.1.

Fig. 4.9 illustrates the initial moduli, normalized to the initial modulus for the individual materials at a strain rate of 3 microstrain per second, versus strain rate (in this case, $\dot{\epsilon}_{5-20}$). These normalized results lie within a very narrow band, indicating similar effects of strain rate on the initial moduli of cement paste and mortar. Like the strain-rate response of strength, the strain-rate response of E_1 appears to be independent of both water-cement ratio and sand-cement ratio. The overall relationship is approximately linear. For each order of magnitude increase in strain-rate, the initial modulus of elasticity of these materials increases about 9 percent. This change in E_1 indicates that strain rate plays an important role in material response at very low as well as high stresses. In addition, a change in E_1 at strains at which little load induced cracking is expected (Table 3.1) strongly implicates the importance of moisture movement in materials response. It also indicates that, for saturated cement paste and mortar, the concept of a material modulus which is independent of strain rate is incorrect. That is, even the so-called elastic properties of these materials are firmly tied to the rate of loading. Thus, the response of these materials appears to be highly complex, since the material moduli, as well as the strength, depend upon strain rate. This picture contrasts with the strain rate response of mild steel (10). Steel exhibits an increase in strength, but no change in modulus of elasticity with increasing strain rate.

4.5 Effect of Sand Content

Sand, in general, increases the initial modulus of elasticity and reduces the strength and ductility of cement paste. As observed earlier,

sand acts as a stress raiser, increasing the local compressive and lateral tensile strains within the material. This increase in stress reduces both strength and strain capacity. However, the effect of strain rate on the strength and stiffness of cement paste and mortar appear to be the same at all strain rates, indicating that the controlling mechanisms are not strongly influenced by either water-cement ratio or sand content.

The specific effects of sand content are illustrated in Table 4.1 and Fig. 4.4 and 4.8. Aside from the scatter in the data, sand content has little effect on the influence of strain rate on relative strength gain.

An increase in sand content does decrease ϵ_p and ϵ_{pp90} . All mortars have a lower strain capacity than cement paste of the same W/C, and at the same W/C, the mortar with the higher sand content has a lower strain capacity than the mortar with the lower sand content. For W/C = 0.3, the ratio of ϵ_{pp90} for mortar A (S/C = 0.97) to cement paste ranges from 0.50 to 0.63. For W/C = 0.4, the ϵ_{pp90} ratio for mortar A (S/C = 1.59) to cement paste ranges from 0.47 to 0.62, and the ϵ_{pp90} ratio for mortar B (S/C = 1.97) to cement paste ranges from 0.44 to 0.59. For W/C = 0.5, the ϵ_{pp90} ratio ranges from 0.63 to 0.76 for mortar B (S/C = 1.29), and from 0.47 to 0.60 for mortar A (S/C = 2.28). These figures emphasize the role of sand as a stress raiser and/or a vehicle for the introduction of flaws into cement paste.

The relative reduction in strain capacity with increased sand content generally decreases as both strain rate and water-cement ratio increase (Table 4.1). The lower relative sensitivity at higher strain rates may be due to the fact that at higher velocities, cracks have less opportunity to interact with the sand particles, thus cement paste and mortar behave in a

more similar manner. The lower sensitivity at high water-cement ratios may be due to a reduced sensitivity to flaws in this material.

4.6 Submicrocracks

A limited study of submicrocracking in cement paste with $W/C = 0.3$ was carried out using the new image analysis techniques. The surface crack density is compared to compressive strain for one nonloaded specimen and two specimens loaded to a strain of 0.004 in Fig. 4.10.

The data was obtained on a longitudinal surface only. The loaded specimens differed in that one was loaded at a strain rate ($\dot{\epsilon}_{0-100}$) of 300,000 microstrain per second while the other was loaded at 3 microstrain per second (note this is about half the strain rate used in phase 1). The results are significant in that the total amount of cracking is considerably greater than that observed in phase 1 (Fig. 3.8). In phase 1, crack density increased from 22.3 in./in.² (0.88 mm/mm²) for a non-loaded specimen to 32.8 in./in.² at (1.29 mm/mm²) for a compressive strain of 0.004. As pointed out in Section 3.1, these values are an order of magnitude greater than obtained for bond and mortar microcracking in concrete. For the new data, crack densities increase by another order of magnitude, with corresponding values of 577 in./in.² (22.7 mm/mm²) at zero strain and 663 in./in.² (26.1 mm/mm²) at a strain of 0.004 for the lower strain rate. At the higher strain rate, the crack density is 708 in./in.² (27.9 mm/mm²) for a strain of 0.004. The differences in crack density between non-loaded and loaded specimens at the two strain rates, 86 and 131 in./in.² (3.39 and 5.16 mm/mm²), compare to a value of 10.5 in./in.² (0.41 mm/mm²) observed in the earlier tests.

On the surface, these drastically different results might lead to conclusions that 1) submicrocracks play a much greater role than suggested

in the phase 1 study and 2) the results of the phase 1 study are not useful. However, an analysis shows that neither of these conclusions is correct.

Table 4.2 presents a summary of the estimated three-dimensional crack data obtained from the new surface data and compares those estimates to results from phase 1. The phase 2 parameters are only estimates since crack data from transverse surfaces was not obtained. To make these estimates, it is assumed that the relative amount of cracking on the longitudinal and transverse surfaces is the same as obtained in phase 1. It is also assumed that the relationship between the mean crack size, $\langle a \rangle$, and the mean surface crack length is the same as obtained in phase 1.

Table 4.2 illustrates that the number of cracks per unit volume, N_V , is two orders of magnitude greater with the new techniques than obtained with the techniques used in phase 1. However, the mean crack sizes are considerably smaller than those obtained with phase 1. Thus, small cracks have provided the largest contributions to the increase in crack density observed with the new techniques. In addition, a comparison of volumetric crack densities, $N_V \langle a^3 \rangle$, shows that while the volumetric crack densities are higher than observed in phase 1, the increases in volumetric crack density are of the same order of magnitude. The estimated increase in volumetric crack density, $\Delta N_V \langle a^3 \rangle$, at a strain of 0.004 ($\dot{\epsilon} = 3$ microstrain per second) is 0.070 compared to a value of 0.054 for phase 1. The estimated change in $N_V \langle a^3 \rangle$ is 0.105 for $\dot{\epsilon} = 300,000$ microstrain per second. The fact that the values of $N_V \langle a^3 \rangle$ for phase 1 and phase 2 are not an order of magnitude apart is due to the fact that the volumetric crack density depends on the mean of the cube of the crack size $\langle a^3 \rangle$. The large cracks measured in phase 1 provide the greatest contribution to this term. Thus, the phase 1 procedures did capture a major portion of the material response.

4.7 Strain Due to Submicrocracking

The data obtained with the new procedures is used to estimate the strain caused by submicrocracking. The results summarized in Table 4.3 are based on the conservative assumption that the matrix remains linear. In addition, it is assumed that $K = -0.24$ (same as phase 1) and -0.33 (an educated guess) for the slower and faster strain rates, respectively. As illustrated in Table 4.3, the strain caused by submicrocracking increases from about 37 to about 49 percent of the total inelastic strain for the specimen loaded at the lower strain rate. This represents a 34 percent increase in the strain that may be attributed to submicroscopic cracking. Fig. 4.11 compares the portion of the stress strain curve attributed to cracking in phase 1 with an approximation based on the new data.

There is no comparable data for the higher strain rate from phase 1. The results, however, indicate that cracking plays a more important role for material loaded at the higher strain rate, accounting for 55 percent of the total inelastic strain at a strain of 0.004 (Fig. 4.12). This increase in the importance of the role of cracking at higher strain rates is likely due to the greatly reduced time available for other nonlinear behavior to provide strain relief within the material.

CHAPTER 5

SUMMARY AND CONCLUSIONS

5.1 Summary

Submicroscopic cracking and the strain-rate response of cement paste and mortar under uniaxial compression were measured and correlated with the applied strain. Cement paste specimens with water-cement ratios of 0.3, 0.4, 0.5, and 0.7 and mortar specimens with water-cement ratios of 0.3, 0.4, and 0.5 were subjected to monotonic load at strain rates ranging from 0.3 to 300,000 microstrain per second. Specimens were tested at ages ranging from 27 to 29 days. After loading, slices of material were removed from selected specimens for study at magnifications of 1250x and 2500x in a scanning electron microscope. Image analysis instrumentation was used in later stages of the study. Cracks on transverse and longitudinal surfaces were measured, and three-dimensional crack distributions were obtained from the crack data. The portion of the nonlinear material response caused by the cracks was estimated using a self-consistent material model.

5.2 Conclusions

The following conclusions are drawn from the test results and analyses presented in this report. The term "crack density" refers to both surface and volumetric submicrocrack densities.

1. Crack density in cement paste and mortar increases with increasing uniaxial compressive strain, starting at strains as low as 0.0005.
2. The density of surface cracks in cement paste and mortar is one to two orders of magnitude greater than the density of bond and mortar microcracks in concrete at the same values of compressive strain.

3. Under uniaxial compressive loading, the mean size of submicroscopic cracks increases with increasing strain, while the number of cracks per unit volume decreases. This suggests that as compressive strain increases, small cracks join to form larger cracks.
4. Under increasing uniaxial compression, three-dimensional distributions of submicroscopic cracks become skewed towards the direction of applied stress.
5. On the average, three-dimensional crack distributions in cement paste show only small variations with water-cement ratio. However at high strains, volumetric crack density increases more rapidly the lower the water-cement ratio.
6. Crack density is initially lower but increases more rapidly in mortar than in cement paste.
7. For uniaxial compressive loading of cement paste and mortar, submicroscopic cracks contribute to the decrease in the modulus of elasticity with increasing strain.
8. Submicrocracking accounts for a significant portion of the nonlinear response of cement paste and mortar at all levels of applied compressive strain. The role of submicrocracking decreases in relation to other mechanisms, such as large microcracks, macrocracks, and creep, with increasing applied strain.
9. For cement pastes of the same age at a given strain, the percentage of inelastic strain due to submicrocracking is larger the lower the water-cement ratio. This suggests that submicrocracks are relatively more important for higher strength materials than for lower strength materials.

10. The increase in average strain on the descending branch of the stress-strain curve of mortar is due largely to mechanisms other than submicrocracking.
11. Under uniaxial compression, the Poisson effect in cement paste and mortar appears to be controlled by mechanisms other than submicrocracking.
12. The compressive strength of cement paste and mortar increases with increasing strain rate.
13. The initial modulus of elasticity of cement paste and mortar also increases with increasing strain rate, but to a lesser extent than strength.
14. The relative effects of strain rate on strength and stiffness are largely independent of water-cement ratio and sand-cement ratio.
15. With increasing strain rate, the strain at the peak of the stress-strain curve decreases and then increases.
16. Strain capacity increases with strength. Increases in water-cement ratio and sand-cement ratio cause a decrease in strain capacity.
17. Sand particles in mortar act as stress raisers and/or introduce flaws which result in a greater degree of softening and a lower strain capacity for mortar than for cement paste. The effect of sand particles decreases somewhat with increasing strain rate.
18. Crack density and the role of submicroscopic cracking in the nonlinear behavior of cement paste increases with strain rate.
19. Image analysis techniques greatly improve the resolution and accuracy of crack data obtained from cement paste and mortar.

5.3 Future Studies

1. The observations in Phase 2 suggest that a more detailed picture of crack formation can be obtained with the scanning electron microscope and image analysis system than obtained in phase 1. The new instrumentation has a higher resolution and thus provides a more complete picture of the sub-microcracks in cement paste and mortar. The new system also has the ability to do chemical analysis, using an energy dispersive spectrometer and back-scattered electron detectors. These capabilities can be used to provide a clearer picture of the nature of the features through which the cracks pass. From a scientific point of view, the observations obtained in phase 2 are only preliminary and should be followed up. Crack studies should be combined with non-destructive techniques to measure the change in the moduli of the materials during and after loading. The measured moduli should be compared with the theoretical moduli obtained from the three-dimensional crack distributions. This research can provide important new information about the behavior of the constituents of concrete under load and greatly improve our understanding of this important construction material.

2. The current study has exploited only a small portion of the potential of the image analysis system. The capabilities of the combined system can be utilized to obtain fully automated crack surveys. To achieve this goal, a number of aspects of specimen preparation need additional study, including the use of frozen saturated and freeze dried specimens.

3. Crack survey procedures can be extended to materials subjected to environmental attack. For many applications, poor durability represents a greater problem than low strength. Freeze-thaw cycles, the alkali-aggregate reaction, sulfate attack, and D-cracking are of special concern. The combination of automated crack surveys with more traditional procedures for

evaluating concrete damage will improve our understanding of the basic nature of the damage and the damage mechanisms. The new techniques can be extended to fine-grained materials, such as rock, and to a wider range of load regimes, e.g., tension and multi-axial loading.

4. In the current study, stereological techniques were used to convert two-dimensional crack distributions to three-dimensional distributions, and a self-consistent model was used to estimate material moduli based on measured crack distributions. Extensions of this work should be pursued. The current stereological techniques can handle crack distributions only with mild degrees of anisotropy. Modifications to the procedure to handle crack distributions with more general degrees of anisotropy (even simple cases such as nearly parallel cracks) cannot yet be handled analytically. The self-consistent model should be extended to account for closed cracks that undergo frictional sliding and general anisotropic crack distributions. These extensions will broaden the applicability of the current analytical techniques to cover a wider range of loading conditions.

REFERENCES

1. Abrams, D. A., "The Effect of Rate of Application of Load on Compressive Strength of Concrete," Proceedings of the American Society for Testing, V. 17, Part II, 1917, pp. 364-365.
2. Attiogbe, Emmanuel and Darwin, David, "Submicrocracking in Cement Paste and Mortar in Compression," SM Report No. 16, University of Kansas Center for Research, Lawrence, Kansas, Nov. 1985, 439 pp.
3. Attiogbe, Emmanuel and Darwin, David, "Correction of Window Size Distortion of Crack Distributions on Plane Sections," Journal of Microscopy, V. 144, PT. 1, Oct. 1986, pp 71-82.
4. Attiogbe, Emmanuel and Darwin, David, "Self-Consistent Model for a Cracked Solid," Journal of Engineering Mechanics, ASCE, V. 113, No. 7, July 1987, pp. 984-999.
5. Beres, L., "Relationship of Deformational Processes and Structure Changes in Concrete," Proceedings of the Southampton 1969 Civil Engineering Conference, Editor: M. Te'eni, London and New York, Wiley-Interscience, 1971, Part 1, pp. 643-651.
6. Bieniawski, Z. T., "Time Dependent Behaviour of Fractured Rock," Journal of the International Society of Rock Mechanics, V. 2, 1970, pp. 123-137.
7. Budiansky, Bernard, "On the Elastic Moduli of some Heterogeneous Materials," Journal of Mechanics and Physics of Solids, V. 13, 1965, pp. 223-226.
8. Budiansky, Bernard and O'Connell, Richard J., "Elastic Moduli of a Cracked Solid," International Journal of Solids and Structures, V. 12, No. 2, 1976, pp. 81-97.
9. Carrasquillo, Ramon L., Slate, Floyd O., and Nilson, Arthur H., "Microcracking and Behavior of High Strength Concrete Subject to Short-Term Loading," ACI Journal, Proceedings V. 78, No. 3, May-June 1981, pp. 179-186.
10. Chang, K.-C. and Lee, G. C., "Strain Rate Effect on Structural Steel under Cyclic Loading," Journal of Engineering Mechanics, ASCE, V. 113, No. 9, Sep. 1987, pp. 1292-1301.
11. Cook, D. J. and Chindaprasirt, P., "Influence of Loading History Upon the Compressive Properties of Concrete," Magazine of Concrete Research (London), V. 32, No. 111, June 1980, pp. 89-100.
12. Darwin, David and Slate, Floyd O., "Effect of Paste-Aggregate Bond Strength on Behavior of Concrete," Journal of Materials, V. 5, No. 1, March 1970, pp 86-98.

13. Darwin, D., and Dewey, G. R., "Image Analysis of Microcracks," Proceedings, France-U.S. CNS-NSF Workshop on Strain Localization and Size Effect due to Cracking and Damage, Caohan, France, Sep. 6-9, 1988, Elsevier Applied Science Publishers, Ltd., 11 pp., in press.
14. Derucher, Kenneth N., "Application of the Scanning Electron Microscope to Fracture Studies of Concrete," Building and Environment, V. 13, No. 2, 1978, pp. 135-141.
15. Dhir, R. K. and Sangha, C. M., "A Study of Relationships between Time, Strength, Deformation, and Fracture of Plain Concrete," Magazine of Concrete Research (London), V. 24, No. 81, December 1972, pp. 197-208.
16. Evans, R. H., "The Effect of Rate of Loading on the Mechanical Properties of Some Materials," Journal of the Institution of Civil Engineers (London), V. 18, June 1984, pp. 296-306.
17. Gaede, K. "Influence of the Rate of Loading upon the Compressive Strength of Concrete Cubes," Zement-Kalk-Gips, V. 5, June 1952, p. 195.
18. Hill, R., "A Self-Consistent Mechanics of Composite Materials," Journal of Mechanics and Physics of Solids, V. 13, No. 2, 1965, pp. 213-222.
19. Hoenig, Alan, "Elastic Moduli of a Non-Randomly Cracked Body," International Journal of Solids and Structures, V. 15, No. 2, 1979, pp. 137-154.
20. Horii, H. and Nemat-Nasser, S., "Overall Moduli of Solids with Microcracks: Load-Induced Anisotropy," Journal of Mechanics and Physics of Solids, V. 31, No. 2, 1983, pp. 155-171.
21. Hsu, Thomas C., Slate, Floyd O., Sturman, Gerald M., and Winter, George, "Microcracking of Plain Concrete and the Shape of the Stress-Strain Curve," ACI Journal, Proceedings V. 60, No. 2, Feb. 1963, pp. 209-224.
22. Hughes, B. P. and Watson, A. J., "Compressive Strength and Ultimate Strain of Concrete under Impact Loading," Magazine of Concrete Research (London), V. 30, No. 105, December 1978, pp. 189-199.
23. Jones, P. G. and Richart, P. E., "The Effect of Testing Speed on Strength and Elastic Properties of Concrete," Proceedings of the American Society for Testing Materials, V. 36, Part II, 1936, pp. 380-391.
24. Kaplan, S. A., "Factors Affecting the Relationship between Rate of Loading and Measured Compressive Strength of Concrete," Magazine of Concrete Research (London), V. 32, No. 111, June 1980, pp. 79-88.

25. Maher, Ataullah and Darwin, David, "Microscopic Finite Element Model of Concrete," Proceedings, First International Conference on Mathematical Modeling (St. Louis, Aug.-Sept. 1977), University of Missouri-Rolla, V. III, 1977, pp. 1705-1714.
26. Maher, Ataullah and Darwin, David, "Mortar Constituent of Concrete in Compression," ACI Journal, Proceedings V. 79, No. 2, March-April 1982, pp. 100-109.
27. Mainstone, R. J., "Properties of Materials at High Rates of Straining or Loading," Materials and Structures: Research and Testing, V. 8, No. 44, March-April 1975, pp. 102-116.
28. McHenry, D. and Shideler, J. J., "Review of Data on Effect of Speed in Mechanical Testing of Concrete," Symposium on Speed of Testing of Non-Metallic Materials, STP 185, Philadelphia, American Society for Testing Materials, 1956, pp. 72-82.
29. Meyers, Bernard L., Slate, Floyd O., and Winter, George, "Relationship between Time Dependent Deformation and Microcracking of Plain Concrete," ACI Journal, Proceedings V. 66, No. 1, Jan. 1969, pp. 60-68.
30. Moore, O. L., "Report of Working Committee of Committee C-1 on Plastic Mortar Tests for Portland Cement," Proceedings of the American Society for Testing Materials, V. 34, Part 1, 1934, p. 322.
31. Ollivier, J. P. and Grandet, J., "Disorientation of Portlandite Crystals in the 'Aureole of Transition'", presented at the International Symposium on Bonds between Cement Pastes and Other Materials, I.N.S.A., Toulouse, France, November 3-5, 1982.
32. Shah, Surendra P. and Winter, George, "Inelastic Behavior and Fracture of Concrete," ACI Journal, Proceedings, V. 63, No. 9, Sept. 1966, pp. 925-980.
33. Shah, Surendra P. and Chandra, Sushil, "Critical Stress, Volume Change and Microcracking of Concrete," ACI Journal, Proceedings V. 65, No. 9, Sept. 1968, pp. 770-781.
34. Slate, Floyd O. and Matheus, Ramon E., "Volume Changes on Setting and Curing of Cement Paste and Concrete from Zero to Seven Days," ACI Journal, Proceedings, V. 64, No. 1, January 1967, pp. 34-39.
35. Slate, Floyd O. and Olsefski, Stanley, "X-Rays for Study of Internal Structure and Microcracking of Concrete," ACI Journal, Proceedings V. 60, No. 5, May 1963, pp. 575-588.
36. Sparks, P. R. and Menzies, J. R., "The Effect of Rate of Loading upon the Static and Fatigue Strengths of Plain Concrete in Compression,"

- Magazine of Concrete Research (London), V. 25, No. 83, June 1973, pp. 73-80.
37. Spooner, D. C., "Stress-Strain-Time Relationships for Concrete," Magazine of Concrete Research (London), V. 23, No. 75-76, June-September 1971, pp. 127-131.
 38. Spooner, D. C., "The Stress-Strain-Time Relationship for Hardened Concrete," Magazine of Concrete Research (London), V. 24, No. 29, June 1972, pp. 85-92.
 39. Spooner, David C. and Dougill, John W., "A Quantitative Assessment of Damage Sustained in Concrete During Compressive Loading," Magazine of Concrete Research (London), V. 27, No. 92, Sept. 1975, pp. 151-160.
 40. Spooner, David C., Pomeroy, C. Duncan, and Dougill, John W., "Damage and Energy Dissipation in Cement Pastes in Compression," Magazine of Concrete Research (London), V. 28, No. 94, March 1976, pp. 21-29.
 41. Thaulow, S., "Rate of Loading for Compressive Strength Tests," Betong., V. 38, No. 1, 1953, pp. 11-15.
 42. Rusch, H., "Researches Towards a General Flexural Theory for Structural Concrete," ACI Journal, Proceedings, V. 57, No. 1, July 1960, pp. 1-28.
 43. Watstein, D., "Effect of Straining Rate on the Compressive Strength and Elastic Properties of Concrete," ACI Journal, Proceedings, V. 49, No. 8, April 1953, pp. 729-744.
 44. Weibel, Ewald R., Stereological Methods, Academic Press, V. 2, 1980, 340 pp.
 45. Wright, P. J. F. and Garwood, M. A., "The Effect of the Method of Test on the Flexural Strength of Concrete," Magazine of Concrete Research (London), V. 4, No. 11, October 1952, pp. 67-76.

TABLE 3.1
THREE-DIMENSIONAL CRACK PARAMETERS

Maximum Compressive Strain	Degree of Anisotropy	Crack Aspect Ratio	Mean Characteristic Crack Size $\langle a_{\psi} \rangle^*$	Variance of Characteristic Crack Size $\text{var}(a_{\psi})^*$	Number of Cracks per Cubic Inch	Measure of Volumetric Crack Density $N_V \langle a^3 \rangle$
	K	r	10^{-3} in.	10^{-6} in. ²	N_V	10^6 in. ⁻³
			CEMENT PASTE, W/C = 0.7			
0.0	-0.02	1.0	1.58	0.73	1.73	0.014
0.0005	-0.05	1.0	2.10	0.64	1.40	0.020
0.001	-0.07	1.0	$1.5 \times 10^{-3} \psi + 2.16$	0.93	1.12	0.021
0.002	-0.16	0.92	$1.0 \times 10^{-2} \psi + 2.23$	$1.3 \times 10^{-3} \psi + 1.26$	1.19	0.036
0.004	-0.26	0.95	$1.1 \times 10^{-2} \psi + 3.47$	$1.7 \times 10^{-3} \psi + 1.58$	0.63	0.082
0.006	-0.31	0.90	$1.0 \times 10^{-2} \psi + 3.68$	$1.6 \times 10^{-3} \psi + 2.37$	0.51	0.097
			CEMENT PASTE, W/C = 0.5			
0.0	0.00	1.0	1.50	0.84	2.32	0.015
0.0005	-0.07	1.0	2.06	0.83	1.91	0.020
0.001	-0.11	1.0	$1.3 \times 10^{-3} \psi + 2.12$	1.25	1.38	0.024
0.002	-0.16	0.9	$1.0 \times 10^{-2} \psi + 2.27$	$1.6 \times 10^{-3} \psi + 1.47$	1.03	0.033
0.004	-0.27	0.85	$1.0 \times 10^{-2} \psi + 3.13$	$1.5 \times 10^{-3} \psi + 1.75$	0.72	0.076
0.006	-0.30	0.87	$1.2 \times 10^{-2} \psi + 3.60$	$1.8 \times 10^{-3} \psi + 2.14$	0.68	0.105

TABLE 3.1, Continued
THREE-DIMENSIONAL CRACK PARAMETERS

Maximum Compressive Strain	Degree of Anisotropy	Crack Aspect Ratio	Mean Characteristic Crack Size * $\langle a_{\psi} \rangle$	Variance of Characteristic Crack Size * $\text{var}(a_{\psi})$	Number of Cracks per Cubic Inch N_V	Measure of Volumetric Crack Density $N_V \langle a^3 \rangle$
	K	r	10^{-3} in.	10^{-6} in. ²	10^6 in. ⁻³	
CEMENT PASTE, W/C = 0.3						
0.0	-0.02	1.0	1.51	0.63	2.41	0.017
0.0005	-0.05	1.0	1.96	0.85	1.93	0.021
0.001	-0.09	1.0	2.09	0.92	1.41	0.024
0.002	-0.15	0.95	$0.9 \times 10^{-2} \psi + 2.27$	1.36	1.32	0.031
0.003	-0.18	0.90	$1.0 \times 10^{-2} \psi + 2.75$	1.57	1.14	0.042
0.004	-0.24	0.90	$1.0 \times 10^{-2} \psi + 3.01$	$1.4 \times 10^{-3} \psi + 1.53$	0.92	0.071
0.006	-0.31	0.85	$1.1 \times 10^{-2} \psi + 3.56$	$1.6 \times 10^{-3} \psi + 1.84$	0.81	0.109
MORTAR, W/C = 0.5						
0.0	0.00	1.0	1.35	0.55	1.54	0.008
0.0005	-0.07	1.0	2.08	0.54	1.22	0.018
0.001	-0.08	1.0	2.14	0.82	1.19	0.022
0.002	-0.15	0.95	2.54	1.16	1.13	0.040
0.003	-0.18	1.0	$0.9 \times 10^{-2} \psi + 3.21$	$1.2 \times 10^{-3} \psi + 0.92$	0.71	0.072
0.004	-0.24	0.90	$1.0 \times 10^{-2} \psi + 3.52$	$1.4 \times 10^{-3} \psi + 1.74$	0.60	0.088

* ψ in degrees.

Note: 1 in. = 25.4 mm

TABLE 3.2
EFFECTIVE MODULI AND AXIAL STRAIN DUE TO SUBMICROCRACKING -
LINEAR MATRIX MATERIAL, PRE-EXISTING CRACKS

ϵ	σ psi	E_3 10^6 psi	$\frac{E_3}{E_1}$	ν	ν_{31}	$\epsilon_{ec} = \frac{\sigma}{E_3}$	$\epsilon_c = \sigma \left(\frac{E_1 - E_3}{E_1 E_3} \right)$	$\frac{\epsilon_c}{\epsilon - \epsilon_e}$ %
CEMENT PASTE, W/C = 0.7								
$E_1 = 1.78 \times 10^6$ psi $\nu_1 = 0.24^*$								
$E_m = 1.837 \times 10^6$ psi; $\nu_m = 0.243$								
.0005	830	1.763	.9904	--	.241	.000471	.000005	14.8
.001	1581	1.758	.9876	--	.241	.000899	.000011	9.8
.002	2657	1.750	.9831	--	.242	.001518	.000026	5.1
.004	3740	1.578	.8866	--	.246	.002370	.000269	14.2
.006	4070	1.512	.8494	--	.249	.002692	.000405	10.9
CEMENT PASTE, W/C = 0.5								
$E_1 = 2.54 \times 10^6$ psi $\nu_1 = 0.24$								
$E_m = 2.620 \times 10^6$ psi; $\nu_m = 0.243$								
.0005	1195	2.515	.9902	.239	.240	.000475	.000005	16.9
.001	2310	2.507	.9870	.240	.240	.000921	.000012	13.3
.002	4128	2.490	.9803	.242	.241	.001658	.000033	8.8
.004	6036	2.309	.9091	.248	.244	.002614	.000238	14.7
.006	6687	2.156	.8482	.273	.253	.003102	.000469	13.9
CEMENT PASTE, W/C = 0.3								
$E_1 = 3.31 \times 10^6$ psi $\nu_1 = 0.24$								
$E_m = 3.423 \times 10^6$ psi; $\nu_m = 0.243$								
.0005	1581	3.288	.9934	.238	.240	.000480	.000003	13.4
.001	3137	3.280	.9909	.240	.241	.000956	.000009	17.2
.002	6051	3.264	.9861	.247	.241	.001854	.000026	15.2
.003	8195	3.105	.9381	.252	.242	.002639	.000163	31.1
.004	9860	2.942	.8888	.264	.245	.003351	.000373	36.5
.006	11503	2.819	.8517	.294	.254	.004081	.000605	24.0
MORTAR, W/C = 0.5								
$E_1 = 4.79 \times 10^6$ psi $\nu_1 = 0.20$								
$E_m = 4.874 \times 10^6$ psi; $\nu_m = 0.202$								
.0005	2205	4.718	.9850	.212	.199	.000467	.000007	17.7
.001	3697	4.664	.9737	.247	.199	.000793	.000021	9.2
.002	5398	4.628	.9662	.288	.200	.001166	.000039	4.5
.003	5804	4.216	.8802	.375	.207	.001377	.000165	9.2
.004	4066	4.060	.8476	.480	.218	.001001	.000153	4.9

*Estimated

E_1, ν_1 = Initial Moduli; E_m, ν_m = Calculated Matrix Moduli

Note: 1 psi = 6.89 kPa

TABLE 3.3
 MODULI OF MATRIX AND AXIAL STRAIN DUE TO SUBMICROCRACKING -
 NONLINEAR MATRIX MATERIAL, PRE-EXISTING CRACKS

ϵ	σ psi	E_m 10^6 psi	ν_m	$\epsilon_m = \frac{\sigma}{E_m}$	$\epsilon_c = \epsilon - \epsilon_m$	$\frac{\epsilon_c}{\epsilon - \epsilon_e}$ %
CEMENT PASTE, W/C = 0.7						
.0005	830	1.725	.242	.000481	.000019	55.9
.001	1581	1.654	.242	.000956	.000044	39.4
.002	2657	1.450	.243	.001832	.000168	33.2
.004	3740	1.094	.246	.003419	.000581	30.6
.006	4070	0.835	.264	.004875	.001125	30.2
CEMENT PASTE, W/C = 0.5						
.0005	1195	2.485	.242	.000481	.000019	64.6
.001	2310	2.416	.241	.000956	.000044	48.6
.002	4127	2.217	.242	.001862	.000138	36.7
.004	6036	1.758	.246	.003433	.000567	34.9
.006	6687	1.375	.262	.004863	.001137	33.8
CEMENT PASTE, W/C = 0.3						
.0005	1581	3.286	.242	.000481	.000019	85.4
.001	3137	3.271	.244	.000959	.000041	78.5
.002	6051	3.198	.247	.001892	.000108	62.8
.003	8195	3.034	.250	.002701	.000299	57.0
.004	9860	2.870	.258	.003436	.000564	55.2
.006	11503	2.363	.289	.004868	.001132	44.8
MORTAR, W/C = 0.5						
.0005	2205	4.575	.214	.000482	.000018	45.4
.001	3697	3.855	.249	.000959	.000041	18.0
.002	5398	2.919	.290	.001880	.000151	17.3
.003	5804	2.150	.352	.002700	.000300	16.8
.004	4066	1.231	.441	.003303	.000697	22.1

Note: 1 psi = 6.89 kPa

TABLE 3.4
 MODULI OF MATRIX AND AXIAL STRAIN DUE TO SUBMICROCRACKING -
 NONLINEAR MATRIX MATERIAL, NO-PRE-EXISTING CRACKS

ϵ	σ psi	E_m 10^6 psi	ν_m	$\epsilon_m = \frac{\sigma}{E_m}$	$\epsilon_o = \epsilon - \epsilon_m$	$\frac{\epsilon_o}{\epsilon - \epsilon_e}$ %
CEMENT PASTE, W/C = 0.7						
.0005	830	1.718	.242	.000483	.000017	50.2
.001	1581	1.642	.243	.000963	.000037	33.7
.002	2657	1.428	.244	.001861	.000139	27.4
.004	3740	1.054	.248	.003548	.000452	23.8
.006	4070	0.790	.267	.005154	.000846	22.7
CEMENT PASTE, W/C = 0.5						
.0005	1195	2.474	.242	.000483	.000017	59.8
.001	2310	2.401	.242	.000962	.000038	42.3
.002	4127	2.189	.243	.001885	.000115	30.7
.004	6036	1.703	.248	.003544	.000456	28.1
.006	6687	1.313	.265	.005093	.000907	26.9
CEMENT PASTE, W/C = 0.3						
.0005	1581	3.280	.242	.000482	.000018	60.9
.001	3137	3.268	.244	.000960	.000040	76.6
.002	6051	3.168	.248	.001910	.000090	52.3
.003	8195	2.987	.251	.002743	.000257	49.1
.004	9860	2.808	.255	.003512	.000488	47.7
.006	11503	2.251	.258	.005110	.000890	35.2
MORTAR, W/C = 0.5						
.0005	2205	4.556	.214	.000484	.000016	41.1
.001	3697	3.819	.250	.000968	.000032	14.2
.002	5398	2.858	.292	.001889	.000111	12.7
.003	5804	2.069	.355	.002805	.000195	10.9
.004	4066	1.198	.446	.003394	.000606	19.2

Note: 1 psi = 6.89 kPa

TABLE 4.1
SUMMARY OF STRAIN-RATE TESTS

Strain Rate (0 - 100%) με/sec Average (Std. Dev.)	Strain Rate (5 - 20%) με/sec Average (Std. Dev.)	Strain Rate (50 - 99%) με/sec Average (Std. Dev.)	Number of Samples	Maximum Stress, psi Average (Std. Dev.)	ε _p με Average (Std. Dev.)	ε _{pp} με Average (Std. Dev.)	E _i x 10 ⁶ psi Average (Std. Dev.)
0.30 (0)	0.30 (0)	0.30 (0)	2	11658 (955)	9358 (4041)	11151 (3054)	2.94 (0.21)
3.02 (0.02)	3.01 (0.034)	3.02 (0.02)	11	12534 (487)	7450 (794)	7940 (835)	3.396 (0.081)
30.4 (0.07)	30.3 (0.23)	30.7 (0.5)	2	14061 (511)	7326 (755)	7949 (820)	3.406 (0.073)
305 (1.41)	303 (3.9)	308 (2.8)	2	15804 (461)	7036 (318)	7350 (18)	3.649 (0.10)
3052 (34)	3181 (51)	3186 (453)	11	17940 (647)	7037 (716)	7556 (505)	3.792 (0.064)
31662 (98)	40221 (231)	31009 (688)	2	21989 (482)	8571 (220)	8889 (124)	3.985 (0.013)
278156 (11788)	176421 (8202)	402344 (34129)	11	22876 (1377)	7960 (776)	8595 (740)	4.206 (0.075)

CEMENT PASTE, W/C = 0.3

TABLE 4.1, Continued
SUMMARY OF STRAIN-RATE TESTS

Strain Rate (0 - 100%) με/sec Average (Std. Dev.)	Strain Rate (5 - 20%) με/sec Average (Std. Dev.)	Strain Rate (50 - 99%) με/sec Average (Std. Dev.)	Number of Samples	Maximum Stress, psi Average (Std. Dev.)	ε _p με Average (Std. Dev.)	ε _{pp} με Average (Std. Dev.)	E _i x 10 ⁶ psi Average (Std. Dev.)
0.30 (0)	0.30 (0)	0.30 (0)	2	7456 (113)	10703 (694)	11412 (164)	2.256 (0.001)
3.05 (0.02)	3.04 (0.05)	3.05 (0.02)	2	7755 (27)	7007 (1092)	8047 (1475)	2.494 (0.008)
30.5 (0.07)	30.8 (0.25)	30.5 (0.07)	2	8502 (101)	6377 (89)	6883 (250)	2.65 (0.069)
304 (1.41)	298.6 (7.0)	304 (1.4)	2	9544 (321)	6494 (506)	7079 (463)	2.777 (0.007)
3072 (3.5)	3270 (0)	3041 (9.9)	2	10557 (332)	6501 (553)	7099 (465)	2.752 (0.016)
32248 (165)	38718 (161)	30897 (96)	2	11956 (26)	6597 (605)	7309 (110)	2.862 0.023)
282410 (4959)	161384 (1223)	398143 (13625)	2	13406 (235)	6533 (291)	7151 (114)	3.135 (0)

CEMENT PASTE, W/C = 0.4

TABLE 4.1, Continued
SUMMARY OF STRAIN-RATE TESTS

Strain Rate (0 - 100%) με/sec Average (Std. Dev.)	Strain Rate (5 - 20%) με/sec Average (Std. Dev.)	Strain Rate (50 - 99%) με/sec Average (Std. Dev.)	Number of Samples	Maximum Stress, psi Average (Std. Dev.)	ε _p με Average (Std. Dev.)	ε _{pp} με Average (Std. Dev.)	E _i x 10 ⁶ psi Average (Std. Dev.)
0.30 (0)	0.31 (0)	0.30 (0)	2	5048 (112)	7924 (894)	8307 (443)	1.760 (0.049)
3.0 (0.02)	3.01 (0.029)	3.0 (0.02)	11	5896 (333)	6311 (773)	8061 (857)	2.035 (0.102)
30.4 (0.07)	30.5 (0.28)	30.4 (0.07)	2	6551 (54)	5857 (38)	6747 (362)	1.935 (0.047)
305 (2.8)	298.8 (1.48)	305 (2.8)	2	6897 (44)	5358 (370)	6189 (66)	2.114 (0.014)
3048 (21)	3330 (70)	3007 (23)	11	7878 (417)	5568 (669)	6427 (568)	2.339 (0.090)
32863 (235)	38002 (17)	31160 (270)	2	8093 (298)	5198 (370)	6119 (589)	2.289 (0.052)
284722 (9121)	162043 (6360)	391875 (11328)	11	9816 (660)	5886 (579)	6822 (750)	2.678 (0.106)

CEMENT PASTE, W/C = 0.5

TABLE 4.1, Continued
SUMMARY OF STRAIN-RATE TESTS

Strain Rate (0 - 100%) με/sec Average (Std. Dev.)	Strain Rate (5 - 20%) με/sec Average (Std. Dev.)	Strain Rate (50 - 99%) με/sec Average (Std. Dev.)	Number of Samples	Maximum Stress, psi Average (Std. Dev.)	ε _p με Average (Std. Dev.)	ε _{pp} με Average (Std. Dev.)	E _i psi x 10 ⁵ Average (Std. Dev.)
0.30 (0)	0.30 (0.01)	0.30 (0)	2	9831 (219)	4901 (141)	5572 (0)	3.843 (0.595)
3.04 (0)	2.99 (0.4)	3.05 (0.01)	2	10841 (32)	4157 (78)	4675 (93)	4.553 (0.063)
30.3 (0)	30.5 (0.4)	30.2 (0.1)	2	12323 (304)	4164 (79)	4475 (52)	4.906 (0.084)
291 (19)	306 (4)	302 (0)	2	13394 (360)	4183 (52)	4442 (66)	5.070 (0.095)
3090 (13)	3681 (193)	3068 (17)	2	14548 (236)	4226 (262)	4584 (351)	5.008 (0.137)
32155 (1293)	29730 (3014)	31447 (841)	2	15695 (2771)	4377 (134)	4732 (43)	5.955 (0.305)
264352 (10974)	141982 (14162)	465254 (3770)	2	17804 (339)	4636 (47)	5376 (6)	5.675 (0.298)

MORTAR, W/C = 0.3, S/C = 0.97

TABLE 4.1, Continued
SUMMARY OF STRAIN-RATE TESTS

Strain Rate (0 - 100%) Average $\mu\epsilon/\text{sec}$ (Std. Dev.)	Strain Rate (5 - 20%) Average $\mu\epsilon/\text{sec}$ (Std. Dev.)	Strain Rate (50 - 99%) Average $\mu\epsilon/\text{sec}$ (Std. Dev.)	Number of Samples	Maximum Stress, psi Average (Std. Dev.)	ϵ_p $\mu\epsilon$ Average (Std. Dev.)	ϵ_{pp} $\mu\epsilon$ Average (Std. Dev.)	$E_i \times 10^6$ psi Average (Std. Dev.)
0.31 (0)	0.30 (0)	0.30 (0)	2	7356 (54)	4132 (86)	5310 (51)	3.898 (0.141)
3.03 (0.04)	3.00 (0.05)	3.03 (0.05)	2	7841 (84)	3712 (102)	4538 (180)	4.256 (0.064)
30.6 (0.1)	30.4 (0.4)	30.6 (0.01)	2	8812 (113)	3336 (240)	3845 (268)	4.738 (0.216)
306 (1)	293 (10)	306 (1)	2	9588 (260)	3502 (46)	3940 (108)	4.978 (0.112)
3038 (119)	3970 (78)	3080 (42)	2	10398 (255)	3520 (317)	4404 (226)	4.938 (0.445)
32262 (779)	26135 (728)	31776 (779)	2	11278 (209)	3721 (188)	4230 (277)	5.100 (0.199)
267708 (6044)	126581 (5167)	521089 (35628)	3	12547 (142)	3620 (221)	4298 (340)	5.817 (0.231)

MORTAR-A, W/C = 0.4, S/C = 1.59

TABLE 4.1, Continued
SUMMARY OF STRAIN-RATE TESTS

Strain Rate (0 - 100%) μE/sec Average (Std. Dev.)	Strain Rate (5 - 20%) μE/sec Average (Std. Dev.)	Strain Rate (50 - 99%) μE/sec Average (Std. Dev.)	Number of Samples	Maximum Stress, psi Average (Std. Dev.)	ε _p μE Average (Std. Dev.)	ε _{pp} μE Average (Std. Dev.)	E _i × 10 ⁶ psi Average (Std. Dev.)
0.31 (0)	0.30 (0)	0.30 (0)	1	7566	4045	4958	3.888
3.04 (0.02)	3.01 (0.06)	3.03 (0.03)	5	8002 (199)	3272 (169)	3992 (172)	4.618 (0.237)
30.6 (0.1)	30.2 (0.57)	30.4 (0.1)	2	8760 (81)	3200 (13)	3671 (92)	4.851 (0.103)
304 (1)	296 (5)	303 (1)	2	9724 (124)	3267 (173)	3730 (190)	5.195 (0.186)
3111 (31)	3915 (0)	3047 (23)	2	10508 (74)	3142 (154)	3592 (104)	5.450 (0.013)
32345 (1295)	28965 (4273)	31692 (1380)	3	11515 (71)	3398 (93)	3906 (147)	5.689 (0.259)
264199 (5354)	123744 (691)	512384 (21886)	2	12720 (302)	3568 (206)	4234 (359)	5.978 (0.034)

MORTAR-B, W/C = 0.4, S/C = 1.97

TABLE 4.1, Continued
SUMMARY OF STRAIN-RATE TESTS

Strain Rate (0 - 100%) με/sec Average (Std. Dev.)	Strain Rate (5 - 20%) με/sec Average (Std. Dev.)	Strain Rate (50 - 99%) με/sec Average (Std. Dev.)	Number of Samples	Maximum Stress, psi Average (Std. Dev.)	ε _p με Average (Std. Dev.)	ε _{pp} με Average (Std. Dev.)	E _i × 10 ⁶ psi Average (Std. Dev.)
0.31 (0)	0.30 (0.01)	0.31 (0)	3	5379 (80)	3503 (532)	4905 (202)	3.490 (0.225)
3.01 (0.02)	2.98 (0.09)	3.01 (0.03)	12	5582 (291)	2827 (193)	3791 (246)	4.024 (0.170)
30.4 (0.1)	30.1 (0.3)	30.5 (0.1)	3	6407 (149)	2908 (132)	3538 (352)	4.147 (0.126)
307 (1)	293 (1)	305 (2)	3	7090 (86)	2948 (56)	3550 (145)	4.561 (0.067)
3080 (29)	4211 (271)	3017 (23)	12	7434 (282)	2907 (188)	3469 (179)	4.584 (0.156)
34645 (257)	27487 (949)	34071 (364)	3	8824 (326)	3135 (153)	3689 (141)	5.050 (0.197)
219728 (15836)	97292 (6599)	438418 (31313)	12	9391 (611)	2839 (165)	3525 (212)	5.451 (0.185)

MORTAR-A, W/C = 0.5, S/C = 2.28

TABLE 4.1, Continued
SUMMARY OF STRAIN-RATE TESTS

Strain Rate (0 - 4) μE/sec Average (Std. Dev.)	Strain Rate (5 - 20%) μE/sec Average (Std. Dev.)	Strain Rate (50 - 99%) μE/sec Average (Std. Dev.)	Number of Samples	Maximum Stress, psi Average (S-d. Dev.)	ε _p μE Average (Std. Dev.)	ε _{pp} μE Average (Std. Dev.)	E _i × 10 ⁶ psi Average (Std. Dev.)
0.30 (0)	0.31 (0.01)	0.30 (0)	2	5712 (69)	4284 (0)	6180 (4)	3.020 (0.258)
3.03 (0.01)	2.96 (0.03)	3.03 (0.01)	5	6240 (157)	3745 (224)	4765 (227)	3.500 (0.124)
30.3 (0)	29.8 (0)	30.3 (0.1)	2	6626 (76)	3626 (38)	4252 (16)	3.690 (0.045)
304 (1)	298 (6)	302 (1)	2	7297 (17)	3637 (163)	4119 (59)	3.923 (0.172)
3078 (6)	3580 (58)	3038 (34)	2	7908 (255)	3680 (56)	4296 (64)	3.952 (0.146)
32637 (1529)	34218 (824)	30982 (1467)	2	8273 (192)	3900 (44)	4625 (117)	3.714 (0.282)
293825 (11970)	137452 (11546)	532744 (4390)	2	10040 (466)	3699 (47)	4390 (98)	4.891 (0.255)

MORTAR-B, W/C = 0.5, S/C = 1.29

TABLE 4.2
 COMPARISON OF THREE-DIMENSIONAL CRACK
 PARAMETERS FOR CEMENT PASTE, W/C = 0.3

Maximum Compressive Strain	Mean Characteristic Crack Size $\langle a_{\psi} \rangle^*$ 10^{-3} in.	Number of Cracks per Cubic Inch N_V in. ⁻³	Measure of Volumetric Crack Density $N_V \langle a^3 \rangle$	Change in Volumetric Crack Density $\Delta N_V \langle a^3 \rangle$
PHASE 1, $\dot{\epsilon} = 6.67$ MICROSTRAIN PER SECOND				
0.0	1.51	2.41×10^6	0.017	0
0.004	3.46*	0.92×10^6	0.071	0.054
PHASE 2, $\dot{\epsilon} = 3.0$ MICROSTRAIN PER SECOND ^t OR 300,000 MICROSTRAIN PER SECOND ^{tt}				
0.00	0.385	9.90×10^8	0.112	0
0.004 ^t	0.627	5.16×10^8	0.182	0.070
0.004 ^{tt}	0.689	4.55×10^8	0.217	0.105

Note: 1 in. = 25.4 mm

*For $\psi = 45^\circ$

TABLE 4.3

ESTIMATED EFFECTIVE MODULI AND AXIAL STRAIN
DUE TO SUBMICROCRACKING
LINEAR MATERIAL - PHASE 2

CEMENT PASTE, W/C = 0.3

ϵ	σ	E_3	$\frac{E_3}{E_1}$	$\epsilon_c = \frac{\sigma}{E_3}$	$\epsilon_c = \sigma \left(\frac{E_1 - E_3}{E_1 E_3} \right)$	$\frac{\epsilon_c}{\epsilon - \epsilon_e}$
	psi	10^6 psi				%
$\dot{\epsilon} = 3$ MICROSTRAIN PER SECOND						
$E_1 = 3.31 \times 10^6$ psi						
0.004	9,860	2.84	0.857	0.003475	0.000497	48.8
$\dot{\epsilon} = 300,000$ MICROSTRAIN PER SECOND						
$E_1 = 4.92 \times 10^6$ psi						
0.004	14,700	4.15	0.843	0.003544	0.000556	54.9

Note: 1 psi = 6.89 kPa

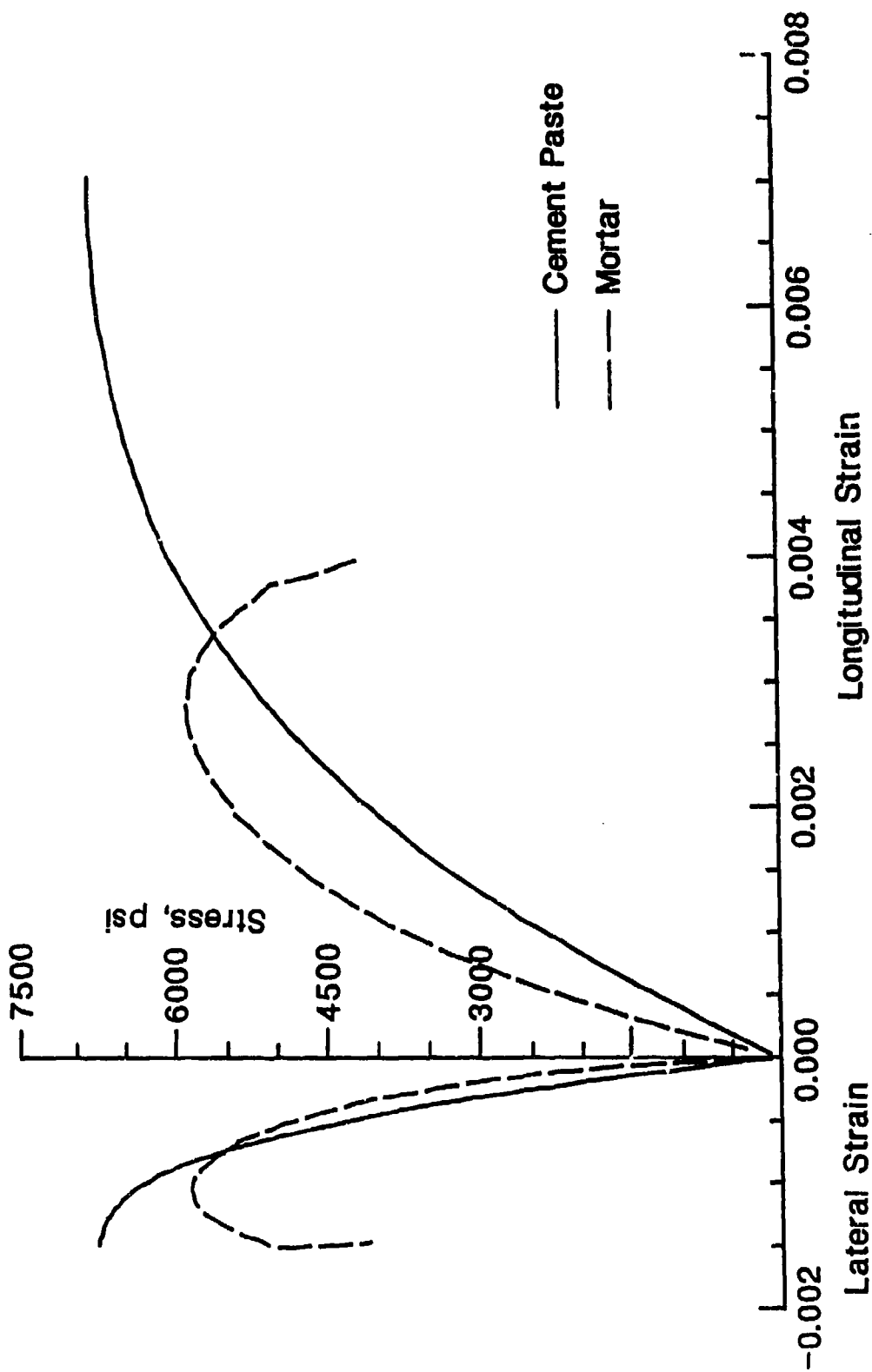


Fig. 3.1 Stress-strain curves for cement paste and mortar, $W/C = 0.5$ (1
psi = 6.89kPa)

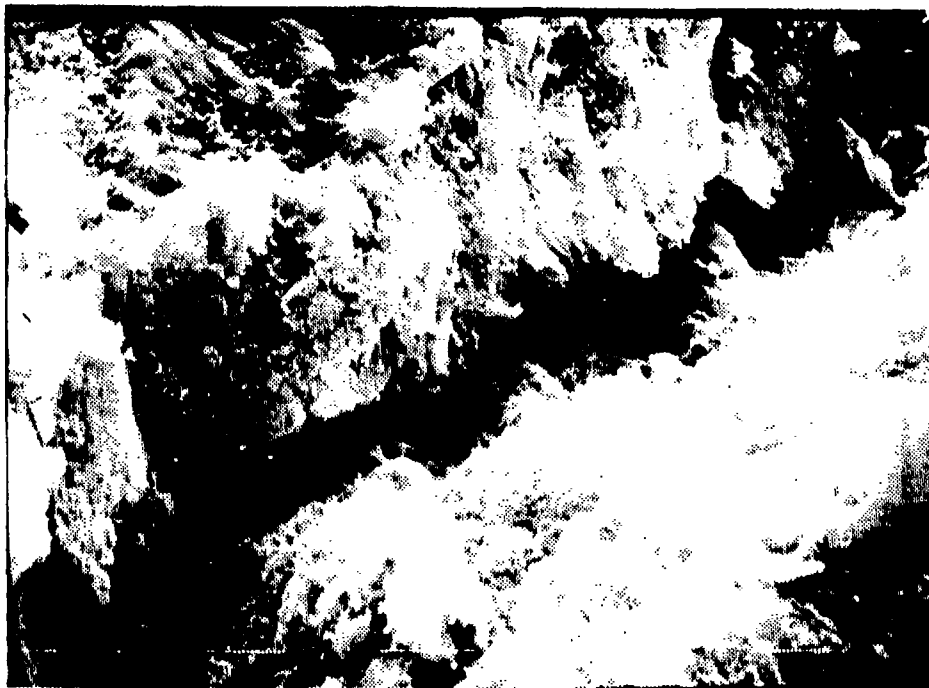


Fig. 3.3 Crack through calcium silicate hydrate and calcium hydroxide in cement paste, μ marker = 3.6×10^{-4} in. ($9.1 \mu\text{m}$)



Fig. 3.4 Sand grain adjacent to calcium silicate hydrate in mortar. Cracks at interface and within calcium silicate hydrate, μ marker = 3.6×10^{-3} in. ($90.9 \mu\text{m}$)

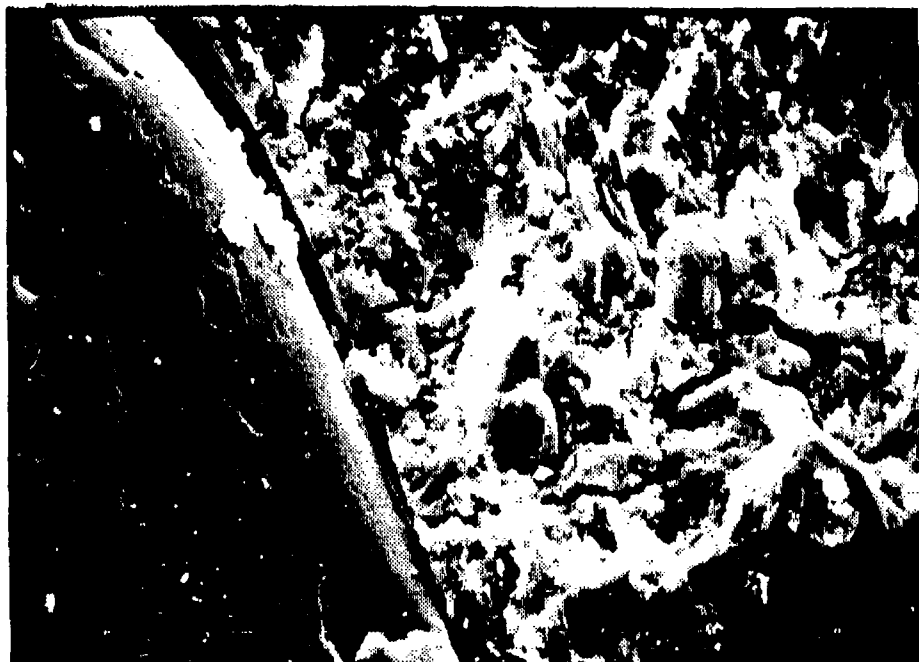


Fig. 3.2 Crack through calcium silicate hydrate in cement paste, μ marker
= 3.6×10^{-4} in. (9.1 μ m)

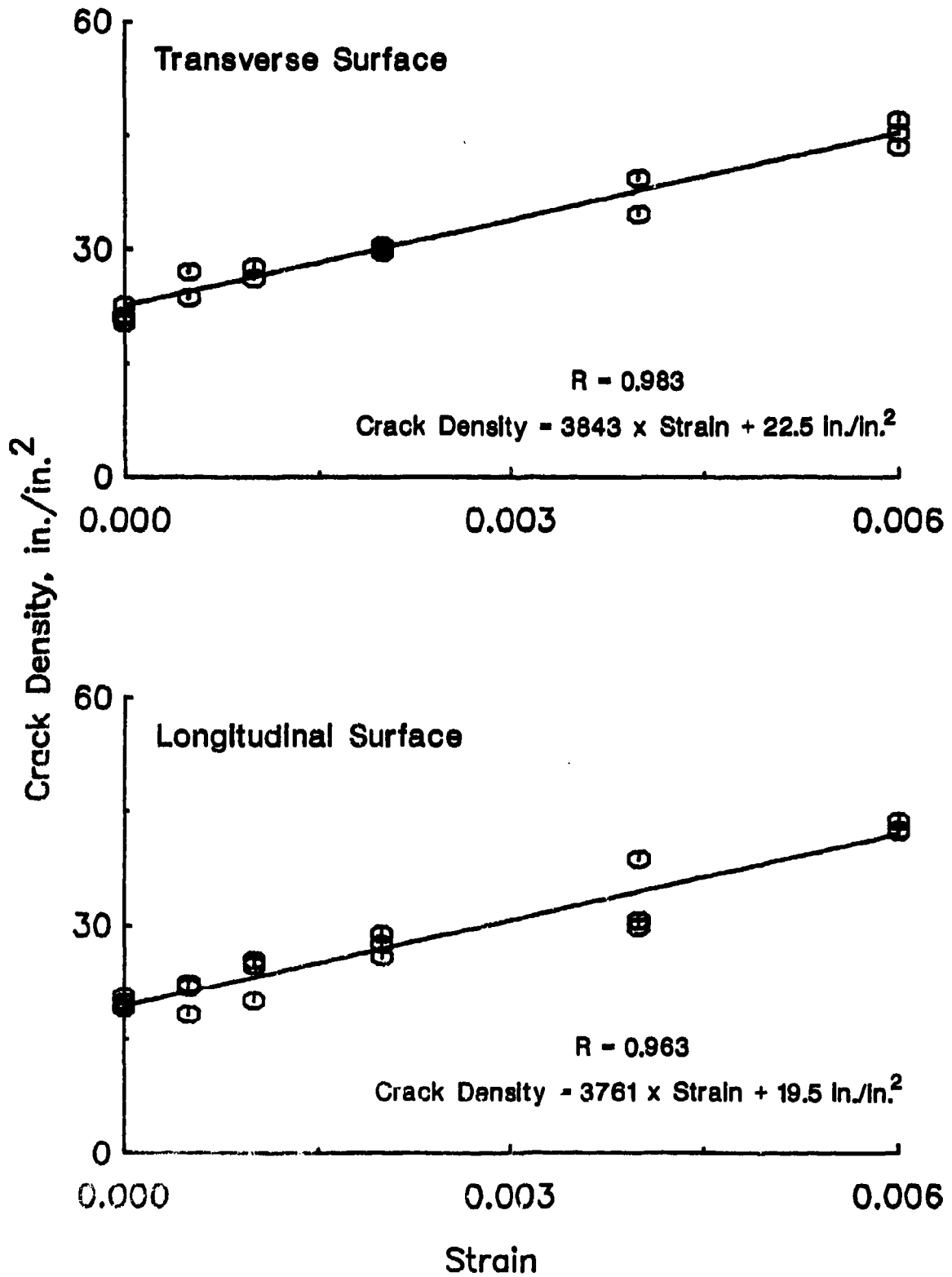


Fig. 3.5 Surface crack density versus compressive strain for cement paste, W/C = 0.5 (1 in./in.² = 0.039 mm/mm²)

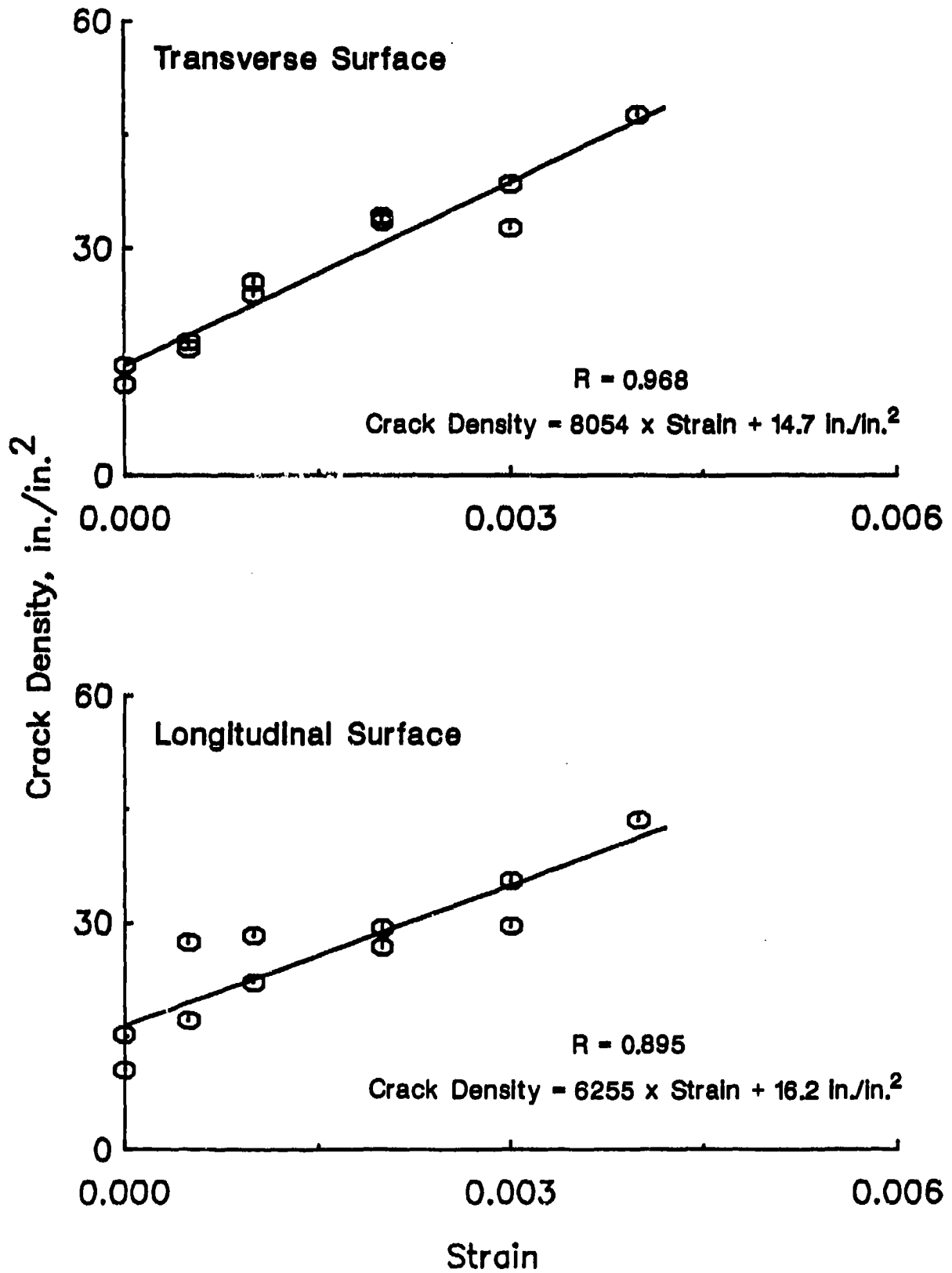


Fig. 3.6 Surface crack density versus compressive strain for mortar, W/C = 0.5 (1 in./in.² = 0.039 mm/mm²)

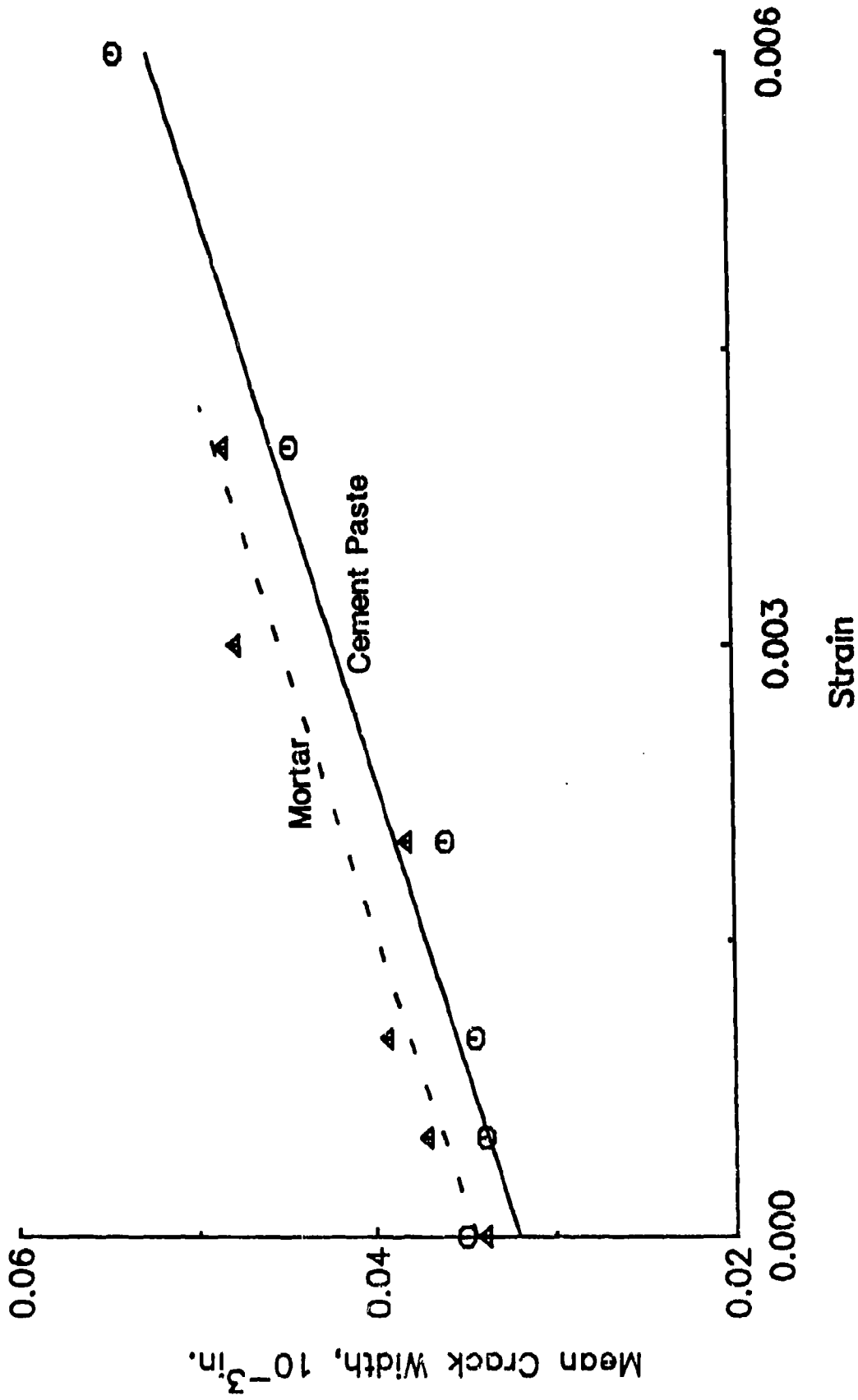


Fig. 3.7 Mean crack width versus compressive strain for cement paste and mortar, W/C = 0.5 (1 in. = 25.4 mm)

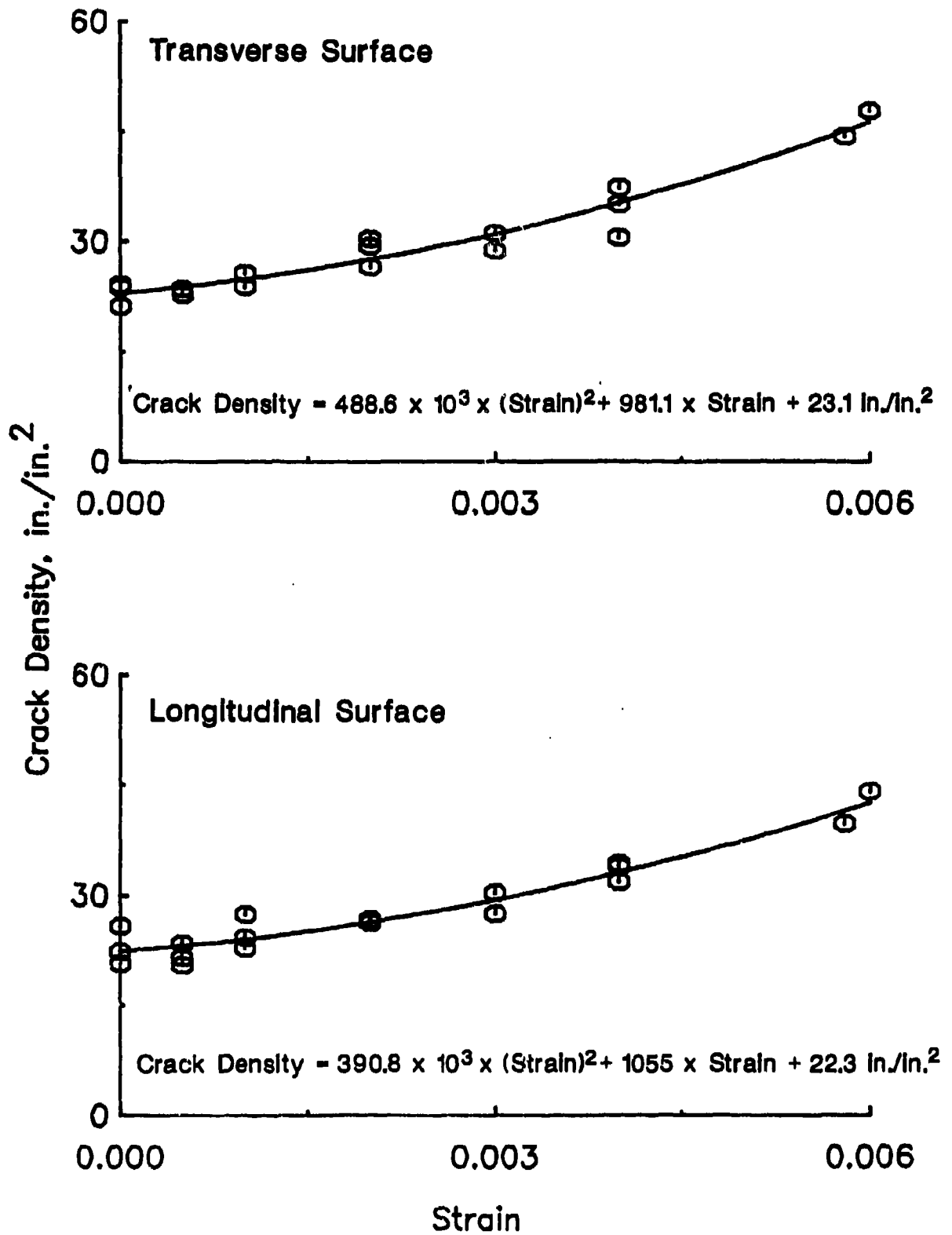


Fig. 3.8 Surface crack density versus compressive strain for cement paste
W/C = 0.3 (1 in./in.² = 0.039 mm/mm²)

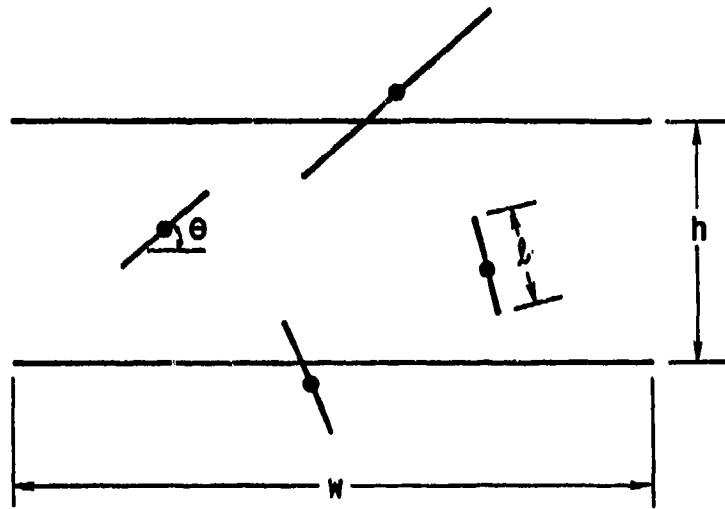


Fig. 3.9 Cracks as seen with limited field of view

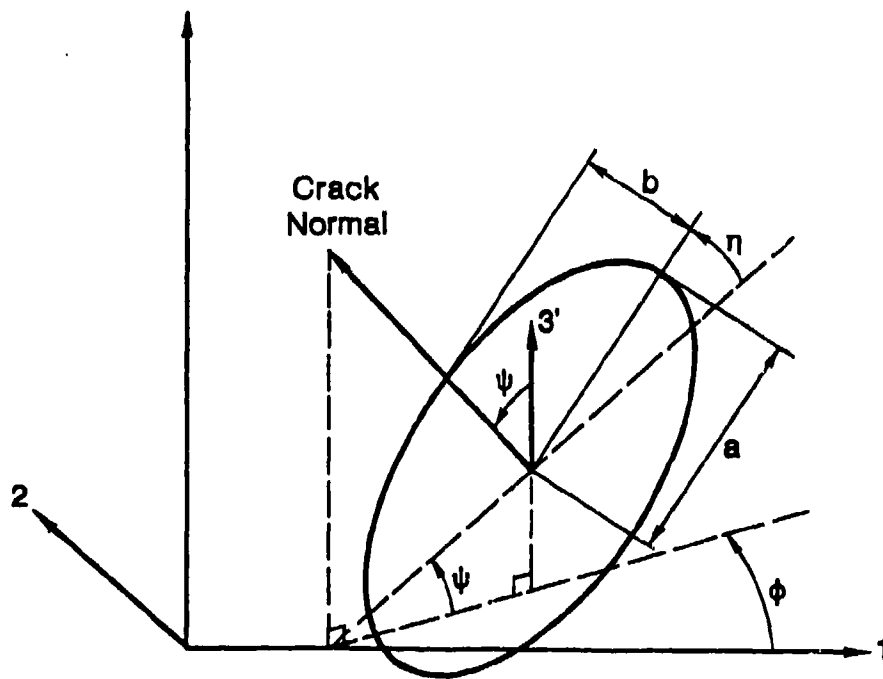


Fig. 3.10 Elliptic crack

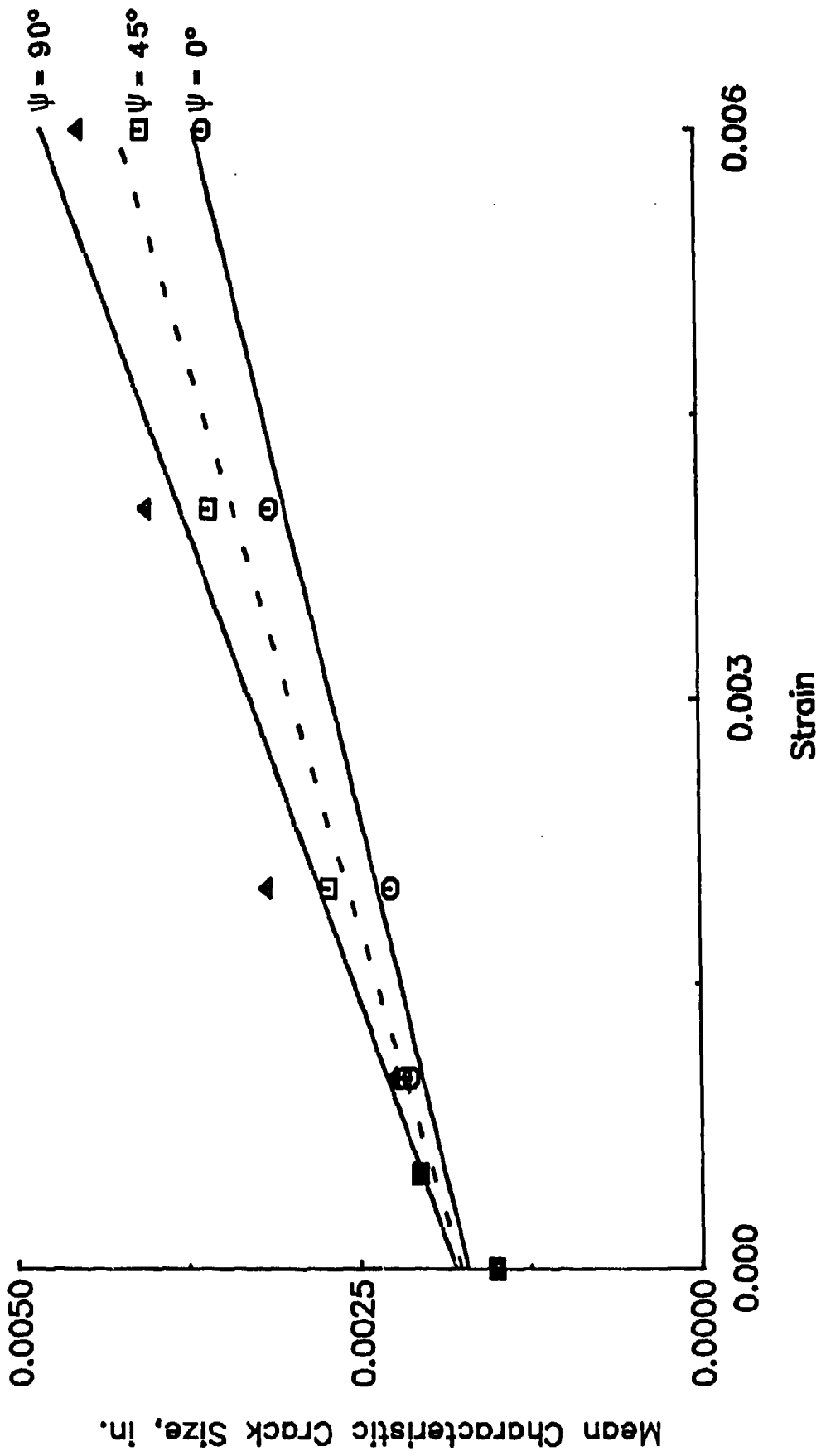


Fig. 3.11 Mean characteristic crack size, $\langle a_v \rangle$, versus compressive strain for cement paste, $W/C = 0.5$ (1 in. $\psi = 25.4$ mm)

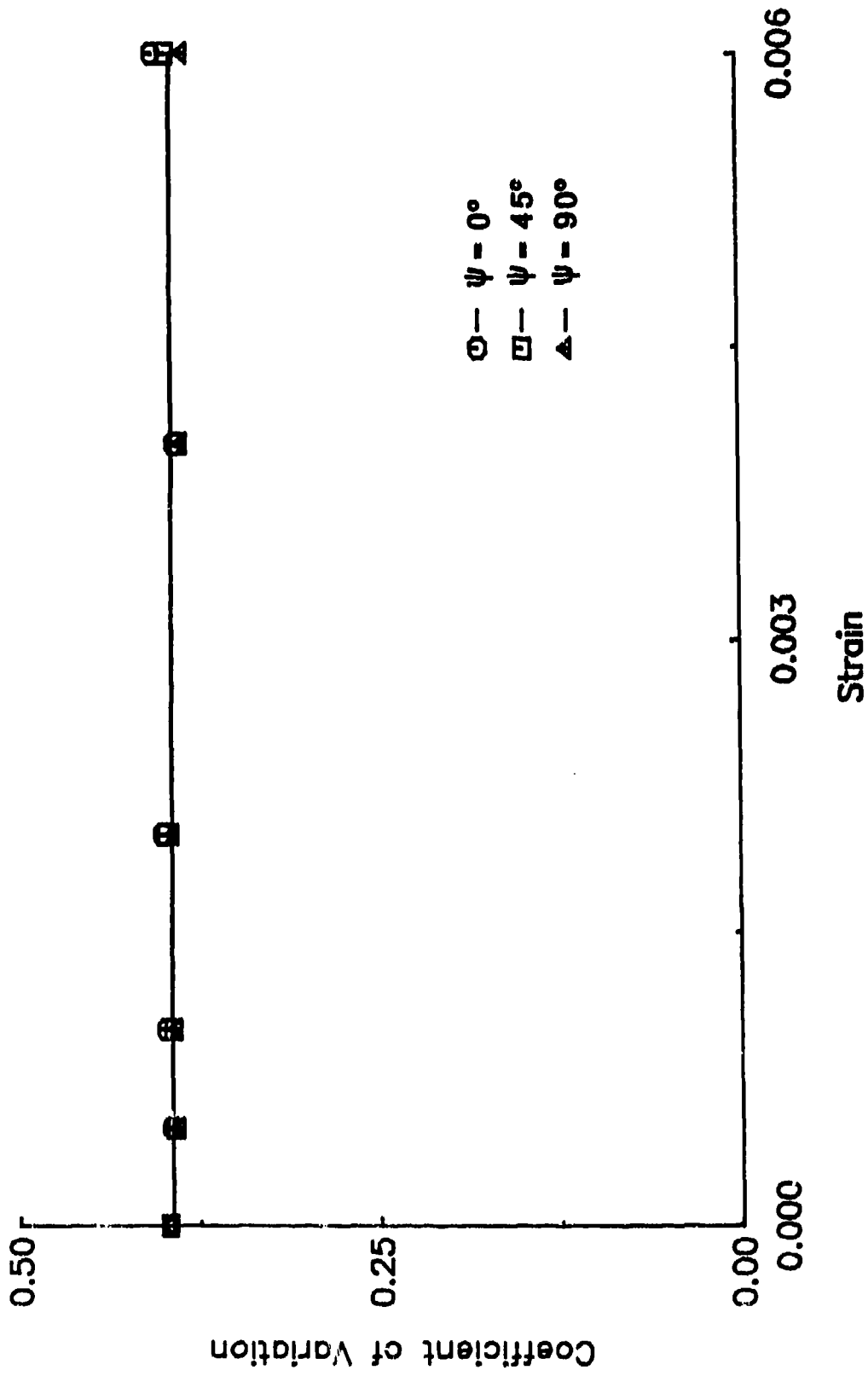


Fig. 3.12 Coefficient of variation of crack size versus compressive strain for cement paste, $W/C = 0.5$ (1 in. = 25.4 mm)

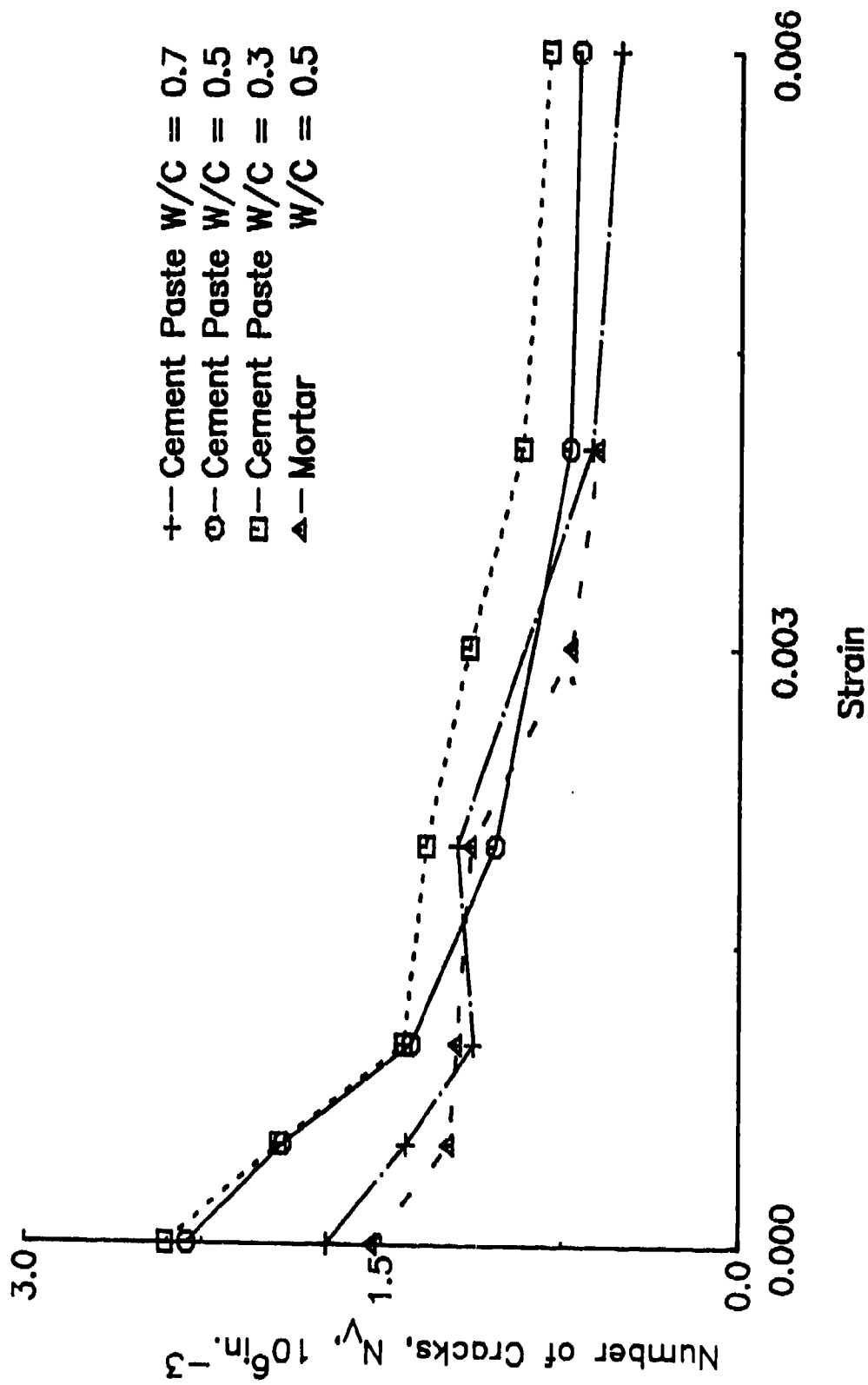


Fig. 3.13 Number of cracks per unit volume versus compressive strain for cement paste, W/C = 0.7, 0.5, and 0.3, and mortar, W/C = 0.5 ($10^6 \text{ in.}^3 = 61 \text{ mm}^3$)

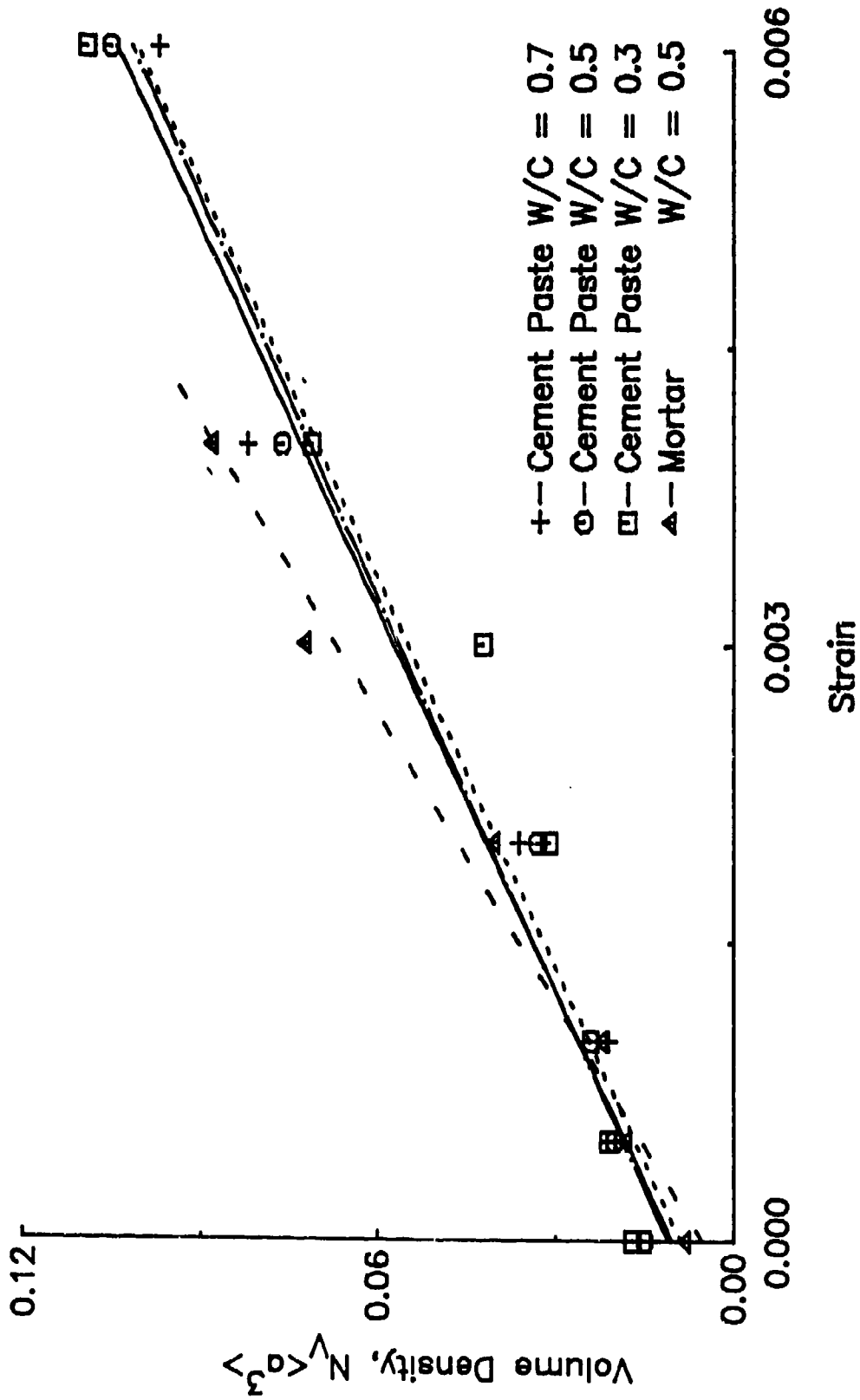


Fig. 3.14 Measure of volumetric crack density, $N_v \langle a^3 \rangle$, versus compressive strain for cement paste, W/C = 0.7, 0.5, 0.3, and mortar, W/C = 0.5

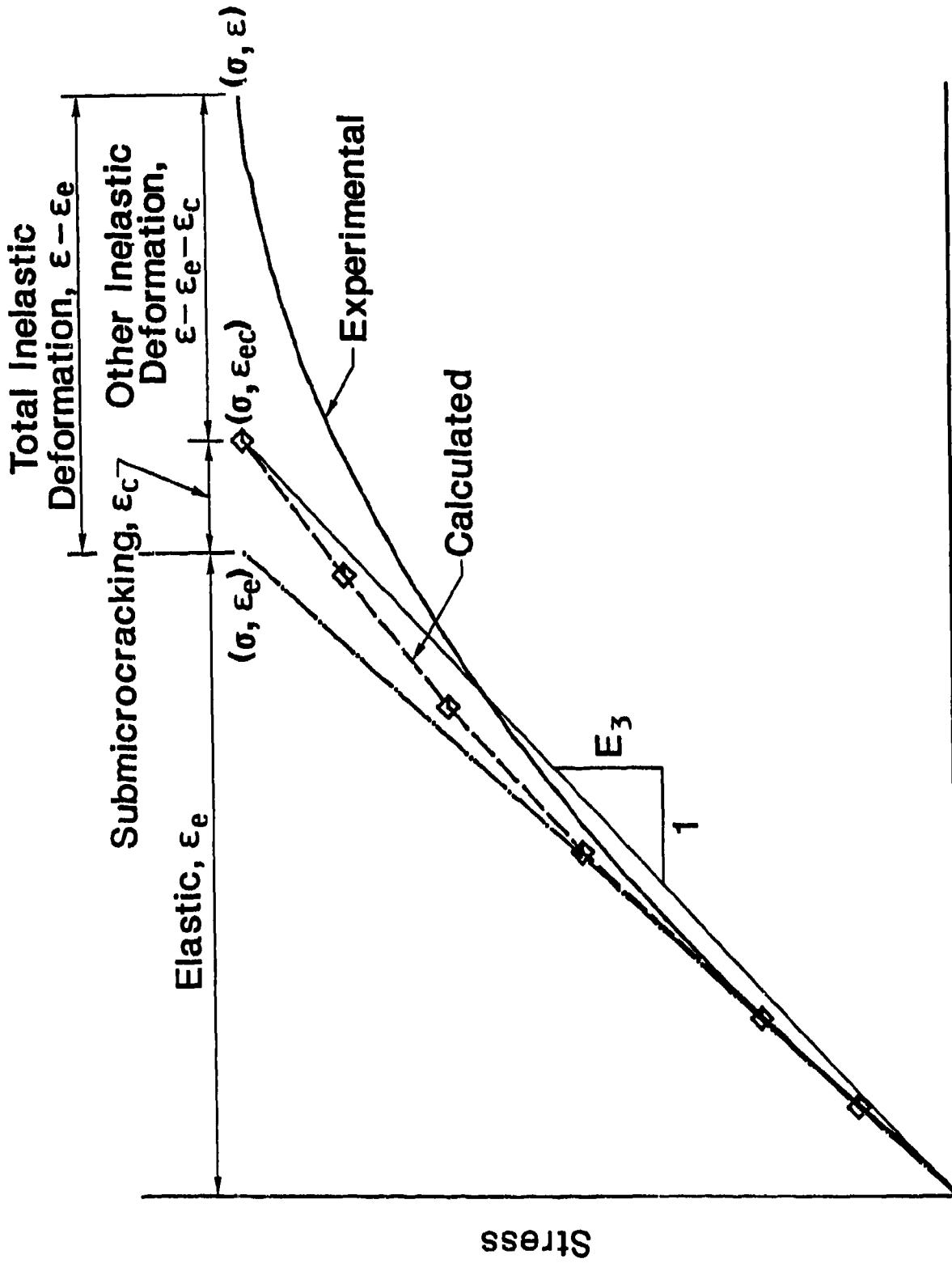


Fig. 3.15 Secant modulus, E_3 , and strain associated with submicrocracking and other inelastic deformation

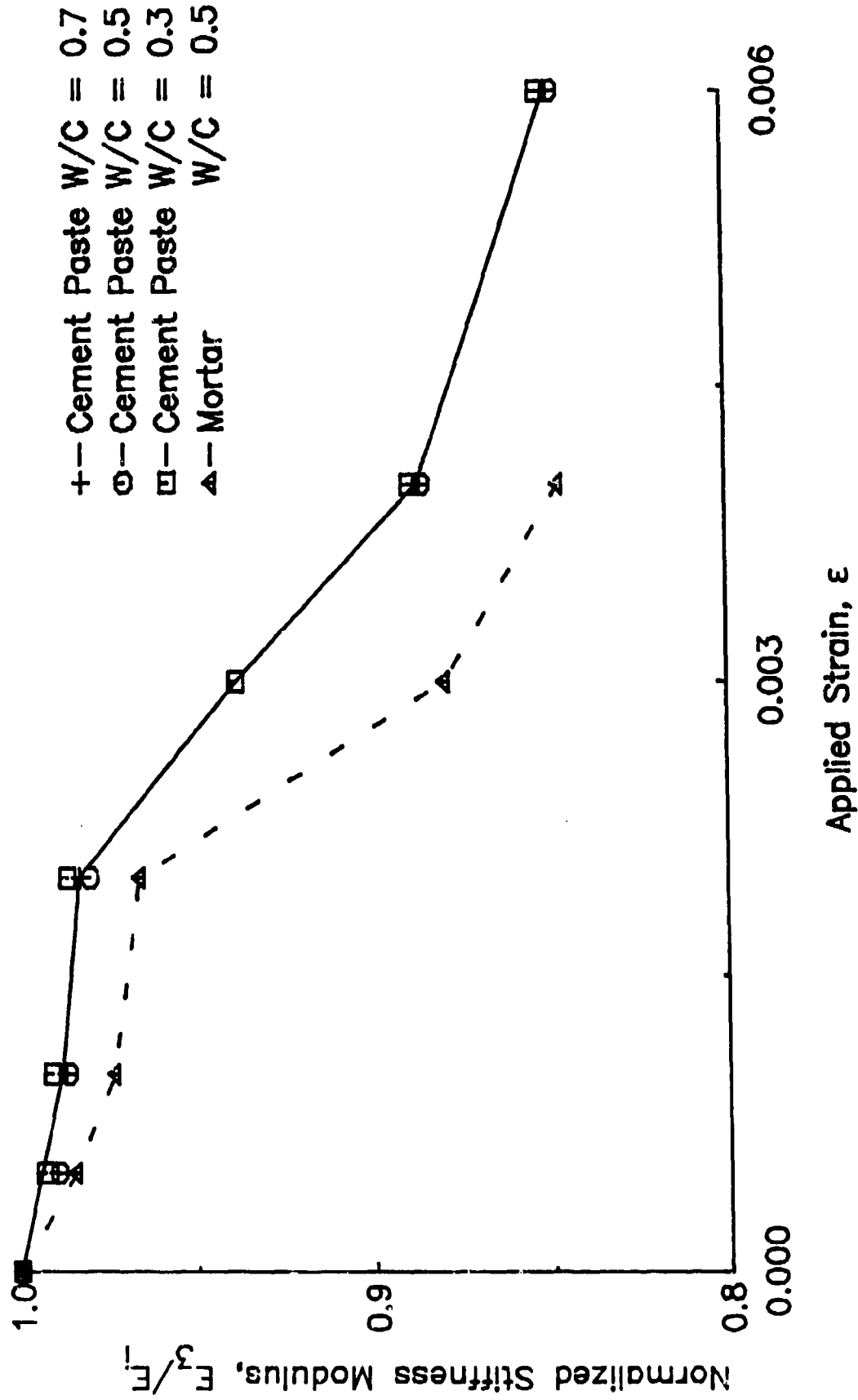


Fig. 3.16 Normalized calculated secant stiffness moduli versus compressive strain for cement paste, W/C = 0.7, 0.5, and 0.3, and mortar, W/C = 0.5

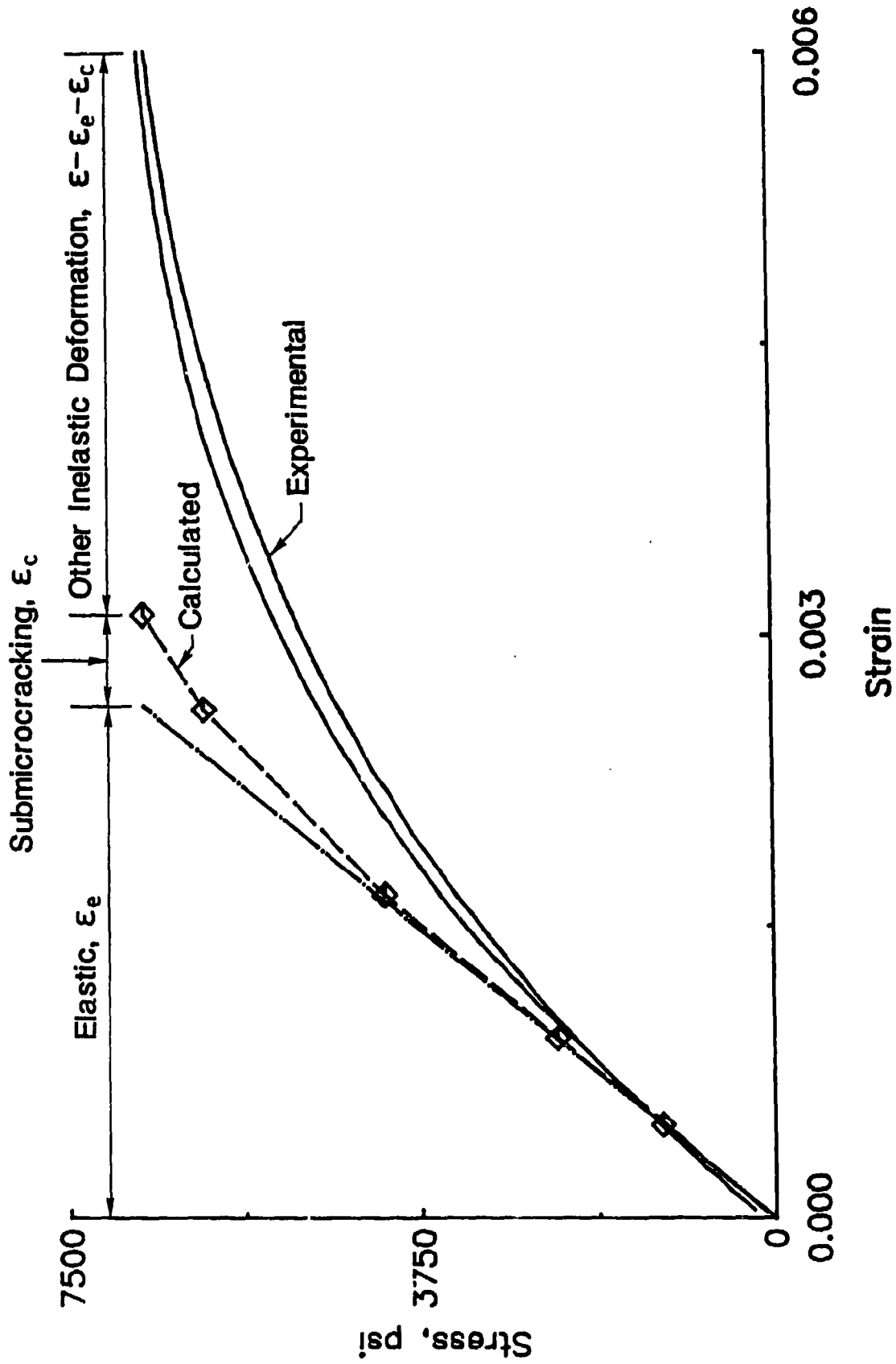


Fig. 3.17 Stress-strain curves for cement paste, W/C = 0.5. Linear matrix
(1 psi = 6.89 kPa)

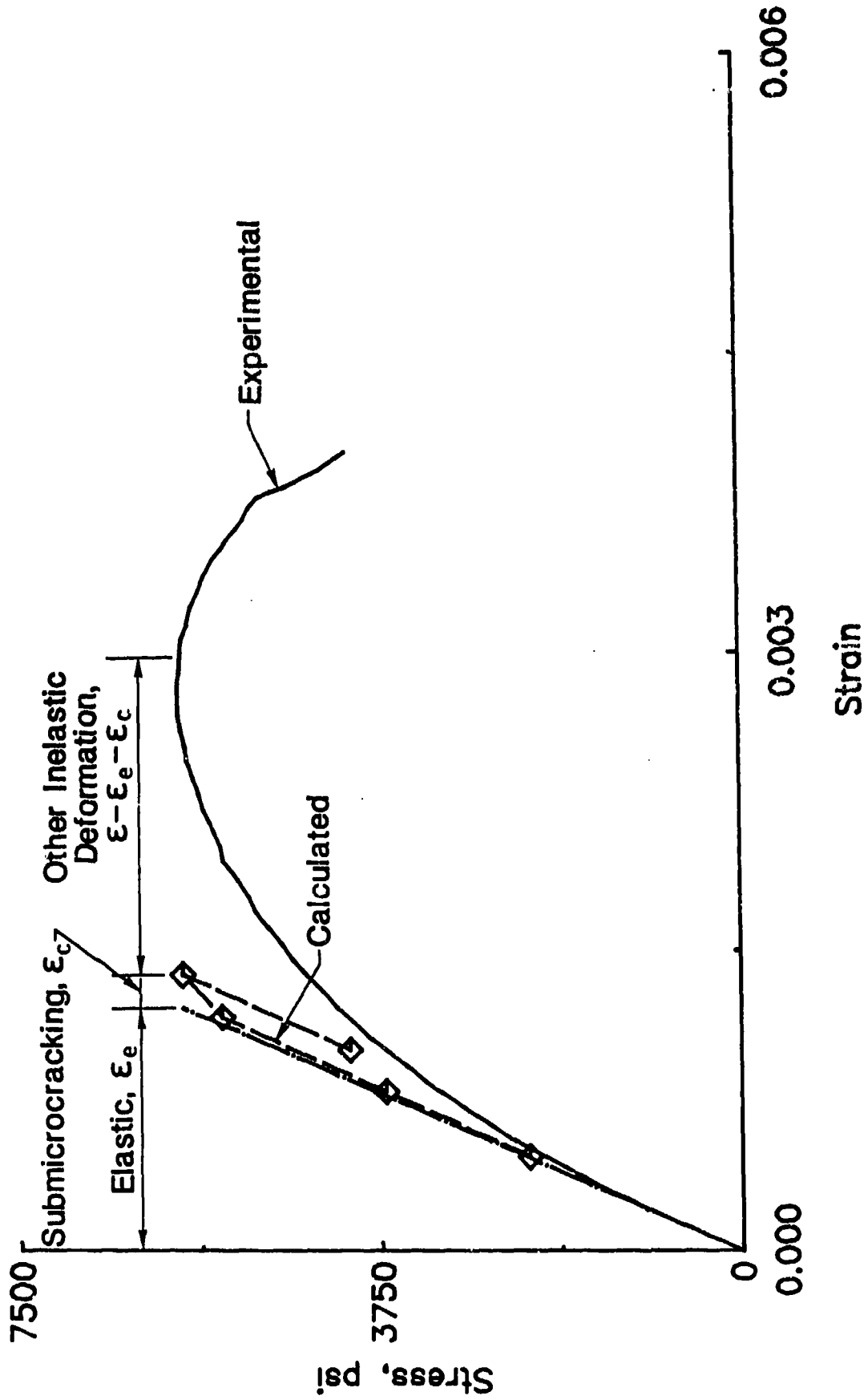


Fig. 3.18 Stress-Strain curves for mortar, W/C = 0.5. Linear matrix (1 psi = 6.89 kPa)

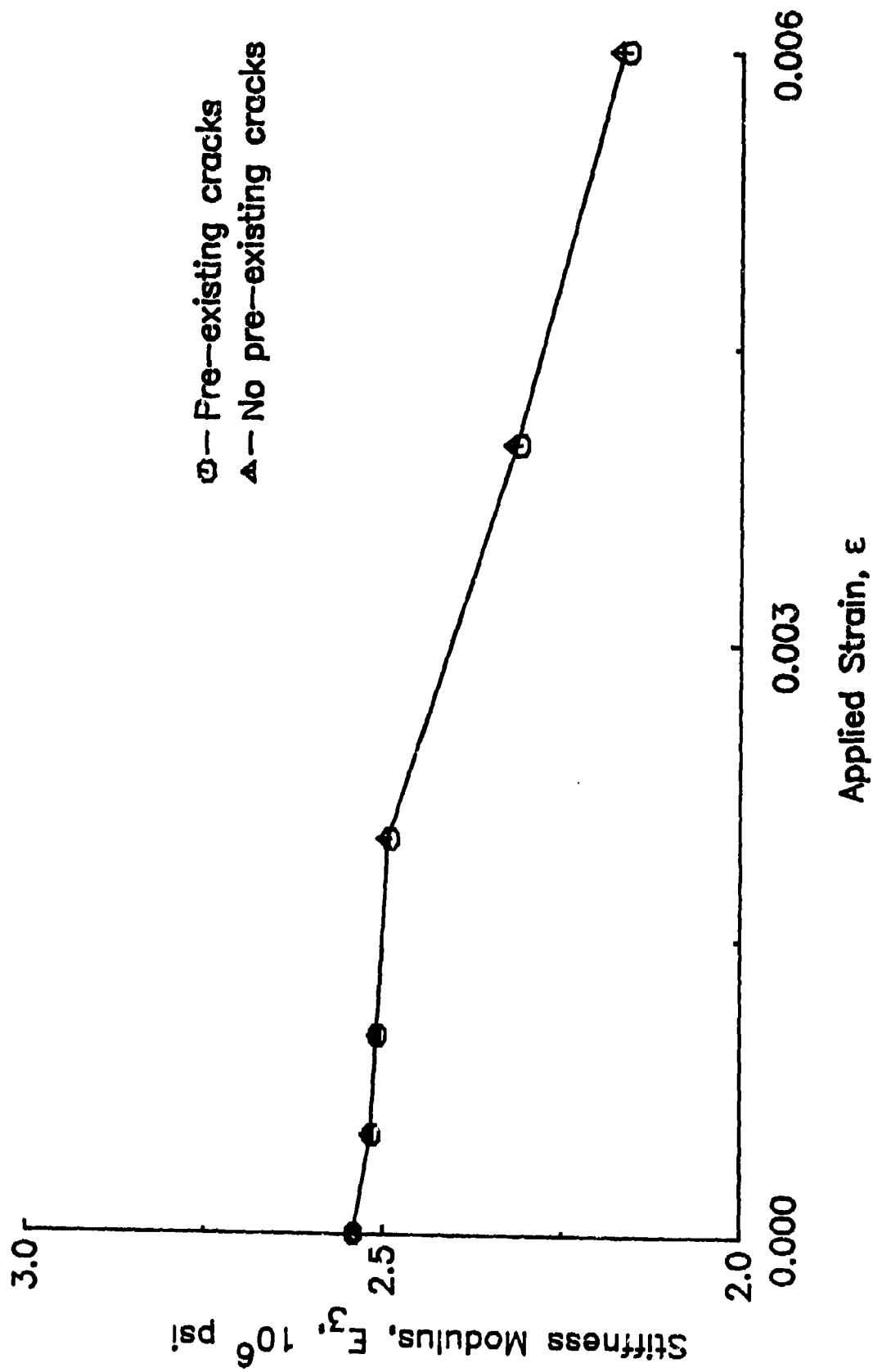


Fig. 3.19 Comparison of calculated secant stiffness moduli of cement paste, W/C = 0.5, with and without pre-existing cracks. Linear matrix (1 psi = 6.89 kPa)

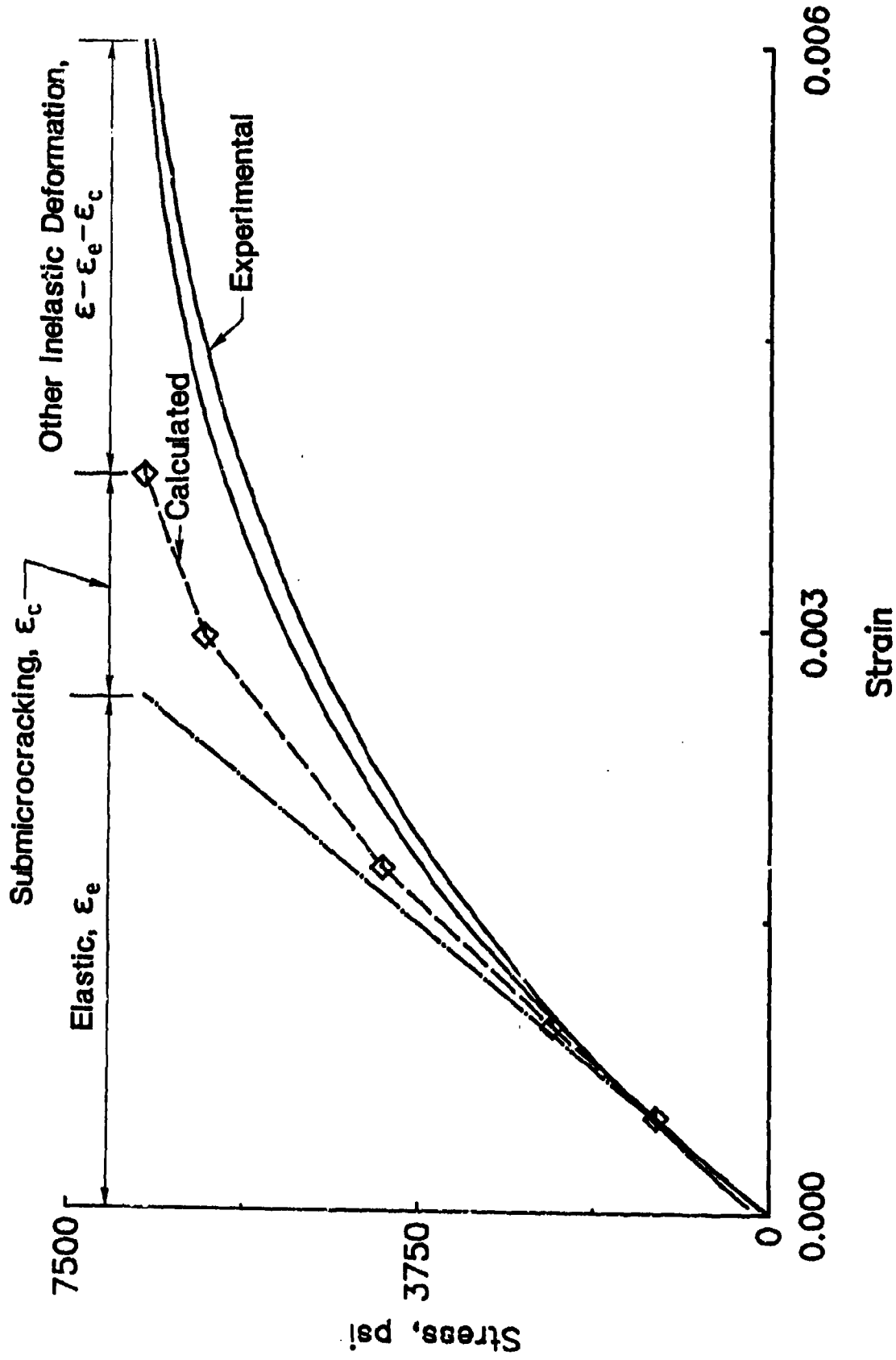


Fig. 3.20 Stress-strain curves for cement paste, $W/C = 0.5$. Nonlinear matrix (1 psi = 6.89 kPa)

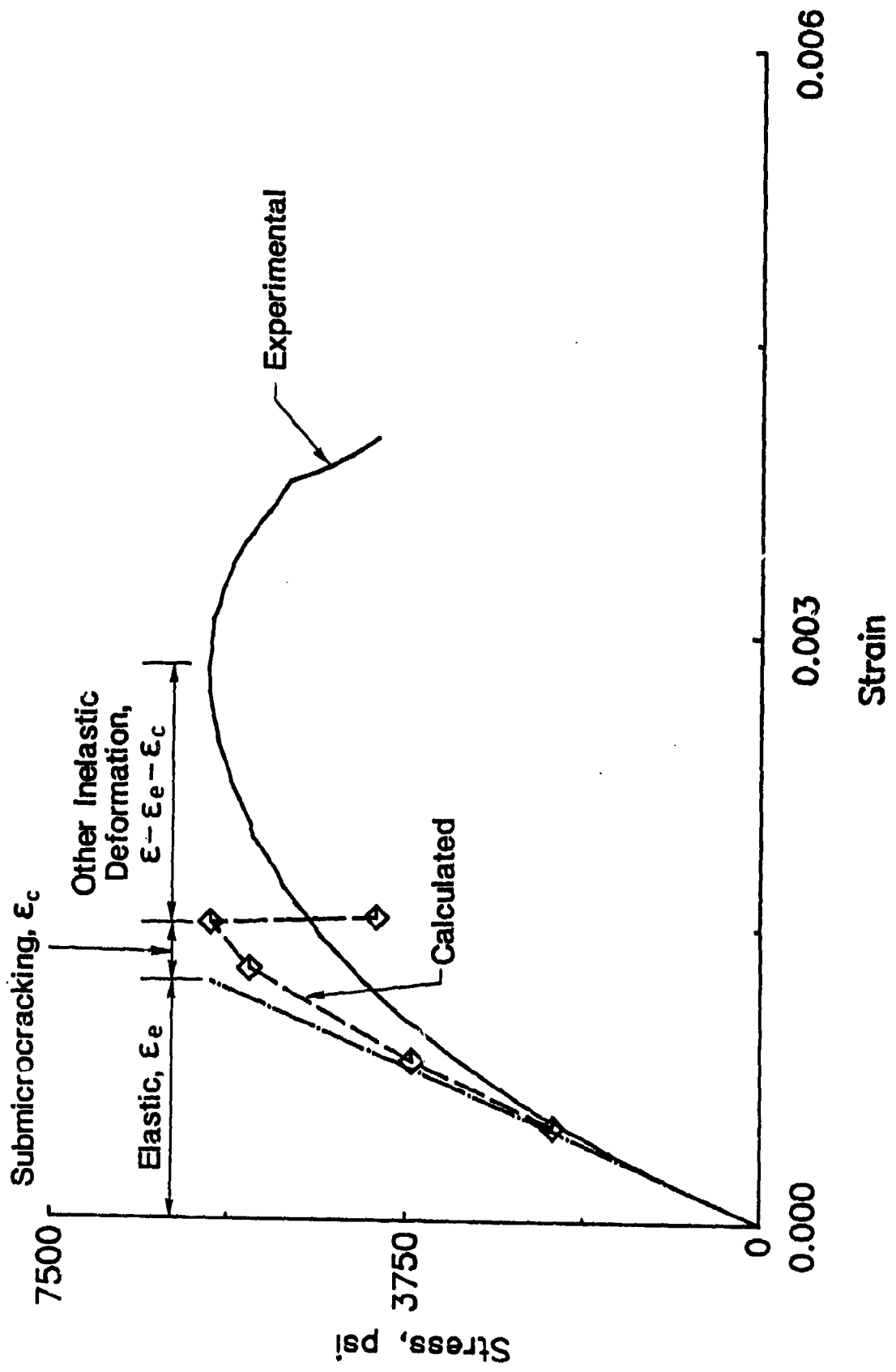


Fig. 3.21 Stress-strain curves for mortar, W/C = 0.5. Nonlinear matrix (1 psi = 6.89 kPa)

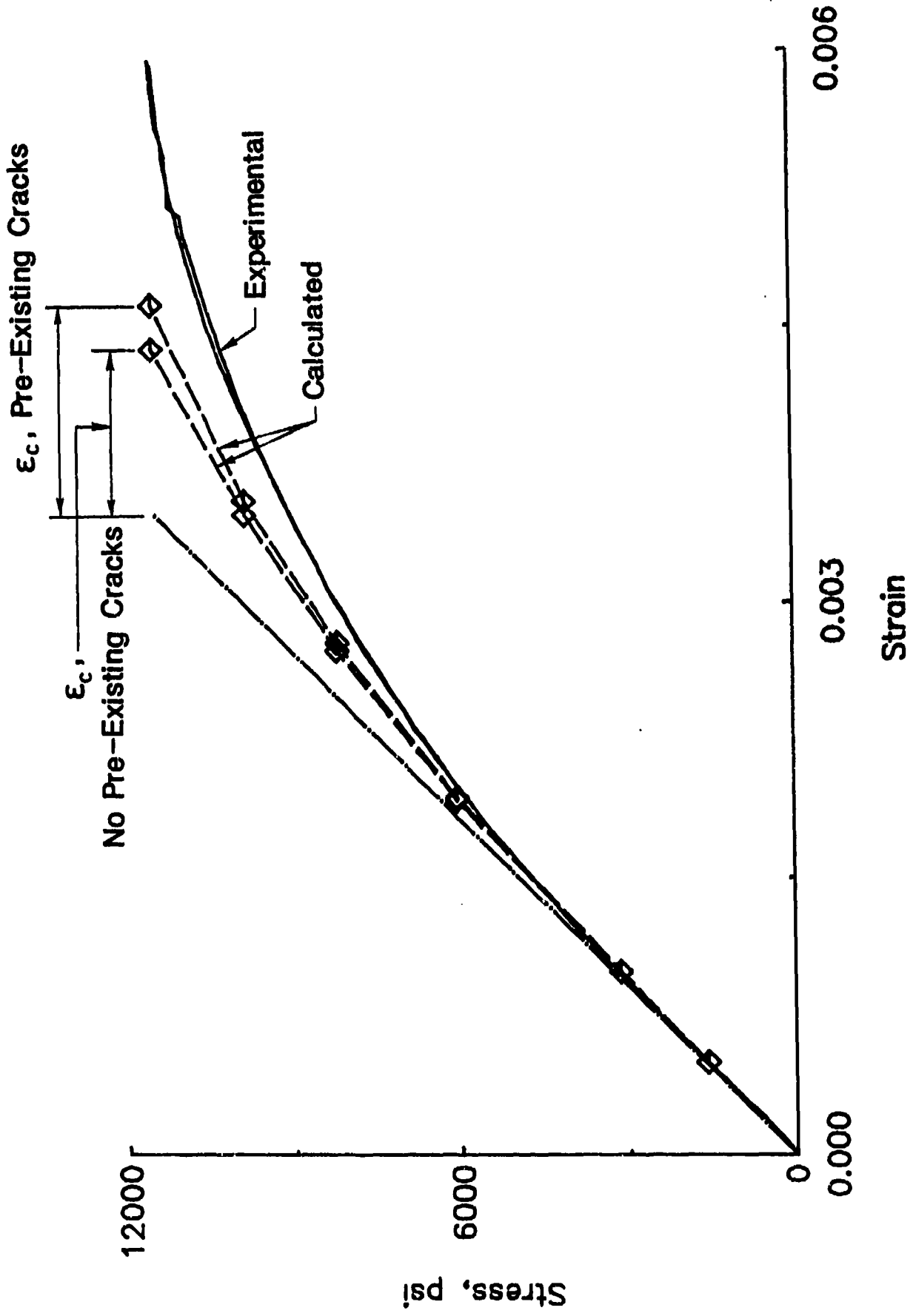


Fig. 3.22 Stress-strain curves for cement paste, W/C = 0.3. Calculated curves both with and without pre-existing cracks. Nonlinear matrix (1 psi = 6.89 kPa)

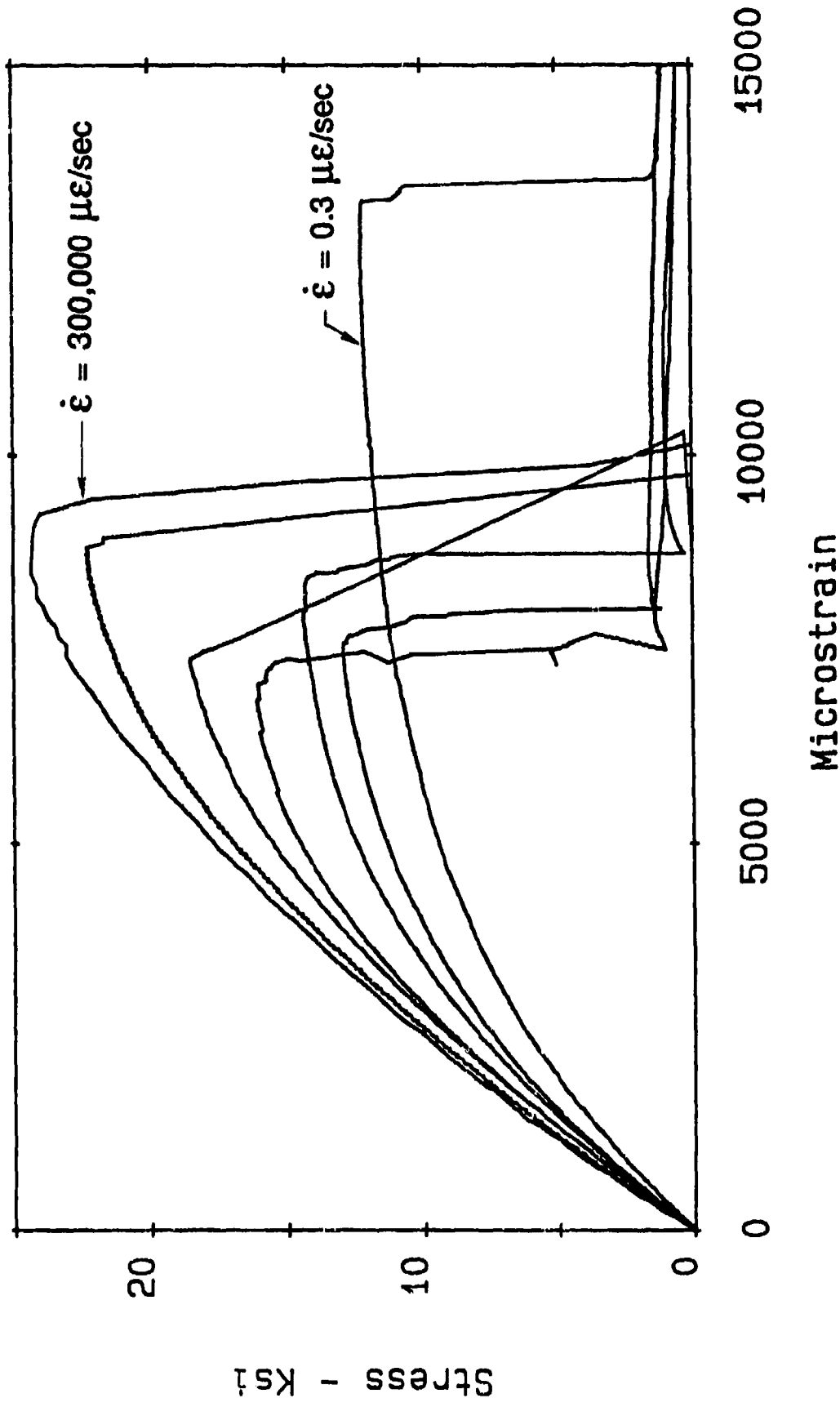


Fig. 4.1 Stress-strain curves for cement paste, W/C = 0.3, strain rates = 0.3, 3.0, 30, 300, 3000, 30,000 and 300,000 microstrain per second

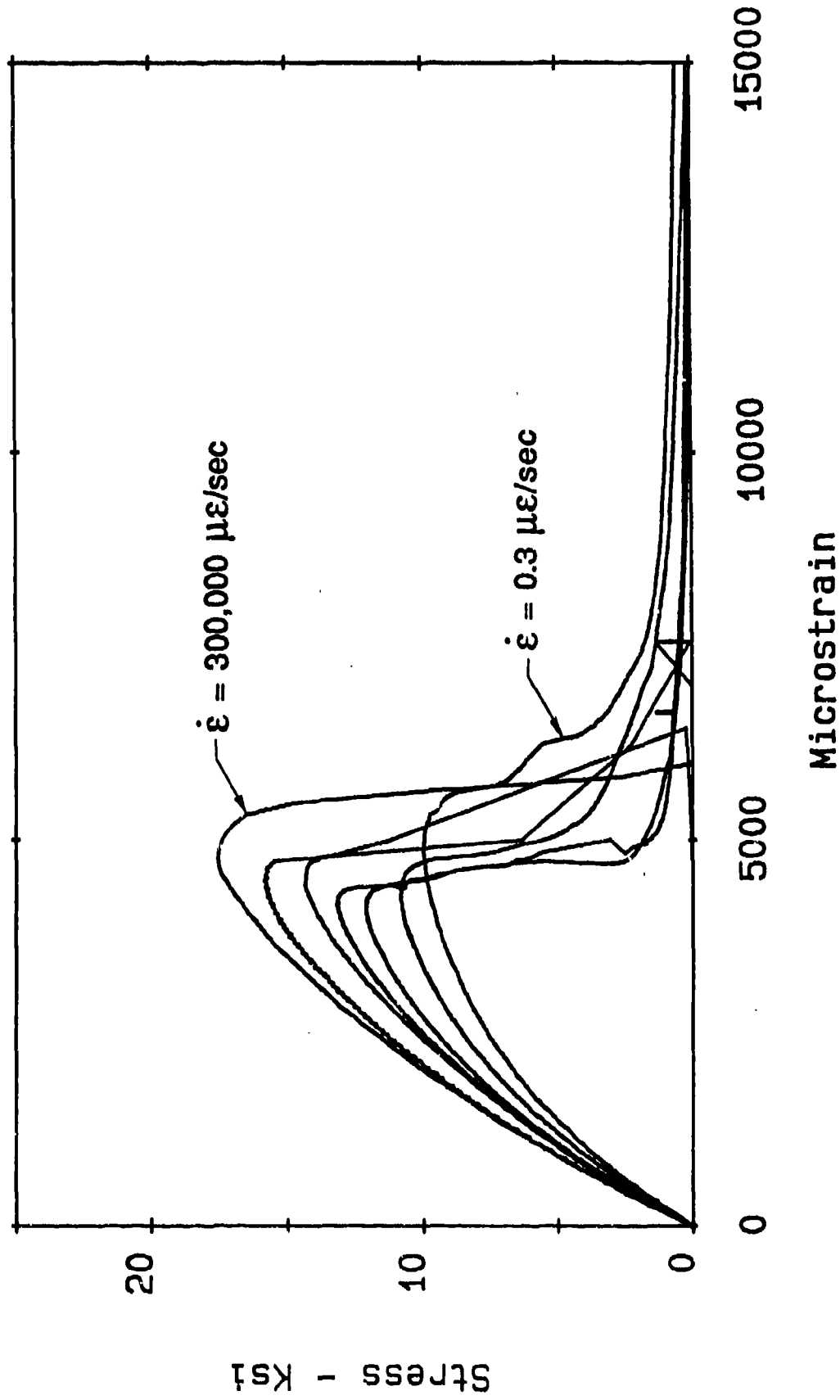


Fig. 4.2 Stress-strain curves for mortar, W/C = 0.3, strain rates = 0.3, 3.0, 30, 300, 3000, 30,000 and 300,000 microstrain per second.

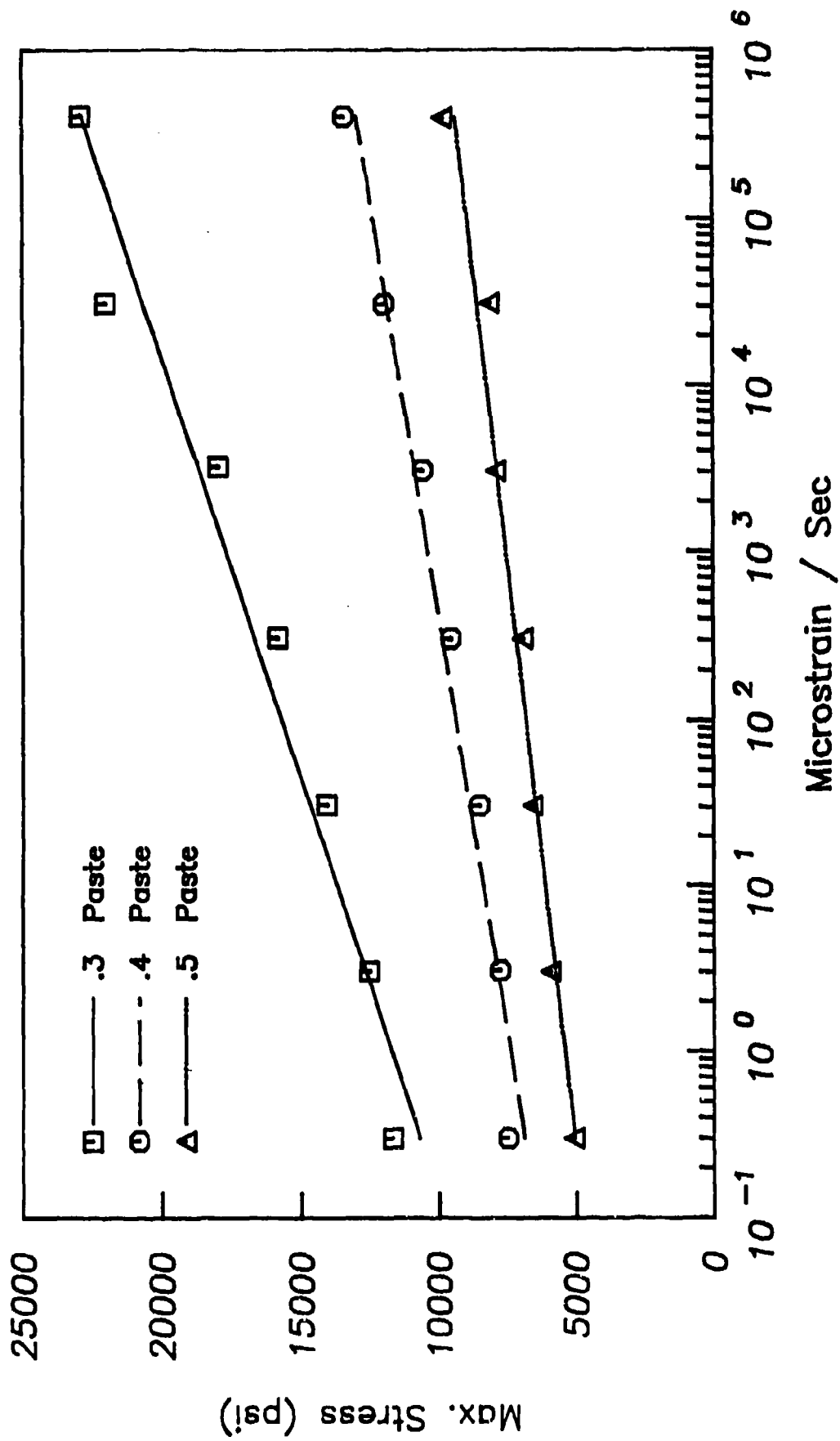


Fig. 4.3 Compressive strength versus strain rate ($\dot{\epsilon}_{50-99}$) for cement paste, W/C = 0.3, 0.4, and 0.5

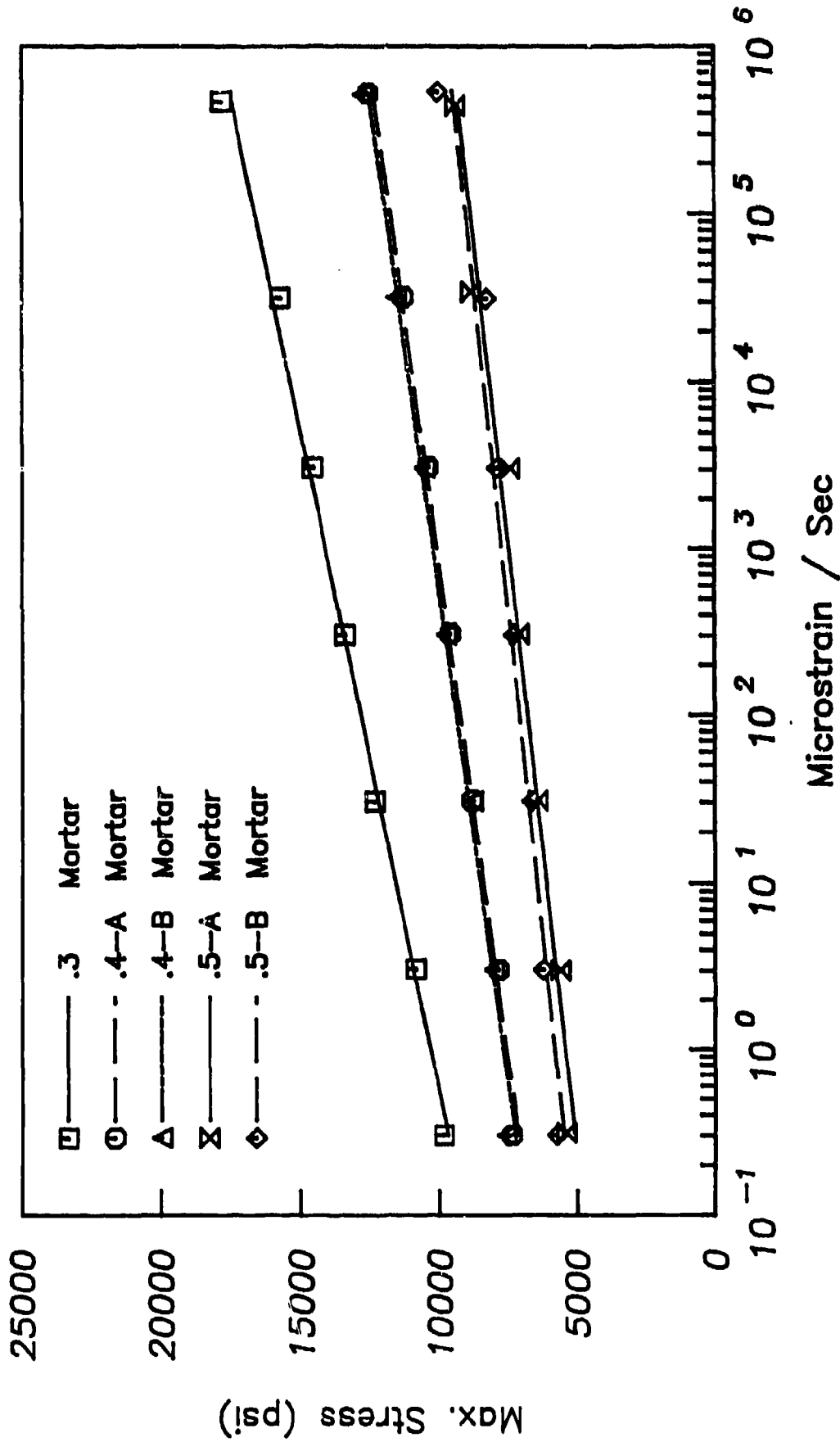


Fig. 4.4 Compressive strength versus strain rate ($\dot{\epsilon}_{50-99}$) for mortar, W/C = 0.3, 0.4, and 0.5

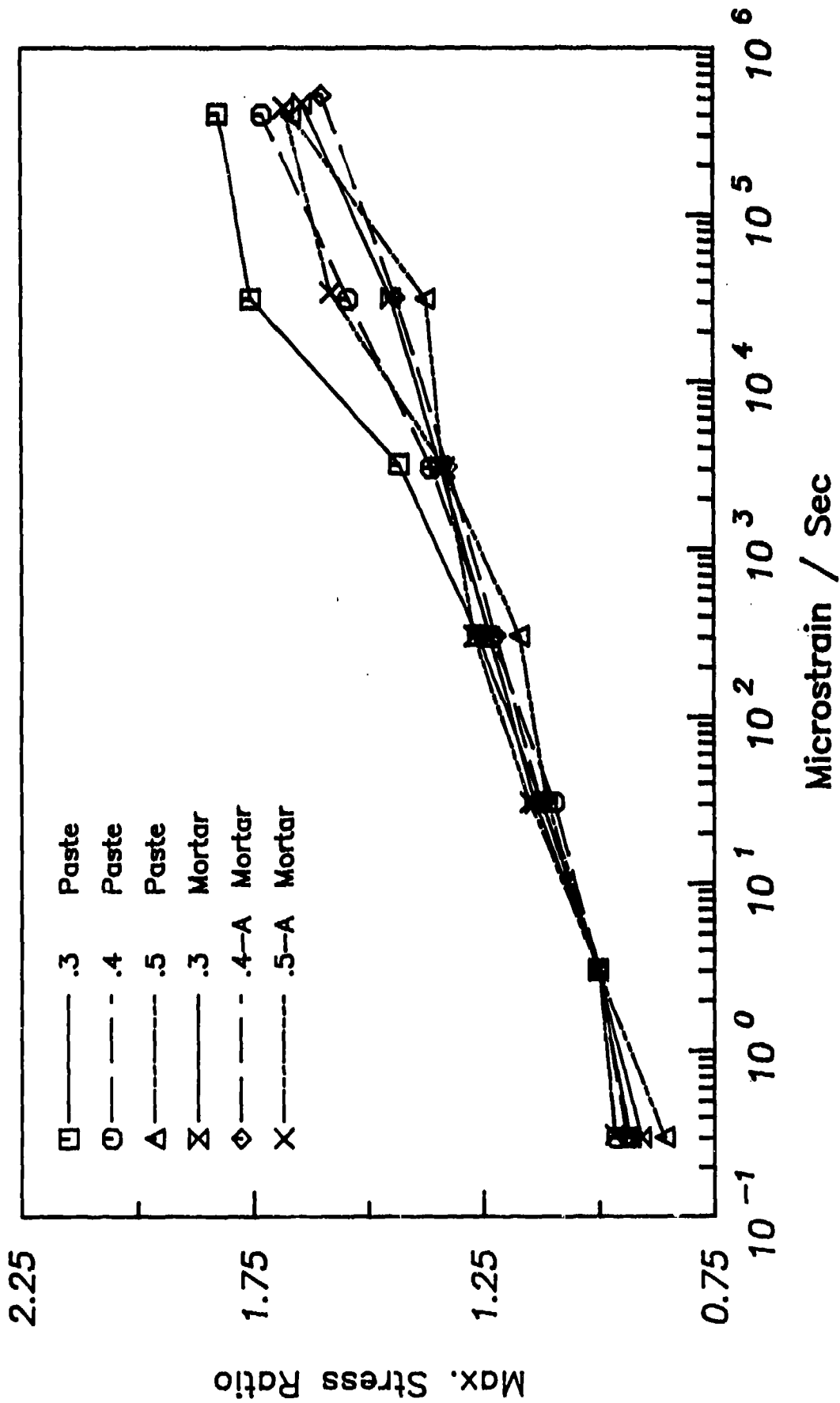


Fig. 4.5 Maximum stress ratios for cement paste and mortar versus strain rate (ϵ_{50-99})

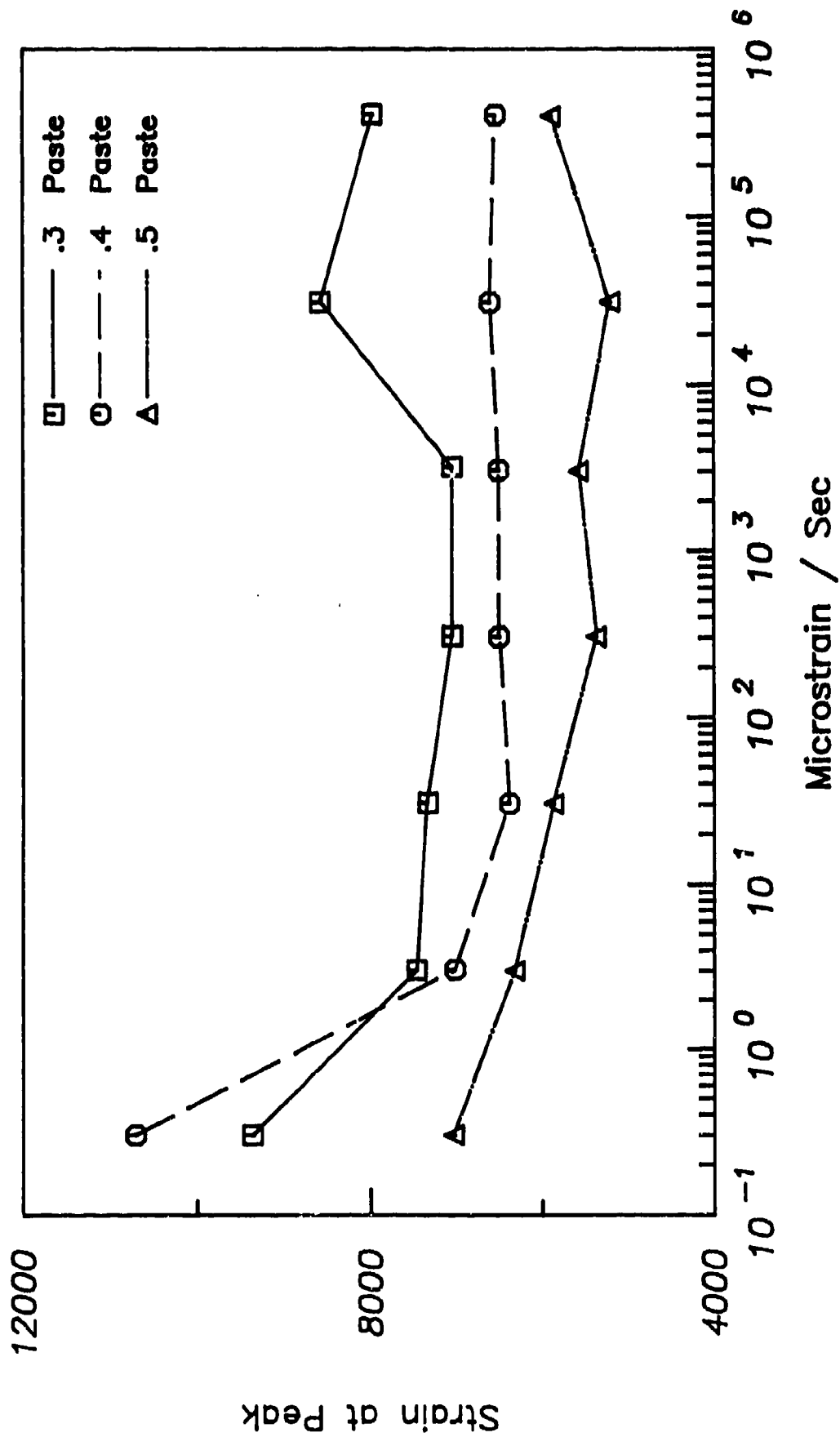


Fig. 4.6 Strain at the peak of the stress-strain curve versus strain rate ($\dot{\epsilon}_{50-99}$) for cement paste, W/C = 0.3, 0.4, and 0.5

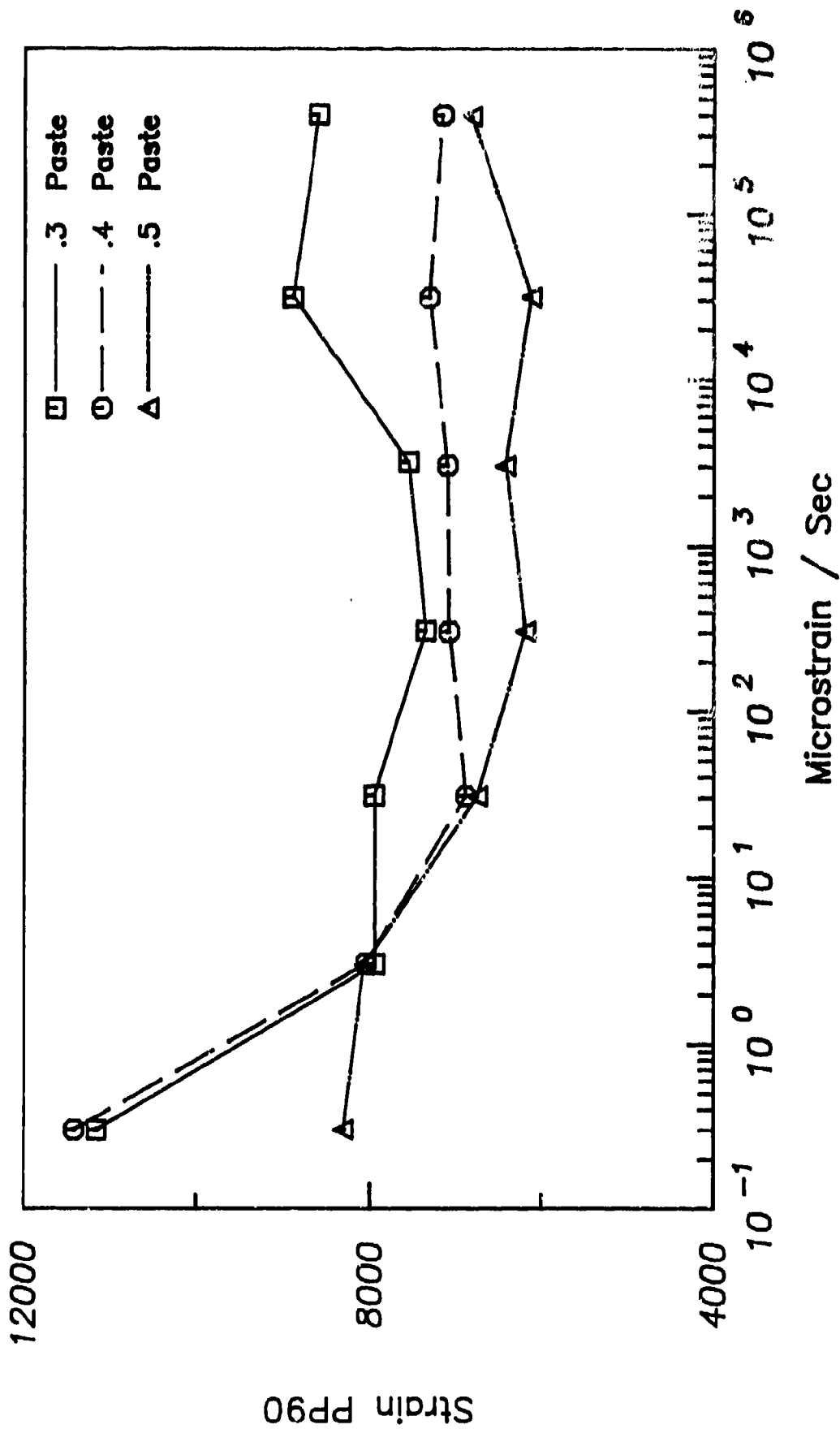


Fig. 4.7 Post-peak strain at a stress equal to 90 percent of the peak stress versus strain rate (ϵ_{50-99}) for cement paste, W/C = 0.3, 0.4, and 0.5

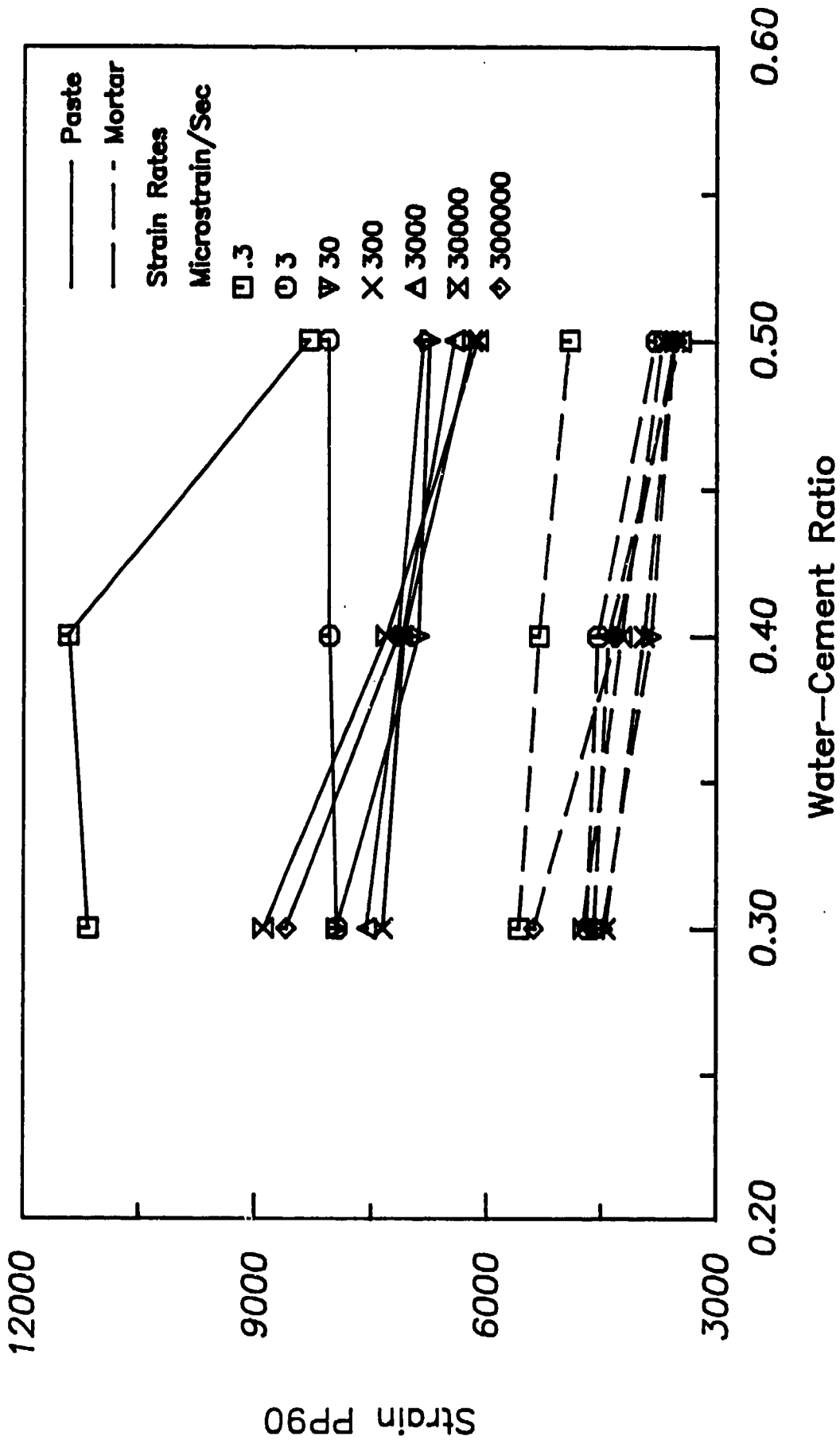


Fig. 4.8 Post-peak strain at a stress equal to 90 percent of the peak stress versus water-cement ratio for cement paste and mortar at different strain rates (ϵ_{50-99})

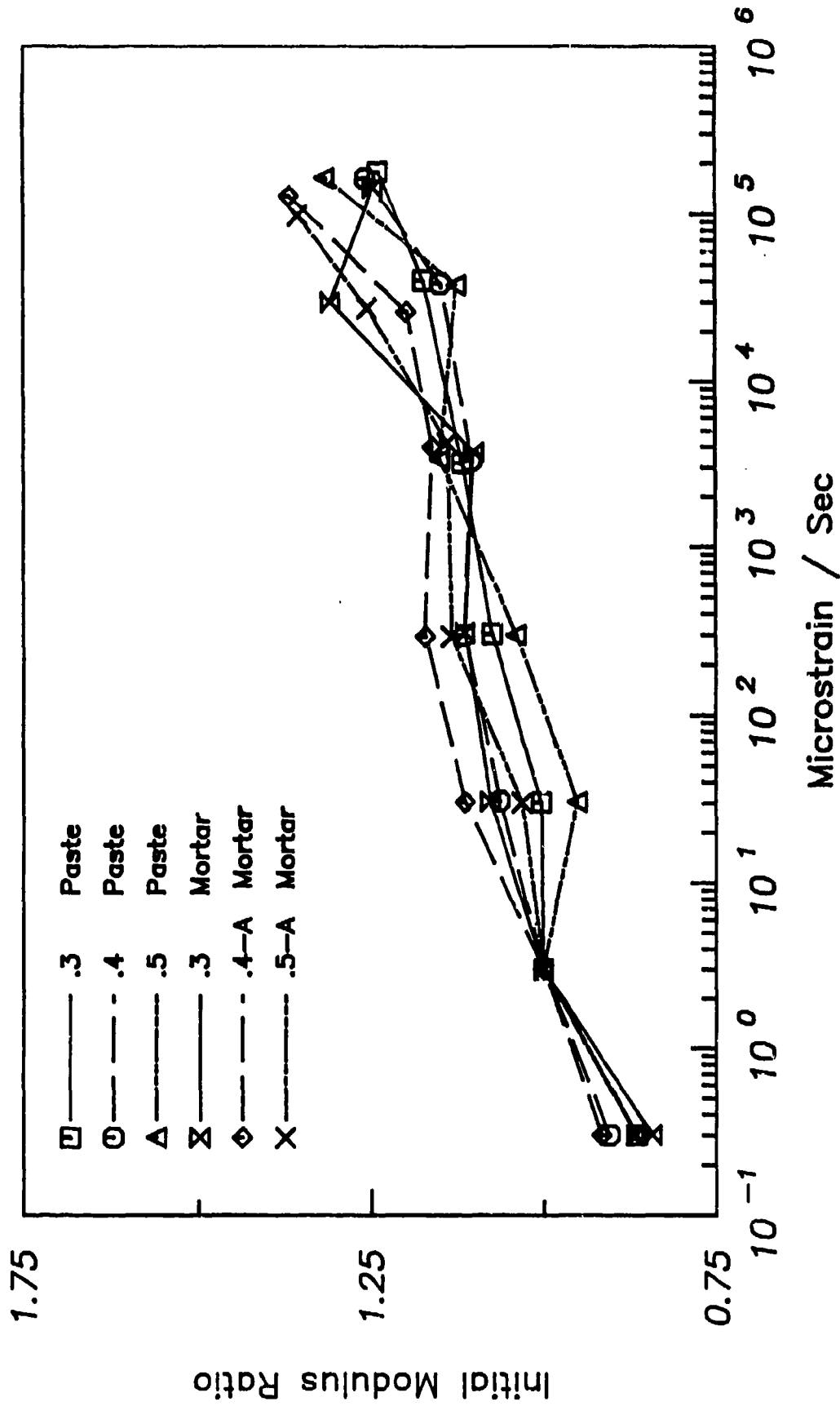


Fig. 4.9 Ratio of initial modulus of elasticity to modulus at $\dot{\epsilon} = 3.0$ microstrain per second versus strain rate (ϵ_{5-20})

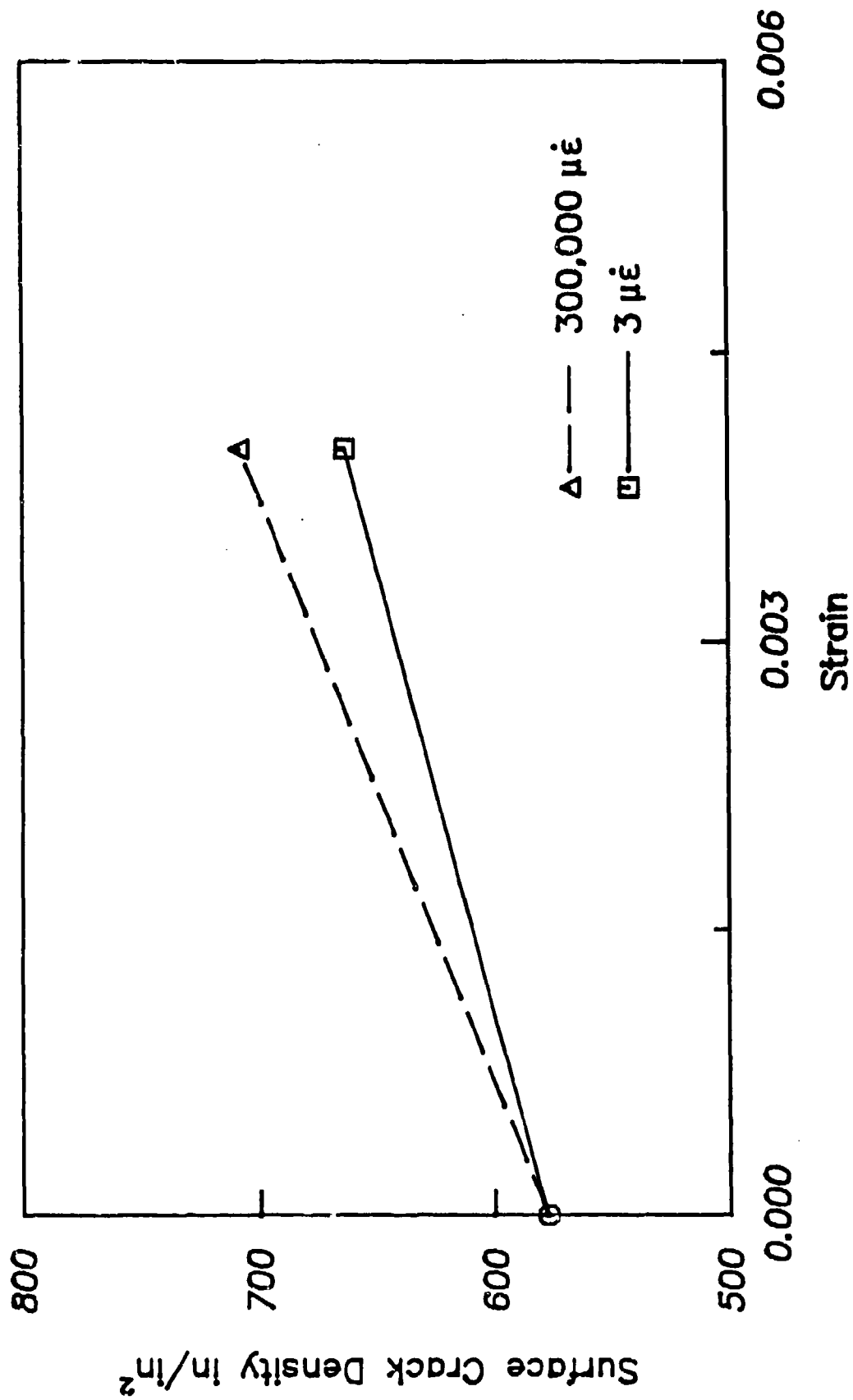


Fig. 4.10 Crack density measured with image analysis system versus compressive strain for cement paste, $W/C = 0.3$, for $\epsilon = 3.0$ and $300,000$ microstrain per second ($1 \text{ in./in.}^2 = 0.039 \text{ mm/mm}^2$)

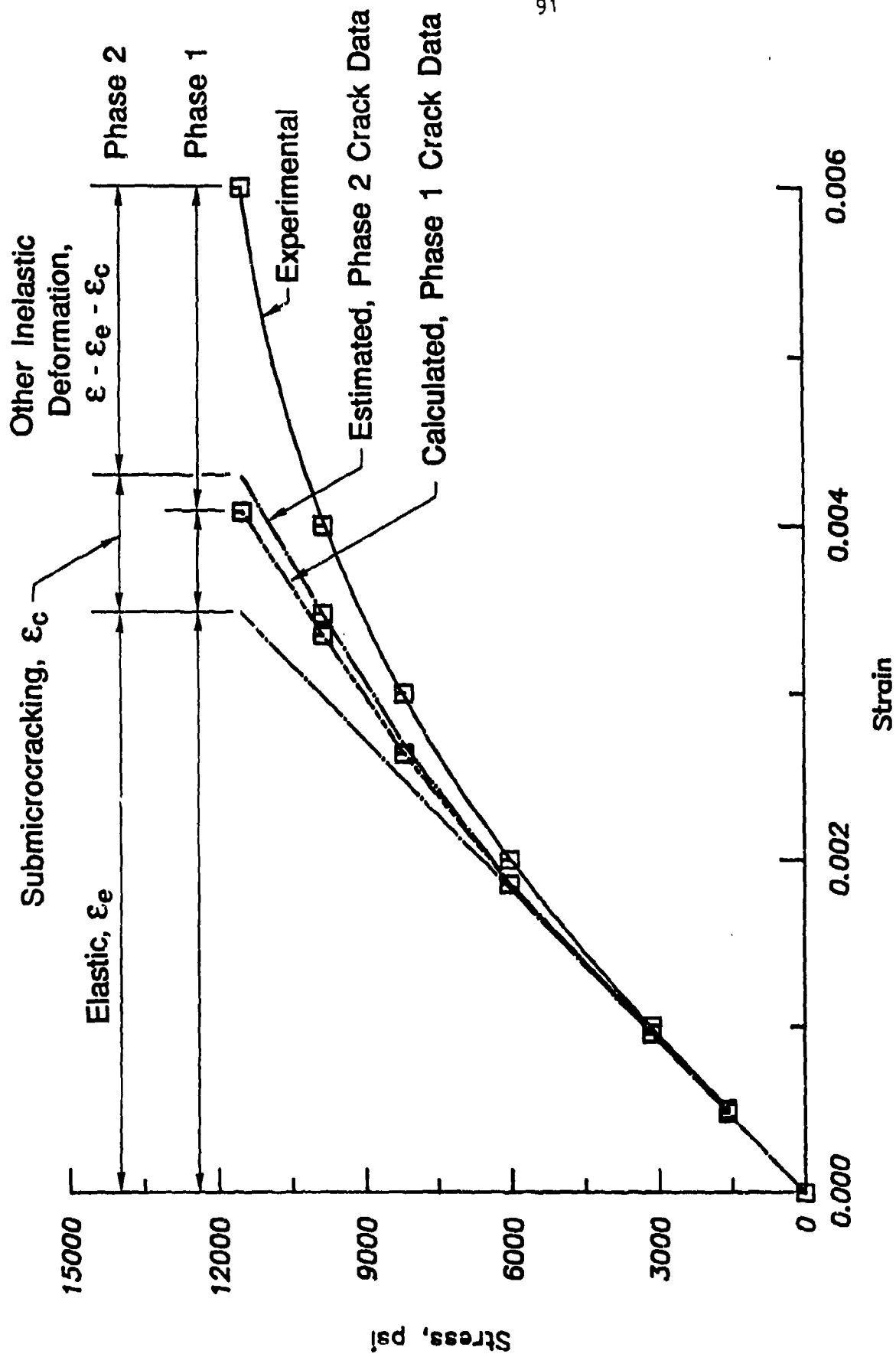


Fig. 4.11 Stress-strain curves for cement paste, W/C = 0.3. Linear matrix, $\epsilon = 3.0$ microstrain per second

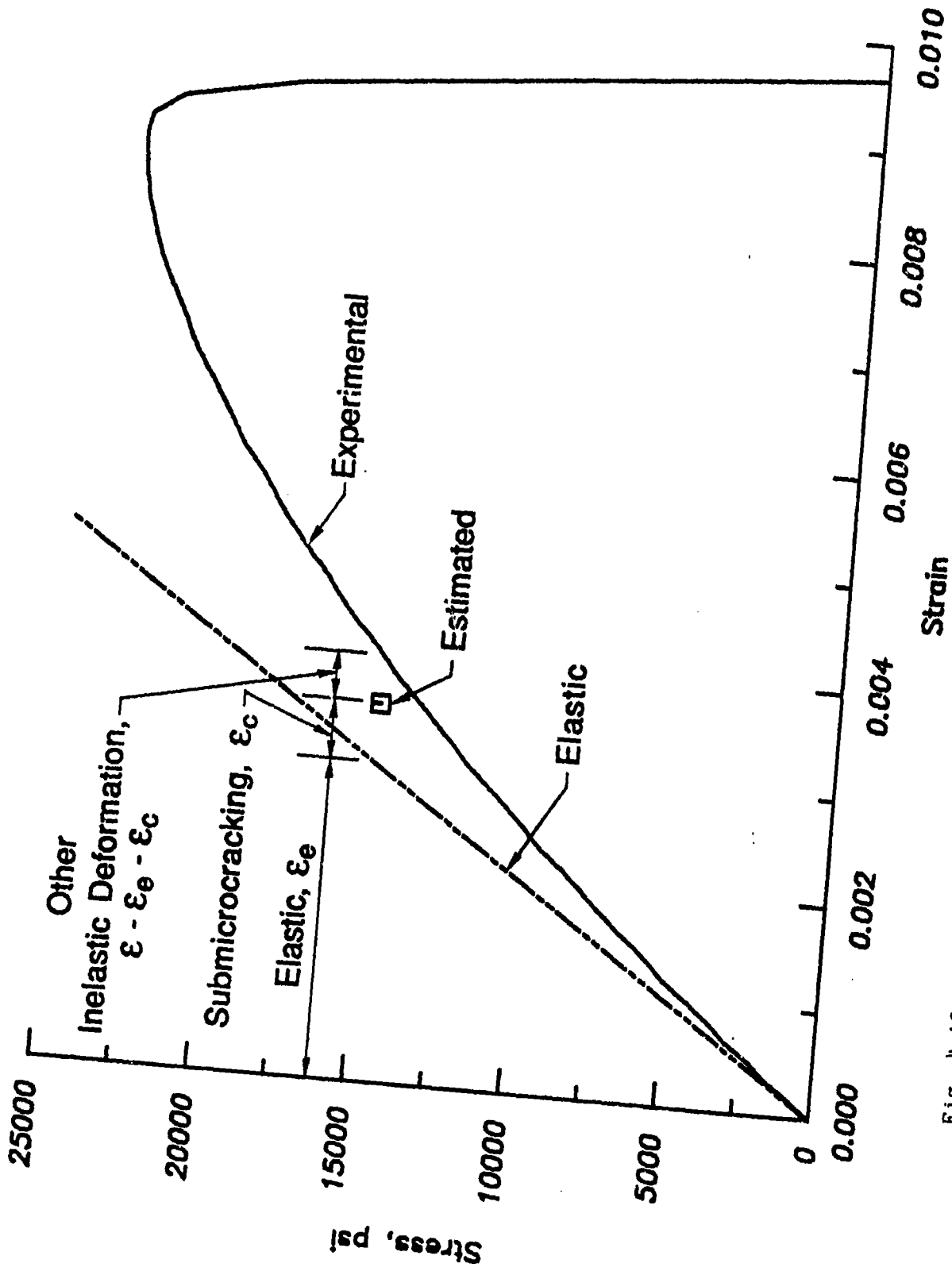


Fig. 4.12 Stress-strain curve for cement paste, $W/C = 0.3$. Linear matrix, $\dot{\epsilon} = 300,000$ microstrain per second

APPENDIX A

NOTATION

a	length of major semi-axis of elliptic crack = "characteristic" crack size
$\langle a_\psi \rangle$	mean characteristic crack size for orientation ψ
b	length of minor semi-axis of elliptic crack
E_1	initial stiffness modulus (= secant modulus between 5 and 20 percent of compressive strength for strain rate study)
E_m	secant stiffness modulus of matrix material
E_1	secant stiffness modulus perpendicular to direction of loading
E_3	secant stiffness modulus in direction of loading
$f(a \psi)$	three-dimensional crack size distribution for orientation ψ
$f(\psi)$	three-dimensional crack orientation distribution
G_{12}	secant shear modulus in plane perpendicular to direction of loading
G_{31}	secant shear modulus in direction of loading
K	measure of degree of anisotropy for three-dimensional crack distributions
N_V	number of cracks per unit volume
$N_V \langle a^3 \rangle$	measure of volumetric crack density
r	crack aspect ratio = b/a
$\text{var} \langle a_\psi \rangle$	variance of crack size distribution for orientation ψ
α, β	parameters of gamma distribution
$\Delta N_V \langle a^3 \rangle$	change in measure of volumetric crack density
$\Delta \Phi$	strain energy change due to cracks
ϵ	applied axial strain

ϵ_c	strain due to submicroscopic cracks
ϵ_e	elastic strain = σ/E_1
ϵ_{ec}	elastic strain plus cracking strain
ϵ_m	strain in matrix material = σ/E_m
ϵ_p	strain at peak of stress-strain curve
ϵ_{pp90}	strain past the peak of the stress-strain curve corresponding to 90 percent of the peak stress
$\dot{\epsilon}$	strain rate
$\bar{\epsilon}$	average strain rate from zero stress to peak stress
$\dot{\epsilon}_{5-20}$	average strain rate between strains corresponding to 5 and 20 percent of peak stress
$\dot{\epsilon}_{50-99}$	average strain rate from strain corresponding to 50 percent of peak stress to a strain past the peak of the stress-strain curve corresponding to 99 percent of the peak stress
η	angular rotation of crack about its normal, see Fig. 3.10
θ	crack trace angle, see Fig. 3.9
ν_1	initial Poisson's ratio
ν	Poisson's ratio
ν_m	Poisson's ratio of matrix material
ν_{12}	Poisson's ratio in plane perpendicular to direction of loading
ν_{31}	Poisson's ratio in plane parallel to direction of loading
σ	stress normal to crack plane
ϕ	strain energy of uncracked solid
ϕ_c	strain energy of cracked solid
ϕ	angular crack coordinate in plane perpendicular to longitudinal axis, see Fig. 3.10
ψ	three-dimensional crack orientation, see Fig. 3.10

APPENDIX B

REPORTS AND PUBLICATIONS SUPPORTED BY THE AIR FORCE OFFICE OF SCIENTIFIC RESEARCH UNDER GRANT AFOSR-85-0194

1. Attiogbe, E. K. and Darwin, D., "Submicroscopic Cracking of Cement Paste and Mortar in Compression," SM Report No. 16, University of Kansas Center for Research, Inc., Lawrence, Kansas, November 1985, 439 pp.
2. Darwin, D. and Attiogbe, E. K., "Effects of Loading Rate on Cracking of Cement Paste in Compression," Cement-Based Composites: Strain Rate Effects on Fracture, S. Mindess and S. P. Shah, Eds., Materials Research Society Symposia Proceedings, Vol. 64, 1986, pp. 167-180.
3. Attiogbe, E. K. and Darwin, D., "Correction of Window Size Distortion of Crack Distributions on Plane Sections," Journal of Microscopy, Vol. 144, Pt. 1, October 1986, pp. 71-82.
4. Attiogbe, E. K. and Darwin, D., "Self-Consistent Model for a Transversely Isotropic Cracked Solid," Journal of Engineering Mechanics, ASCE, Vol. 113, No. 7, July 1987, pp. 984-999.
5. Attiogbe, E. K. and Darwin, D., "Submicrocracking in Cement Paste and Mortar," ACI Materials Journal, Vol. 84, No. 6, November-December 1987, pp. 491-500.
6. Attiogbe, E. K. and Darwin, D., "Strain Due to Submicrocracking in Cement Paste and Mortar," ACI Materials Journal, Vol. 85, No. 1, January-February 1988, pp 3-11.
7. Darwin, D.; Shen Z.; and Harsh, S., "Silica Fume, Bond Strength, and the Compressive Strength of Mortar," Bonding in Cementitious Composites, S. Mindess and S. P. Shah, Eds., Materials Research Society Symposium Proceedings, Vol. 114, 1988, pp. 105-110.
8. Darwin, D. and Dewey, G. R., "Image Analysis of Microcracks," Proceedings, France-U.S. CNRS-NSF Workshop on Strain Localization and Size Effect due to Cracking and Damage, Cachan, France, September 6-9, 1988, Elsevier Applied Science Publishers, Ltd., 11 pp. in press.
9. Darwin, D.; Attiogbe, E. K.; Harsh, S.; Shen, Z.; and Dewey, G. R., "Submicroscopic Deformation in Cement Paste and Mortar at High Load Rates," SL Report 88-1, University of Kansas Center for Research, Inc., Lawrence, Kansas, August 1988.